

# Control and enhancement of supercontinuum in photonic crystal fibres

Dane R. Austin

Submitted in Partial Fulfillment of the Requirements for the Degree of Master of Science

Supervised by Professor C. Martijn de Sterke and Professor Benjamin J. Eggleton

Center for Ultrahigh bandwidth Devices for Optical Systems  
The University of Sydney



2010

# Abstract

Supercontinuum generation in femtosecond-pumped photonic crystal fibres is a dramatic spectral broadening process with significant applications. We present a detailed study of dispersive wave generation, an important mechanism for the production of blue-shifted radiation, which shows that the standard model which involves fundamental solitons perturbed by higher-order dispersion needs to be augmented by considering the rapid red-shift of the pump caused by spectral recoil. We also develop an intuitive physical explanation for narrow-band supercontinuum enhancements caused by fibre Bragg gratings, and show that this effect is a specific case of a universal property of self-phase modulation by which narrowband phase features can be converted into a spectral enhancement.

## Chronological note

The work contained in this thesis was performed in January to September 2006. At the end of this period, the author left the University of Sydney to commence a doctoral degree elsewhere. Because of the doctoral thesis, the writing of this thesis was deferred until December 2010.

# Publications and presentations

The following publications arose from this thesis:

D.-I. Yeom, J. A. Bolger, G. D. Marshall, D. R. Austin, B. T. Kuhlmeier, M. J. Withford, C. M. de Sterke, and B. J. Eggleton, “Tunable spectral enhancement of fiber supercontinuum,” *Opt. Lett.* **32**, 1644–1646 (2007).

D. R. Austin, J. A. Bolger, C. M. de Sterke, B. J. Eggleton, and T. G. Brown, “Narrowband supercontinuum control using phase shaping,” *Opt. Express* **14**, 13142–13150 (2006).

D. R. Austin, C. M. de Sterke, B. J. Eggleton, and T. G. Brown, “Dispersive wave blue-shift in supercontinuum generation,” *Opt. Express* **14**, 11997–12007 (2006).

The following refereed conference presentations arose from this thesis:

D. R. Austin, J. A. Bolger, C. M. de Sterke, D.-I. Yeom, T. G. Brown, and B. J. Eggleton, “Narrow-band spectral enhancement of a self-phase modulated pulse,” in “Conference on Lasers and Electro-optics, Baltimore,” (2007).

D. R. Austin, C. M. de Sterke, T. G. Brown, and B. J. Eggleton, “Grating induced spectral enhancement via four-wave mixing,” in “Australian Conference on Optical Fibre Technology/Australian Optical Society, 2006,” (2006), pp. 127–129.

D. R. Austin, C. M. de Sterke, T. G. Brown, and B. J. Eggleton, “The nonlinear wavenumber in supercontinuum generation,” in “Australian Conference on Optical Fibre Technology/Australian Optical Society, 2006,” (2006), pp. 137–137.

# List of acronyms

**DWGR** dispersive wave generation region

**FBG** fibre Bragg grating

**FWHM** full-width at half-maximum

**GNLSE** generalized nonlinear Schrödinger equation

**LPG** long-period grating

**SPM** self-phase modulation

**ZDW** zero-dispersion wavelength

**PCF** photonic crystal fibre

# Contents

<b>Abstract</b>	<b>2</b>
<b>Publications</b>	<b>3</b>
<b>List of acronyms</b>	<b>4</b>
<b>Contents</b>	<b>5</b>
<b>1 Introduction</b>	<b>6</b>
<b>2 Background</b>	<b>9</b>
2.1 Historical development of spectral broadening . . . . .	9
2.2 Photonic crystal fibres . . . . .	11
2.3 Applications of supercontinuum generation . . . . .	12
2.4 The theory of supercontinuum generation by soliton fission . . . . .	13
2.5 Quantitative modelling . . . . .	16
2.6 Tailoring and controlling supercontinuum generation . . . . .	18
2.7 Outline of this thesis . . . . .	20
<b>3 Dynamics of dispersive wave generation</b>	<b>22</b>
3.1 Dispersive wave generation by a fundamental soliton . . . . .	22
3.2 Dispersive wave blue-shift in supercontinuum generation . . . . .	26
<b>4 Spectral enhancement using narrowband spectral filtering</b>	<b>38</b>
4.1 Background and motivation . . . . .	38
4.2 Theory . . . . .	39
4.3 Example . . . . .	40
4.4 Narrowband supercontinuum control using phase shaping . . . . .	42
<b>5 Summary and outlook</b>	<b>52</b>
5.1 Dispersive wave generation . . . . .	52
5.2 Narrowband spectral enhancements . . . . .	53
<b>A Numerical methods</b>	<b>54</b>
<b>B Conservation laws of the nonlinear Schrödinger equation</b>	<b>55</b>
B.1 Energy conservation . . . . .	55
B.2 Conservation of spectral centre of mass . . . . .	56
B.3 Violation of conservation laws due to self-steepening and Raman scattering . . . . .	56
<b>Bibliography</b>	<b>58</b>

# Chapter 1

## Introduction

Supercontinuum generation is the dramatic spectral broadening of laser light. The result is unique in possessing the spectral width of white light and yet the intensity and coherence of a laser. It has been demonstrated in a variety of nonlinear media since its first observation in 1970 [1, 2], and is a powerful demonstration of the breadth of phenomena made possible by the interaction of several basic linear and nonlinear optical processes. The development of convenient laboratory supercontinuum sources [3] has only broadened its plethora of applications, including solution of the long standing optical frequency metrology problem, deemed worthy for one half of the 2005 Physics Nobel Prize. This thesis explores several different aspects of supercontinuum generation with the aim of controlling and enhancing the process. Besides the direct benefit to applications of supercontinuum, our studies bring fresh insight into the generation process itself.

As a nonlinear spectral broadening process, supercontinuum generation comes about through the self-action of an intense optical pulse in a nonlinear transparent material, producing a spectrum which can cover the entire visible range as shown in Fig. 1.1(a). Roughly speaking, the broadening is proportional to the product of the intensity, the nonlinearity, and the interaction length. High intensities can be achieved using amplified lasers, spatial focusing or pulse compression. Certain materials exhibit high nonlinearities, whilst waveguides can offer any desired interaction length. Each of the many techniques for generating supercontinuum is a means of sufficiently increasing one or more of these factors. Among these techniques, the use of femtosecond titanium-sapphire oscillators to pump photonic crystal fibres (PCFs) [4] stands out as a broadband yet shot-to-shot repeatable light source for numerous applications. Furthermore the mechanism in this technique involves a number of interesting nonlinear effects, making it a powerful platform for studying new physics.

Photonic crystal fibres, an example of which is shown in Fig. 1.1(b), possess a complex transverse microstructure which enables novel optical guidance properties that are impractical or impossible in conventional optical fibres. For supercontinuum generation, their key property is their high waveguide dispersion, which cancels out the intrinsic material dispersion of silica in the visible and near infrared. This enables femtosecond pulses from Ti:Sapphire mode-locked lasers to propagate without temporal broadening. As a result of the technological maturation of PCF, along with ultrafast Ti:Sapphire oscillators, supercontinuum sources based on these devices are being deployed rapidly. A typical setup is shown in Fig. 1.1(c). Although the resulting optical fields are usually quite complex, the basic generation process is now generally well understood [5].

Figure 1.2(a) shows a supercontinuum spectrum simulated using typical experimental parameters. A pump pulse of FWHM bandwidth 13 nm is launched into the fundamental mode of a PCF. After 10 cm of propagation, the spectrum has broadened to approximately 1000 nm. This broadband spectrum carries immediate advantages as a source in metrology, imaging, spectroscopy, and interferometry where data is to be obtained at multiple wavelengths. Additionally, the spectral breadth is directly related to the coherence length, which determines the longitudinal resolution of interferometric volume imaging systems based on the Mach-Zehnder interferometer — optical coherence tomography [7] being the prime example. We note that this bandwidth is not entirely unique — comparable bandwidths can be obtained directly from state-of-the-art oscillators. However, a precisely dispersion-controlled cavity with an additional broadening element is necessary [8], so that at present fibre-based broadening systems are often used in preference to octave-spanning oscillators. Other means of achieving such broadening generally rely on the stronger nonlinear effects achievable with amplified pulses [9].

Since the supercontinuum is generated in a single fundamental mode of the PCF, it has an approximately Gaussian profile with near-perfect spatial coherence and may be focused to a diffraction-limited spot, provided

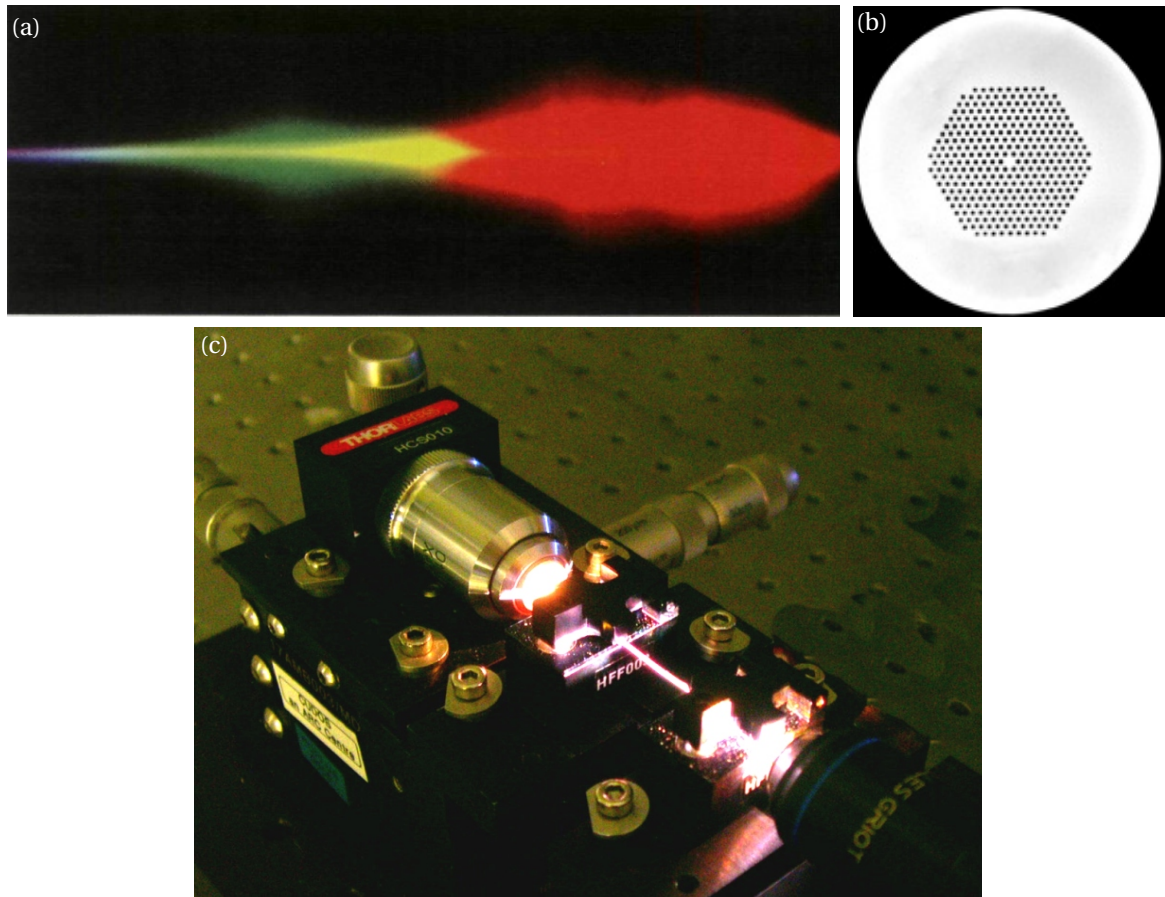


Figure 1.1: (a) Supercontinuum generation by a 100 fs, 625 nm pulse in 1 mm of carbon tetrachloride (taken from ref. [6]); (b) Cross section of a typical PCF — the black circles are air holes running axially through the white surrounding fused silica. (c) A typical setup for supercontinuum generation in a PCF — Ti:Sapphire pulses are coupled into the fibre using a microscope objective and white light generation can occur within several millimetres of propagation.

## 1. INTRODUCTION

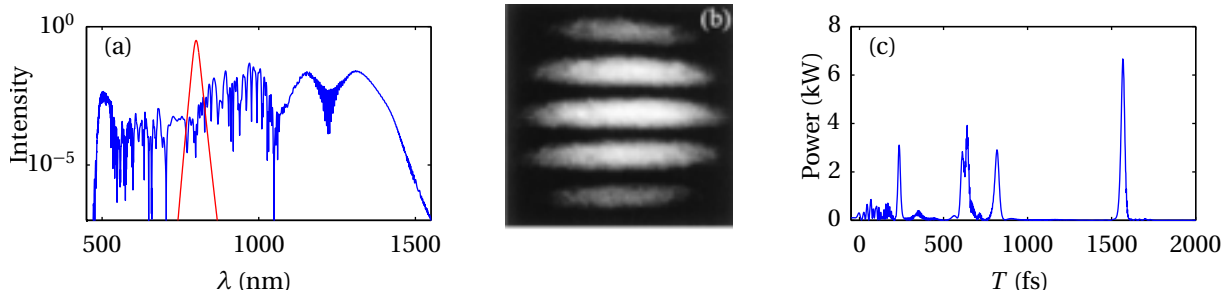


Figure 1.2: (a) Calculated supercontinuum spectrum produced by pumping 10 cm of PCF with a 50 fs pulse at 800 nm with peak power 25 kW. (b) Spatial interference pattern formed between the supercontinuum output of a PCF and a single-mode fibre (taken from ref. [3]). (c) Temporal profile corresponding to the spectrum shown in (a).

chromatic aberrations can be managed. Figure 1.2(b) shows a spatial interference pattern formed between supercontinua from a PCF and the output of a single-mode fibre. The regular high-visibility fringe pattern indicates that only a single spatially coherent mode is present.

Additionally, for pump pulse durations below 100 fs (the regime considered in this thesis), supercontinuum generation is dominated by deterministic processes. Any shot-to-shot variations in the supercontinuum are caused by technical issues such as laser intensity fluctuations. This is a contrast to the inherently stochastic amplification of spontaneous noise underlying the modulational instability, which is a key process when longer pump pulses are used. The shot-to-shot stability of supercontinuum with short pump pulses is essential in several applications including frequency metrology and pulse compression.

The temporal profile corresponding to the spectrum shown in Fig. 1.2(a) is shown in Fig. 1.2(c). The supercontinuum consists of several temporally separated pulses of varying duration and intensity, testament to the fact that supercontinuum generation involves energy transfer and reshaping in the time as well as the frequency domain. A cohesive picture of supercontinuum generation, which accounted for its temporal and spectral properties, emerged in 2002 and is presented in Section 2.4. Notably, the theoretical picture invoked a number of nonlinear wave processes, such as stimulated Raman scattering and dispersive wave generation, which had previously been studied in other contexts. Supercontinuum generation has therefore acted as a novel testbed for nonlinear dynamics, provoking research into exotic phenomena such as rogue wave generation [10] and soliton collisions [11].

The various experimental applications exploit different aspects of the supercontinuum. The key feature in precision frequency metrology, for example, is the octave-spanning spectrum [12], whereas spectroscopists [13] appreciate it as a tunable broadband source. These differing requirements and rapid technological development have prompted timely efforts to tailor supercontinuum for various applications, by varying either the incident laser pulse, the fibre, or both.

One desirable goal would be to extend the supercontinuum spectra further to shorter wavelengths, or to increase the relative intensity at short wavelengths. The difficulty of achieving this motivated the first part of this thesis, a theoretical investigation of blue light production in supercontinuum generation. The conventional theory of supercontinuum attributes blue-shifted radiation to *dispersive wave generation*. Whilst this process is well-understood in isolation [14, 15], we show that in the context of supercontinuum generation, the conventional understanding needs modification to agree with experimental and numerical results.

In the second part of this thesis, we explore a technique to enhance a spectrally narrow region of the supercontinuum spectrum. Theoretically, numerically and experimentally, we show how spectrally narrow phase and amplitude features combine with self-phase modulation to produce spectral enhancements. Besides explaining previously reported experimental observations, this has led to the demonstration of a tunable spectral enhancement technique [16].

This thesis is structured as follows: Chapter 2 provides the necessary background, leading to an outline of the thesis. Chapter 3 presents the investigation of dispersive wave generation, whilst in Chapter 4, spectrally narrow enhancements are studied theoretically and experimentally. Chapter 5 gives a conclusion, summary and outlook.



## Chapter 2

# Background

This thesis presents two major results: a detailed study the dynamics of blue-light generation in femtosecond-pumped supercontinuum generation, and a theory of the mechanism by which narrowband phase features in an ultrashort pulse are converted into spectral intensity modulations by the Kerr nonlinearity. The latter result explains narrowband spectral enhancements observed when supercontinuum generation is carried out in a fibre Bragg grating. This chapter provides the background necessary to motivate and understand these results.

We begin with the historical development of spectral broadening of laser pulses in Section 2.1. This history makes evident the disruptive role played by the invention of photonic crystal fibres, a technology we review in Section 2.3. Several applications of supercontinuum generation are reviewed in Section 2.3, and we focus on those in which blue-light generation and/or narrowband spectral modulation play a significant role. In Section 2.4 we present a qualitative description of femtosecond-pumped supercontinuum generation in photonic crystal fibres. In Section 2.5 we introduce the generalized nonlinear Schrödinger equation (GNLSE) used to model supercontinuum generation. In Section 2.6, we discuss various means of influencing, and to a degree controlling, supercontinuum generation, paying particular attention to the generation of blue-shifted radiation and narrow spectral features. Finally, Section 2.7 outlines the two main results of this thesis.

### 2.1 Historical development of spectral broadening

The generation by Ranka *et al.* [3] of white light spanning 400–1500 nm in a photonic crystal fibre pumped by a nanojoule Ti:Sapphire oscillator, shown in Fig. 2.1(b), sparked a flurry of interest. The unexpected result prompted new theoretical investigations of nonlinear fibre optics as well as finding immediate application in frequency metrology. In this section we examine supercontinuum generation in photonic crystal fibres in the context of nonlinear optics and discuss the reasons for its significance.

The high intensities made possible by the advent of the laser in 1960 enabled direct observation of nonlinear optical effects, in which the anharmonicity of the dielectric response makes a significant contribution to radiation. One of the most important properties of nonlinear optics is the ability to produce light of a different frequency to the applied field, which is not possible in linear optics. This finds wide application in producing laser-like radiation in spectral regions outside the gain bandwidth of any material. Supercontinuum generation is primarily a *spectral broadening* process, in that the new frequencies are adjacent to the existing ones, in contrast to (for example) sum-frequency generation.

Moderate spectral broadening in liquids was reported and interpreted throughout the 1960s [17–20]. In 1970 however, Alfano and Shapiro [2] produced white light by propagating intense picosecond-long pulses through glass. The resulting spectral width was around 300 nm, an order of magnitude greater than in previous experiments, and the new phenomenon was dubbed supercontinuum generation. Visible supercontinua were also demonstrated in noble gases [21] and organic liquids [22] whilst broad coverage of the infrared was produced using dielectrics and semiconductors [23]. An example spectrum is shown in Fig. 2.1(a). Supercontinuum quickly became established as an ultrafast broadband source for use in time-resolved spectroscopy [24]. However, its widespread use was limited by the requirement for amplified lasers with millijoule pulse energies.

To reduce the required intensity and/or achieve greater broadening, it was natural to look to optical fibres as a means of sustaining tight confinement over a long interaction length. Lin and Stolen [25] produced 180 nm wide supercontinua in the visible using microjoule pulses. However, by extending the fibre length the broad-

## 2. BACKGROUND

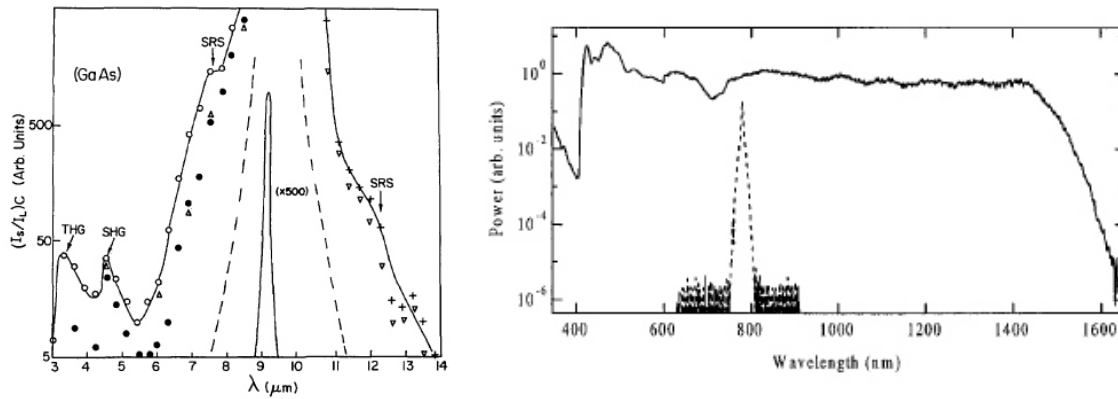


Figure 2.1: (a) Supercontinuum spectrum from a GaAs crystal using 600  $\mu\text{J}$  pulses from a CO<sub>2</sub> laser [23]; (b) Supercontinuum spectrum from a photonic crystal fibre pumped by 8 nJ Ti:Sapphire pulses [3].

ening could not be increased indefinitely, and nor could the required pulse energy be further reduced. Instead the fibre group-velocity dispersion caused temporal spreading of the pulses, reducing their peak intensity and effectively clamping the available nonlinear interaction length.

Hasegawa and Tappert recognized [26] that this need not necessarily be the case. The experiments of Lin and Stolen [25], along with other fibre-based supercontinuum experiments, had used visible light pumping which lay in the *normal dispersion* regime of the fibre, in which red frequencies travel faster than blue frequencies. However, in the *anomalous dispersion* regime, it is possible for the third order nonlinearity, at a certain strength, to effectively cancel the group velocity dispersion, leading to indefinite *fundamental soliton propagation* of pulses without dispersive spreading. Experimental observation of fundamental solitons [27] occurred after the development of ultrashort sources in the anomalous dispersion regime of silica fibres, above 1.3  $\mu\text{m}$ .

Whilst fundamental solitons represent a balance between the third-order nonlinearity and anomalous dispersion, *higher-order solitons* [28] occur when the relative strength of the nonlinearity (the product of the pulse intensity with the intrinsic nonlinearity of the material) over the dispersion is increased beyond this balance. Higher order solitons undergo complex evolution, involving compression and splitting in both the temporal and spectral domains. Experimental [27, 29] and theoretical [30] work established that in the presence of perturbations such as Raman scattering and higher-order dispersion, higher-order solitons initially experience spectral broadening and temporal compression before undergoing *soliton fission*, breaking into a train of constituent fundamental solitons, each of shorter duration than the original pulse. Further experiments at 1.3  $\mu\text{m}$  [31–33] and 1.4  $\mu\text{m}$  [34] demonstrated that soliton fission produces supercontinuum generation. Since the output spectra covered the telecommunications region, these results stimulated research into broadband sources for wavelength division multiplexing [35, 36].

Meanwhile, photonic crystal fibres, which shall be discussed in detail shortly, were being developed. Mogilevstev *et al.* [37] recognized that the anomalous dispersion wavelengths of these fibres could be shifted below 1.3  $\mu\text{m}$ , the intrinsic zero-dispersion wavelength of fused silica, whilst Broderick *et al.* [38] realized that by virtue of their reduced effective mode area compared to standard optical fibres, photonic crystal fibres could possess a higher nonlinearity. After the dramatic demonstration by Ranka *et al.* of octave-spanning white light generation from a photonic crystal fibre with anomalous dispersion above 770 nm pumped by 770 nm light, it was recognized that both these effects were playing a role. However a complete theoretical picture did not emerge until 2002 [5, 39], and invoked essentially the same soliton fission process as in single mode fibre. The importance of the waveguide dispersion and nonlinearity rather than the microstructure itself was demonstrated by tapering a conventional fibre to have dispersive and nonlinear characteristics that were essentially equal to that of a photonic crystal fibre. Using this fibre, Birks *et al.* [40] then generated a comparable supercontinuum using similar pumping conditions to that of a photonic crystal fibre-based experiment. Despite this, the mechanical fragility of such a fibre taper, along with the single-moded guidance property of a photonic crystal fibre, meant that the latter remained the more practical solution.

We can now locate femtosecond pumping of photonic crystal fibres in the anomalous dispersion regime within the broader class of dramatic spectral broadening processes, all described by the term supercontinuum. It is useful to ask which mechanisms act to achieve a sufficiently high product of intensity, interaction length

and material nonlinearity for significant spectral broadening to occur. Several such mechanisms are actually at play: the mode-locked Ti:Sapphire oscillator concentrates the energy into a brief time interval, whilst the tight focusing into the narrow core of the photonic crystal fibre concentrates the light spatially. Higher-order soliton evolution achieves a further temporal compression to yield the ultrabroad supercontinuum spectra. This can be contrasted with the case in bulk media [2], discussed above, where one key ingredient is *self-focusing*, in which the pulse “generates its own focusing lens” via the Kerr effect [41], leading to an explosive increase in peak intensity. Alternatively, self-action is not necessarily required, and supercontinuum can simply be achieved by “brute force” as demonstrated by the experiments pumped in the normal dispersion regime [25].

Much progress since the paper of Ranka *et al.* has focused on pumping using longer pulses of picosecond or nanosecond duration, or even CW sources, mainly driven by the inherent simplicity of such systems. In general, supercontinuum from such sources exhibits lower coherence — which in this context means shot-to-shot repeatability — because the initial spectral broadening is dominated by the *modulational instability* — the Kerr-effect-driven breakup of a smooth intensity envelope into discrete pulses. The corresponding frequency-domain picture is the amplification of spontaneous quantum noise into sidebands that possess a random phase relationship to the pump. The modulational instability is therefore always present; however with femtosecond pumping, particularly below 100 fs, soliton fission dominates the initial dynamics. Seeding the modulational instability using two-color pumping improves the coherence [42, 43]. However, it is fair to say that pumping with pulses shorter than 100 fs is currently the most straightforward way to produce a coherent supercontinuum<sup>1</sup> [4]. This thesis is largely concerned with femtosecond pumping, largely because the modulational instability present with longer pulses produces a huge number of sub-pulses with many interactions, complexifying the physics and generally necessitating a statistical approach. However, the processes studied here — dispersive wave generation and the evolution of short pulses following the application of spectrally narrow features — are also relevant to the picosecond–CW pumping regime.

## 2.2 Photonic crystal fibres

A conventional optical fibre, also known as a step index fibre<sup>2</sup>, guides light by total internal reflection in a core whose refractive index is made slightly higher than the surrounding cladding by the presence of dopants. The small index contrast means that the fibres are *weakly guiding* [45], so that the main contribution to the dispersion comes from the material response of the constituent material, most commonly fused silica, which is normally dispersive at wavelengths below 1.3  $\mu\text{m}$ . Anomalous dispersion in the visible spectrum can be achieved by increasing the contrast — however this could only be accomplished by producing a single strand of silica only a few microns thick, so surrounding air acted as the low-index cladding<sup>3</sup>. Besides their impractical fragility, such fibres tend to be multi-moded, complicating experimental studies of nonlinear propagation.

To circumvent these and other limitations of low-contrast step-index fibres, a transverse microstructure can be introduced into the refractive index profile of the fibre. The design freedom possessed by these *photonic crystal fibres* opens up a wide range of optical and physical properties. As described in Section 2.1 above, for our purposes the relevant qualities are a small mode area and anomalous dispersion around 800 nm. The original and most common design which satisfies these requirement features a solid central core of silica surrounded by an array of air holes running along the length. This combination of air holes and silica acts like the cladding of a conventional fibre, guiding the light down the core by total internal reflection [46]. However, because the area of the air holes relative to the surrounding silica — the *air-fill fraction* — can be made quite large without losing mechanical robustness or single-modedness, the effective refractive index of the cladding can be very close to unity. The result is essentially a high contrast, low loss, mechanically robust single-mode fibre, an impossible feat using a standard stepped-index design.

The discovery that ultrabroadband spectra could be produced from such fibres by Ti:Sapphire pumping was timely, because in 2000 these lasers were becoming commonplace in ultrafast laboratories. Many applications for these supercontinuum sources were quickly discovered, including several with relevance to the results in this thesis. These are the topic of the next section.

<sup>1</sup> Even with sub-100 fs pump pulses, there is degradation of shot-to-shot repeatability with propagation, but since this occurs after the majority of the spectral broadening it can be alleviated by using appropriate fibre lengths — typically a few centimetres.

<sup>2</sup> More elaborate designs exist [44], but the points made in this discussion about stepped index fibres are valid for them also.

<sup>3</sup> Increasing the core index through higher dopant concentrations causes unacceptable loss.

## 2.3 Applications of supercontinuum generation

### 2.3.1 Metrology

Supercontinuum generation in photonic crystal fibres made an immediate impact in optical frequency metrology. The precise synthesis and determination of optical frequencies is desirable for precision spectroscopic tests of fundamental theories because of the low fractional linewidths of resonances in the optical domain. However, the 9.193 GHz cesium hyperfine transition which defines the SI primary standard is some  $5 \times 10^4$  times smaller and establishing a connection between these two domains represented a serious challenge. The first solutions consisted of long chains of phase-coherent oscillators [47] which were as costly as they were complex. For example, the chain described by Schnatz *et al.* [47] consists of ten oscillators connected together by frequency multiplying electronics.

Hänsch and coworkers made a major advance using the concept of the frequency comb, the frequency domain description of the pulse train provided by a mode-locked laser. Fourier theory shows that the spectrum of a periodic pulse train consists of a comb of discrete frequencies separated by the repetition rate. In reality, fluctuations in the repetition rate will of course distort this, but Udem *et al.* showed that in normal Ti:Sapphire oscillators, the comb spacing is constant to 3 parts in  $10^{17}$  [48]. In addition, the repetition rate can be locked to an external source [49], so that the comb spacing is traceable to the cesium standard. The difference between any two frequencies can then be measured by using the comb as a “ruler” [50, 51].

However, the pulse train emitted by a mode-locked laser is not strictly periodic, even when the repetition rate is stabilized. Instead, the pulse accumulates a phase slip during each traversal of the cavity, caused by the difference between the net phase and group delays. In the frequency domain, this manifests as an offset  $\delta$ , so that  $n^{\text{th}}$  frequency of the comb is  $f_n = n\Delta + \delta$ . Prior to 2000, the only way of referring the absolute comb frequencies to the cesium standard was through a long chain of phase-locked oscillators. Supercontinuum generation changed this by enabling  $f$ - $2f$  interferometry, which requires an octave-spanning spectrum. There are several forms of this technique. In one [12], the fundamental and the second harmonic of a stabilized reference laser are mixed with the octave-spanning frequency comb and the radio-frequency beat tone is measured. Another approach is to frequency double the long-wavelength end of the comb and mix it with the short-wavelength end, measuring the radio frequency beat tone [52]. Either way, the phase slip frequency  $\delta$  is measured to high accuracy. Furthermore, the offset can be stabilized and set to zero using closed loop control [53]. This means that the electric fields of each pulse are identical, and this has opened up the study of extreme nonlinear processes such as high-harmonic generation which directly depend on the electric field, rather than just the intensity envelope. Although commercial oscillators are now available which produce octave-spanning spectra, most *carrier-envelope phase stabilization* devices, including some commercial ones<sup>4</sup> employ supercontinuum generation in photonic crystal fibre to generate a sufficiently broad spectrum for  $f$ - $2f$  interferometry.

In Chapter 4, we describe a technique for producing a spectrally narrow enhancement to the supercontinuum spectrum. The in-principle benefit to  $f$ - $2f$  interferometry is clear; the signal to noise ratio of the radio-frequency beat tone is proportional to the product of the spectral amplitudes of the fields which are being heterodyned [54].

### 2.3.2 Interferometry and ultrafast spectroscopy

Supercontinuum has been employed as an experimental source since its discovery in bulk media [55, 56]. As a bright, broadband and spatially coherent field, it is particularly useful for interferometry and spectroscopy. For example, dispersion measurements using a Michelson interferometer [57, 58] have a long free-space reference arm and therefore require a well-collimated source, an ideal role for supercontinuum sources. The development of convenient supercontinuum sources, first in conventional fibre [25] and then in photonic crystal fibres, has increased its utility.

Photonic crystal fibres pumped by Ti:Sapphire oscillators are widely used as a probe for ultrafast pump-probe spectroscopy experiments [13]. The multi-MHz ultrabroadband pulse trains coming directly from an oscillator are beneficial from the perspective of acquisition time and signal to noise ratio. Supercontinuum pulses may be shorter than the pump pulse which created them, so there is no loss of temporal resolution when using them as a probe.

---

<sup>4</sup><http://www.menlosystems.com/xps800.html>

Since the time resolution of these experiments depends on the probe length, it is important to understand the generation dynamics so that supercontinuum duration is as short as possible without compromising the overall bandwidth. Indeed, recent studies have deliberately used short lengths of fibre to produce short supercontinuum probe pulses [59]. This is one motivation for our investigation into the dynamics of *dispersive wave generation*, which produces the short wavelengths in the supercontinuum and is described in Chapter 3. Furthermore, the scheme to increase the local spectral intensity discussed in Chapter 4 can potentially benefit these experimental applications.

### 2.3.3 Microscopy and imaging

Supercontinuum from microstructured fibres has been used as an illumination source for a variety of imaging techniques.

Optical coherence tomography [60] is a non-invasive imaging technique for taking cross sectional images of biological samples on a micrometer scale. In optical coherence tomography, one arm of a Michelson interferometer is reflected from a reference mirror, whilst the other backscatters off the sample under observation. Interference patterns are observed in the recombined beam, thus measuring the amplitude of the light which is reflected from the sample. Transverse resolution is obtained by focusing the beam to a small spot which is raster scanned across the sample, whilst longitudinal resolution is obtained because the light source has low longitudinal spatial coherence due to its broad bandwidth. Only a narrow plane of the sample is at the correct distance to produce fringes. By scanning the sample axially and transversely, an image is obtained. Optical coherence tomography using a supercontinuum source [7] offers unprecedented brightness and resolution and was used in 2002 [61] to obtain submicron axial resolution over a 325 nm spectrum centred at 725 nm.

In confocal laser scanning fluorescence microscopy [62], supercontinuum generation has been used to adapt a Ti:Sapphire oscillator, used for multiphoton excitation, to shorter wavelengths suitable for single-photon excitation. Supercontinuum from photonic crystal fibres is also of sufficient intensity for two-photon microscopy, providing spectral access to previously inaccessible fluorophores [63]. Another application is coherent anti-Stokes Raman scattering microscopy in which the sample is illuminated with two wavelengths separated by the Raman vibration frequency. For example, supercontinuum generation was used to produce blue-shifted radiation at 643 nm, exactly one Stokes shift above the pump at 795 nm, in order to produce high-contrast images of polystyrene beads [64]. In all cases, dispersive wave generation, considered in Chapter 3, is critical in producing the shorter wavelengths.

Having located supercontinuum generation within the context of ultrafast optics and pointed out some of its important applications, we now present the current understanding of the process.

## 2.4 The theory of supercontinuum generation by soliton fission

It took several years from the discovery of Ranka *et al.* for a cohesive picture of supercontinuum generation using femtosecond pulses to emerge. Notably, much insight was gained from numerical models which brought together a number of physical processes that were previously well understood, at least in isolation. The novelty of photonic crystal fibres was the new parameter range that was accessible, with a self-focusing nonlinearity of comparable strength to linear dispersion on the femtosecond time-scale.

As a pedagogical tool, we shall consider a numerical simulation using typical experimental parameters of supercontinuum generation in a photonic crystal fibre pumped by a Ti:Sapphire oscillator. Presentation of the detailed mathematical model is deferred until later — we shall first present the basic physical principles and describe the role they play in supercontinuum generation. Figure 2.3 shows the evolution of the supercontinuum in the time and frequency domains. The initial pulse has a transform-limited hyperbolic-secant-squared profile with full-width at half-maximum (FWHM) intensity  $T_{\text{FWHM}} = 50$  fs, centre wavelength 800 nm and peak power  $P_0 = 2.5$  kW. The fibre is 400 mm long and its parameters are based on commercially available Crystal Fibre NL-2.0-770, depicted in cross section in Fig. 2.2(a). The hole diameter is  $0.93 \mu\text{m}$  and the hole spacing is  $1.31 \mu\text{m}$ . The fibre's dispersion relation, expressed in terms of the second derivative  $\beta_2$  of the longitudinal wavenumber, is shown in Fig. 2.2(b). The nonlinear coefficient, defined as the constant of proportionality between the pulse power and the nonlinear contribution to the phase delay per unit length, is  $\gamma = 0.09 \text{W}^{-1} \text{m}^{-1}$ .

As is clear from Fig. 2.3, the evolution is quite complex, with the appearance of several distinct spectral and temporal features accompanying the main spectral broadening from 0–40 nm. Conceptually, the evolution

## 2. BACKGROUND

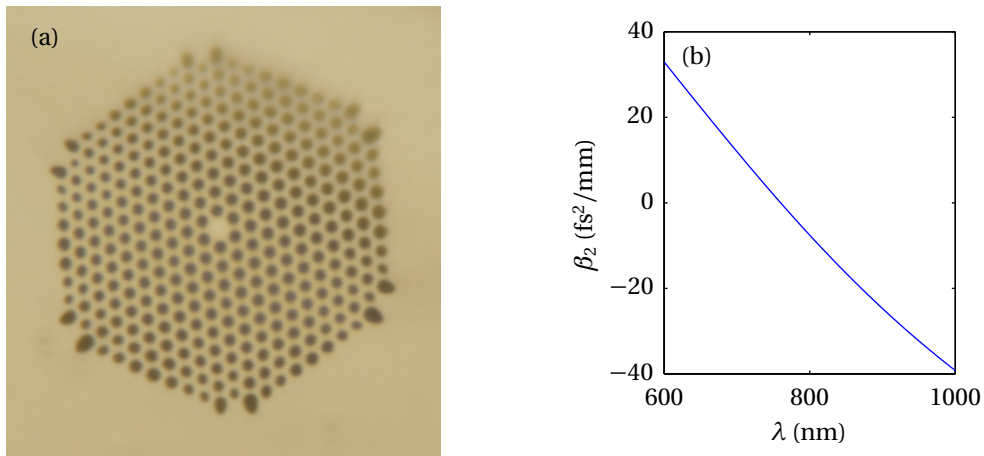


Figure 2.2: (a) Cross section of photonic crystal fibre NL-2.0-770, modelled in several examples throughout this thesis. The dark areas are air holes; the light area is silica. (b) Dispersion of NL-2.0-770.

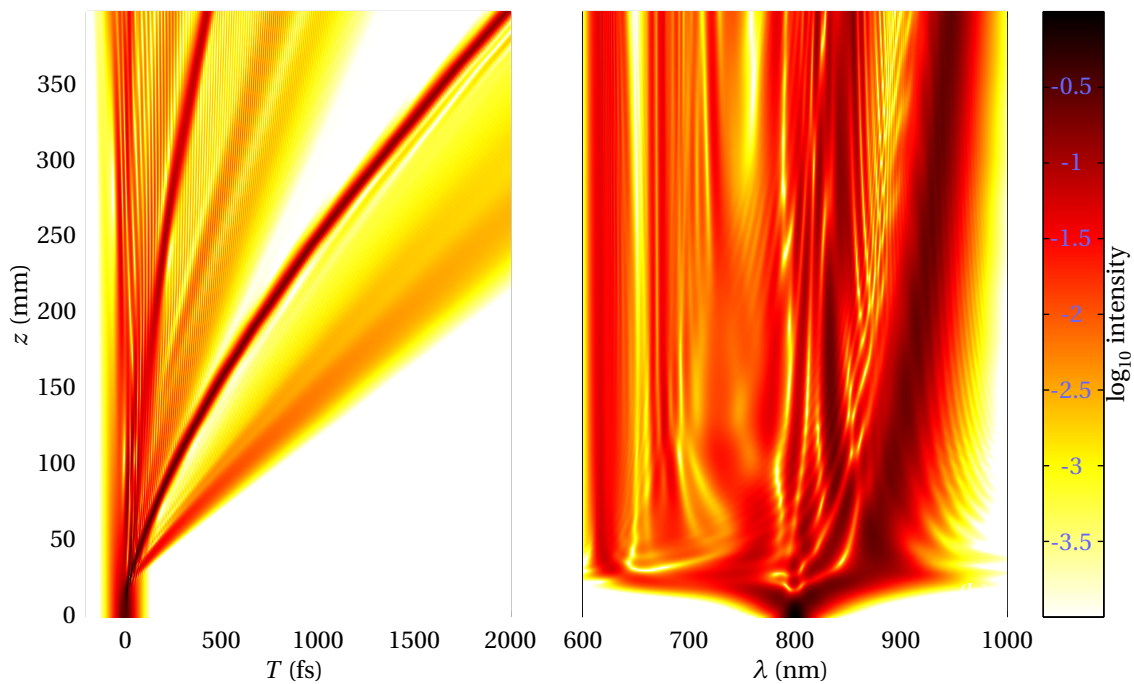


Figure 2.3: Supercontinuum generation by pumping 400 mm of photonic crystal fibre with a pulse of 50 fs FWHM intensity duration, 800 nm centre wavelength and 2.5 kW peak power, corresponding to a fifth-order soliton.

can be divided into three regions. From 0–20 mm, the pulse undergoes near-symmetrical spectral broadening about its centre wavelength, accompanied by temporal compression. From 20–40 mm, the pulse breaks apart into several sub-pulses of different wavelengths. This stage is characterized by the development of a highly modulated spectrum. After 40 mm, the pulses begin to drift away from one another through group-velocity dispersion whilst spectral evolution is more gradual, characterized by a red-shift of the feature at 900 nm. Although dispersion and the third-order nonlinearity are the underlying effects in all three regions, each is amenable to a higher level of interpretation which shall now be presented. Because the discussion involves dynamics in both the time- and frequency-domains, the spectrogram, or short-time Fourier transform, is extensively used to visualize the field. The spectrogram is most conveniently presented as an animation. The accompanying file [SC\\_spectrogram.avi](#) shows the spectrogram of the evolution in Fig. 2.3.

From 0–20 mm, the pulse undergoes symmetric spectral broadening due to self-phase modulation (SPM) [65, 66]. Self-phase modulation is a manifestation of the Kerr effect, the near-instantaneous non-resonant third-order electronic response. The Kerr effect produces an intensity-dependent refractive index, resulting in a decreased phase velocity near the peak of the pulse. On the leading edge of the pulse, the field oscillations are therefore “stretched” leading to a decrease in instantaneous frequency, whilst the opposite occurs on the trailing edge. In the frequency domain, this is seen as symmetric spectral broadening about the centre frequency. These effects are evident in the spectrogram animation at  $z = 15.2$  mm, also reproduced in Fig. 2.4(a).

By 20 mm, the pulse has clearly undergone some temporal compression and has as a result become more intense. This is *soliton effect compression* [67, 68] — anomalous dispersion causes the newly generated frequencies on the leading and trailing edges to be fed back into the centre of the pulse. The rising peak intensity leads to a runaway process accompanied by a sudden increase in bandwidth. At  $z = 28$  mm, the peak power has more than tripled to 8.1 kW, and the bandwidth now extends from 600–950 nm. Given that the further spectral broadening is clearly rather marginal, it may seem prudent to end the fibre at this position and thus produce a broadband single pulse. However, the precise location of this “point of maximum compression” depends on the pump power and fibre parameters and is generally hard to predict. Furthermore, short fibre lengths are often impractical. Therefore, in many experiments the pulse breaks up and develops a highly modulated spectral and temporal profile, as seen for  $z > 50$  mm in Fig. 2.3.

At this point, considerable insight comes from the mathematics of soliton dynamics [69, 70]. Solitons are pulses in which dispersive and nonlinear effects combine to either maintain the pulse profile under propagation or cause it to evolve in a periodic fashion. They arise in a variety of contexts ranging from water waves [71] to Bose-Einstein condensates [72]. An optical soliton represents a balance between SPM and quadratic dispersion. For ordinary materials,  $\chi^{(3)} > 0$  which means that soliton formation requires anomalous dispersion. *Fundamental solitons* represent a balance of the influences of dispersion and nonlinearity, which exactly cancel so that the pulse does not change with propagation [73]. *Higher-order solitons* result when the nonlinearity exceeds the dispersion, and exhibit complex periodic evolution. Mathematically, the soliton order  $N$  is defined as

$$N^2 = \frac{T_0^2 \gamma P_0}{|\beta_2|} \quad (2.1)$$

with fundamental solitons having  $N = 1$ . Here, the pulse duration  $T_0 = 0.567 T_{\text{FWHM}}$  is defined in terms of a hyperbolic secant amplitude profile proportional to  $\text{sech}(T/T_0)$ .

A crucial difference between fundamental and higher-order solitons is that fundamental solitons tend to be robust to higher-order dispersion and higher-order nonlinear effects beyond SPM. However, higher-order solitons are perturbed by these effects, and their periodic evolution is quickly interrupted by *soliton fission* into fundamental solitons, each with shorter duration than the original [28, 30, 74].

In this context, the rapid temporal compression and accompanying spectral broadening, seen in the first 20 mm of propagation in Fig. 2.3, is the first stage of higher-order soliton evolution, which is interrupted at 25 mm by soliton fission caused by higher-order dispersive and nonlinear effects. At the point of soliton fission, energy is spread from 600–950 nm, crossing the zero-dispersion wavelength. Above the zero-dispersion wavelength, where the dispersion is anomalous, fundamental soliton formation is possible and we shall see that this occurs, consistent with the theory of soliton fission. However, below the zero-dispersion wavelength, soliton formation is impossible and instead the radiation is concentrated into linear *dispersive waves* which disperse upon further propagation. The details of dispersive wave generation by the pump pulse is one of the topics of this thesis and shall be discussed in detail in Chapter 3. For the time being, we note that in the literature, dispersive wave emission by a fundamental soliton [14, 75, 76] is usually cited as the relevant mechanism. The emitted wavelengths are determined by a phase-matching condition between the phase of the soliton and the linear dispersion relation of the fibre. This resonance always occurs on the opposite side the zero-dispersion

## 2. BACKGROUND

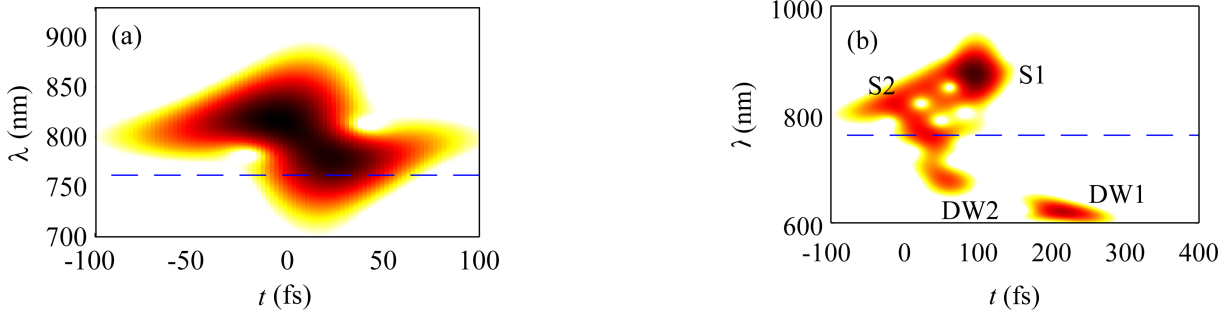


Figure 2.4: Spectrogram at (a)  $z = 15.2$  mm and (b)  $z = 50$  mm. The blue dashed lines show the zero-dispersion wavelength.

wavelength, and is the principal mechanism for efficient conversion to the blue side of the pump in supercontinuum generation. Additional broadening may be caused by cross-phase modulation of the dispersive waves by the solitons [77] or four-wave mixing between the solitons and the dispersive waves [78, 79].

In the spectrogram at  $z = 50$  mm, reproduced in Fig. 2.4(b), the main fission products can be identified. The feature labelled S1 is the most intense of the fundamental solitons, whilst the other solitons, labelled S2, have not separated fully but can be traced in the animation. Dispersive wave packets, labelled DW1 and DW2, are also evident. From this point onwards, the only significant spectral evolution comes from red-shifting of the fundamental solitons. This *soliton self-frequency shift* [80], originates from non-resonant stimulated Raman scattering [81, 82]. The solitons are sufficiently broadband to span the Raman gain bandwidth of silica [66, 83], so that longer wavelengths in the pulse act as Stokes waves for the shorter wavelengths producing a continuous transfer of energy to the red.

This completes the qualitative description of supercontinuum generation. We now introduce the standard mathematical treatment, used for the numerical calculations in this thesis.

## 2.5 Quantitative modelling

The most general approach to optical propagation is Maxwell's equations [5], but for numerical efficiency scalar envelope approaches [30, 84, 85] are used almost universally. The common feature of these approaches is that the resulting equation contains only the first derivative in the propagation direction, potentially limiting its validity for few-cycle or ultra-broadband pulses. However, Brabec and Krausz [86] showed that the envelope concept, and the corresponding first-order propagation equation, are valid down the single-cycle regime. Another common assumption, used here, is that of weak guidance, under which the waveguide is nearly homogeneous and, equivalently, the fields have negligible longitudinal components. This leads to a scalar Helmholtz equation. After incorporation of the linear and nonlinear behavior pertinent for optical fibres, this equation is known as the GNLSE [84]. It has proven quantitatively accurate against experiments and has become the de facto standard [4]. It should be mentioned that since photonic crystal fibres clearly lack transverse homogeneity, the conditions for weak guidance would appear to be violated. Indeed, newly emerging fibres, with subwavelength cores or in which the inhomogeneity plays a greater role, have motivated forms of the GNLSE in which the full vectorial character of the fields is included [87, 88]. However, for the index-guiding fibres considered in this thesis, the strong confinement of the fundamental mode in the homogeneous silica core, which is several times larger than the wavelength, means that weak guidance is sufficiently valid.

In this work, only a single linear polarization is considered. Although manufacturing imperfections do lead to a randomly varying birefringence in typical photonic crystal fibres, it is usually possible to identify principal polarization axes which preserve the polarization over the lengths of fibre under consideration here. Alternatively, one can use polarization maintaining fibres with a deliberately large birefringence. In any case, we assume light is launched into a single polarization mode and remains so throughout the propagation.

The GNLSE is then [4]

$$\frac{\partial A(T, z)}{\partial z} - \sum_{k \geq 2} \frac{i^{k+1}}{k!} \beta_k \frac{\partial^k A}{\partial T^k} + \sum_{k \geq 0} \frac{i^k \alpha_k}{2k!} \frac{\partial^k A}{\partial T^k} = i\gamma_0 \left[ 1 + i\tau_{\text{shock}} \frac{\partial}{\partial T} \right] \left[ A(z, T) \int_{-\infty}^{+\infty} R(T') |A(z, T - T')|^2 dT' \right] \quad (2.2)$$



where  $z$  is distance along the fibre,  $T = t - \beta_1 z$  is time in the comoving frame moving at the group velocity  $\beta_1^{-1}$ ,  $A(T, z)$  is the complex baseband envelope, the  $\alpha_k$ s and  $\beta_k$ s are the Taylor series expansion of the loss  $\alpha(\omega)$  and propagation constant  $\beta(\omega)$  about a central carrier  $\omega_0$ , so that

$$\alpha(\omega) = \alpha_0 + \alpha_1(\omega - \omega_0) + \frac{\alpha_2}{2}(\omega - \omega_0)^2 + \dots \quad (2.3)$$

$$\beta(\omega) = \beta_0 + \beta_1(\omega - \omega_0) + \frac{\beta_2}{2}(\omega - \omega_0)^2 + \dots \quad (2.4)$$

The choice of a comoving frame means that a pulse at the centre frequency remains approximately fixed at constant  $T$ , whilst other frequencies drift away slowly due to group velocity dispersion. The electric field and baseband envelopes are related by

$$E(x, y, z, \omega) = F(x, y, \omega)A(\omega - \omega_0, z) \exp [i\beta_0 z + i\beta_1(\omega - \omega_0)z] + \text{c.c.} \quad (2.5)$$

where  $F(x, y, \omega)$  is scaled so that  $|A(T, z)|^2$  gives the instantaneous power in Watts. The terms on the right-hand side of (2.2) model nonlinear effects, all of which are proportional to

$$\gamma_0 = \frac{\omega_0 n_2(\omega_0)}{c A_{\text{eff}}(\omega_0)} \quad (2.6)$$

where  $n_2(\omega_0)$  is the nonlinear refractive index and  $A_{\text{eff}}(\omega_0)$  the nonlinear effective area defined by [66]

$$A_{\text{eff}}(\omega) = \frac{\left[ \int \int_{-\infty}^{+\infty} |F(x, y, \omega)|^2 dx dy \right]^2}{\int \int_{-\infty}^{+\infty} |F(x, y, \omega)|^4 dx dy}. \quad (2.7)$$

The time derivative in the nonlinear term, proportional to  $\tau_{\text{shock}}$ , models the dispersion of the nonlinearity, associated with self-steepening and shock formation of the pulse trailing edge. The nonlinear response function

$$R(t) = (1 - f_R)\delta(t) + f_R h_R(t). \quad (2.8)$$

includes both the instantaneous electronic contribution, which leads to the Kerr nonlinearity, and the delayed Raman scattering term proportional to  $f_R = 0.18$ , producing the pulse self-frequency shift. In this work we use the Raman gain spectrum  $h_R(t)$  presented by Blow and Wood [84].

Equation (2.2) can be recast in the frequency domain, making the frequency dependence of the various terms more transparent:

$$\frac{\partial A(\omega', z)}{\partial z} = L(\omega)A(\omega', z) + N(\omega', z) \quad (2.9)$$

where  $\omega' = \omega - \omega_0$ , and

$$L(\omega) = [i\beta'(\omega) - \alpha(\omega)/2], \quad (2.10)$$

is the linear operator containing the effects of dispersion and loss. Here,

$$\beta'(\omega) = \frac{\beta_2}{2}(\omega - \omega_0)^2 + \frac{\beta_3}{6}(\omega - \omega_0)^3 + \dots \quad (2.11)$$

is the transformed propagation constant with the effects of phase and group velocity removed and can be thought of as the physical dispersion curve  $\beta(\omega)$  with the tangent at  $\omega_0$  subtracted out. This picture becomes useful in interpreting the physics described in later chapters. The nonlinear source term is

$$N(\omega', z) = i\gamma(\omega) \int d\omega'_1 \int d\omega'_2 A(\omega'_1, z) A(\omega'_2, z) A^*(\omega'_1 + \omega'_2 - \omega') R(\omega' - \omega'_1) \quad (2.12)$$

where the nonlinear coefficient has a linear frequency dependence

$$\gamma(\omega) = \gamma_0 [1 + (\omega - \omega_0)\tau_{\text{shock}}]. \quad (2.13)$$

Finally, the frequency domain form of the nonlinear term makes explicit its interpretation as an integral over all possible four-wave mixing processes of the form

$$\omega_1 + \omega_2 \rightarrow (\omega_1 + \omega_2 - \omega) + \omega. \quad (2.14)$$

We wrote a numerical code to solve the GNLSE, the details of which are presented in Appendix A.

The next section introduces the topic of tailoring supercontinuum generation to suit particular purposes.

## 2.6 Tailoring and controlling supercontinuum generation

The development of the soliton interpretation of supercontinuum generation and the GNLSE gave insight into various methods to control supercontinuum generation towards both specific applications and greater understanding. Some of these methods are a simple variation of the parameters, such as the pump wavelength, whilst others involve modifying the fibre. In this thesis, we are concerned with efforts to extend the short-wavelength edge of the spectrum and to enhance certain narrow spectral regions. This section therefore reviews various means of controlling supercontinuum generation, concentrating on their ability to control the short wavelengths and to enhance certain spectral regions.

### 2.6.1 Varying the pump wavelength

Figure 2.5 shows calculated supercontinua for several different pump wavelengths under otherwise identical conditions. Several trends can be observed, all attributable to the different dispersion experienced by the pump as the wavelength changes. Pumping at 600 nm, well below the zero-dispersion wavelength (ZDW), results in only moderate spectral broadening, caused by some initial self-phase modulation which is quickly quenched by temporal pulse broadening which reduces the intensity to below the threshold for any nonlinearities. As the pump wavelength approaches the ZDW (650 nm and 700 nm), the self-phase modulation causes spectral broadening across the ZDW and into the anomalous dispersion regime. This causes a reduction in the dispersion-induced temporal broadening for these wavelengths, and hence asymmetric spectral broadening. The rapid temporal oscillations on the leading edge of the pulse are characteristic of propagation near the ZDW [89]. As the pump moves above the ZDW, soliton fission begins to play the dominant role, with several discrete solitons becoming evident in the temporal profile. The most intense of these solitons forms the smooth long-wavelength peak in the spectrum, which is red-shifted with respect to the pump by both spectral recoil, caused by dispersive wave emission, and stimulated Raman scattering. Both of these effects weaken with increasing pump wavelength, so that the long-wavelength edge of the spectrum does not change significantly between the 900 nm and 950 nm pump cases.

For anomalous dispersion pumping, the short-wavelength edge shifts to the blue with increasing pump wavelength in an approximately symmetric fashion. This is due to the phase matching conditions for dispersive wave generation. However, the energy content transferred across the ZDW also decreases with increasing pump wavelength because the spectral intensity of the pump at the resonant wavelength decreases. Ultimately, the pump wavelength is limited by fibre loss which becomes significant around 1400 nm.

### 2.6.2 Varying the pump power

Figure 2.6 shows calculated supercontinuum spectra and temporal profiles for a range of pump powers, under conditions that are otherwise identical to Fig. 2.3. The spectrum broadens to both longer and shorter wavelengths with increasing power. The highest shown pump power, 25 kW, corresponds to a launched average power of 112 mW from an 80 MHz oscillator. This approaches the maximum power used in experiments, where the launched power is typically limited by coupling efficiencies of approximately 40%. Accompanying the increased spectral broadening, increasing the input power results in the emergence of a greater number of discrete solitons, spread over a greater temporal extent. This is partly a consequence of the higher soliton order of the pump, as predicted by (2.1), and also a reduction of the soliton fission distance [4].

A major topic of this thesis is the energy and wavelength of the blue-shifted dispersive radiation. Figure 2.6 illustrates that to a certain extent, the dispersive radiation can be pushed to shorter wavelengths simply by increasing the input power. This trend is predicted by the phase matching condition mentioned in Section 2.4, which models the process as dispersive wave emission by a fundamental soliton. However, as we show in Chapter 3, straightforward application of the standard theory considerably underestimates the blue-shift of the dispersive radiation with increasing pump power. An improved picture of dispersive wave generation in supercontinuum which more accurately describes this blue-shift is one of the major results of this thesis.

### 2.6.3 Pulse shaping

Several methods for ultrafast optical *pulse shaping* [90] are now well established. Generally speaking, pulse shapers apply a programmable phase and/or amplitude mask in either the spatial, temporal, or spectral domains. Several classes of pulse shapers have been developed, including direct space-to-time shapers [91],

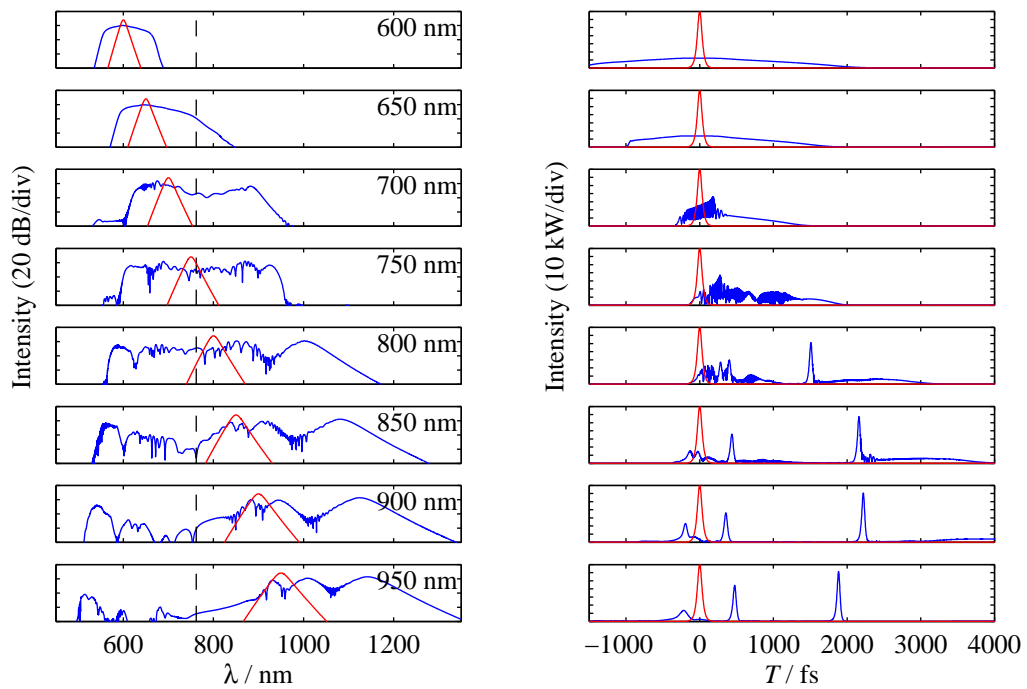


Figure 2.5: Calculated supercontinuum spectra and temporal profiles in 20 cm of Crystal Fibre NL-2.0-770 for various pump wavelengths with pump peak power 5 kW and duration 50 fs (blue). The ZDW is indicated by the black dashed line and the pump pulse is shown in red.

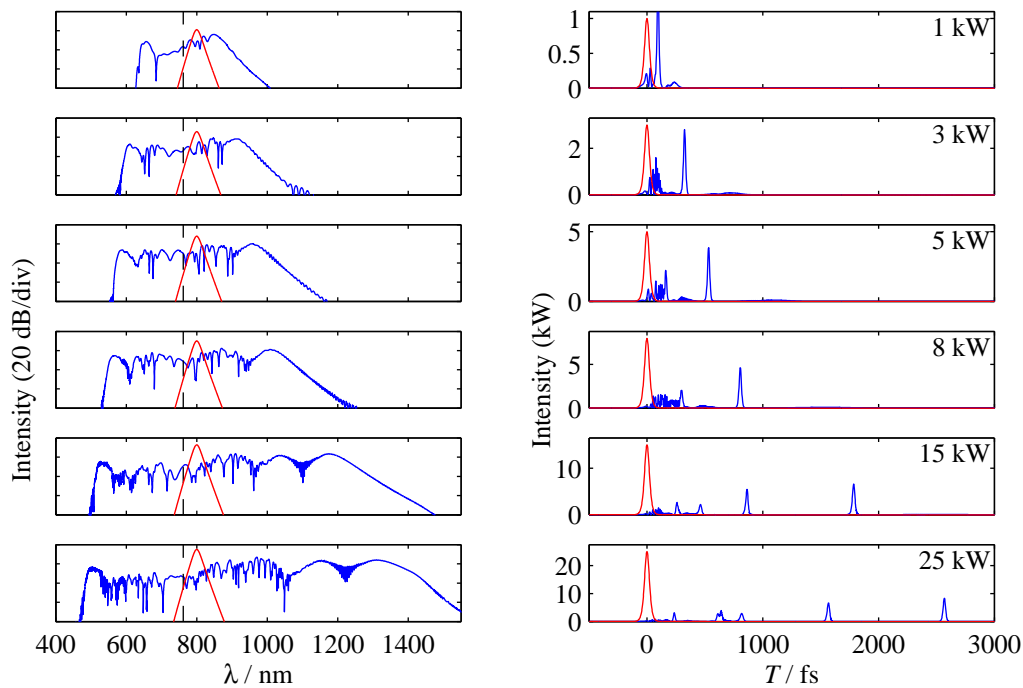


Figure 2.6: Calculated supercontinuum spectra and temporal profiles in 10 cm of Crystal Fibre NL-2.0-770 for various pump powers with pump wavelength 800 nm and duration 50 fs (blue). The ZDW is indicated by the black dashed line and the pump pulse is shown in red.

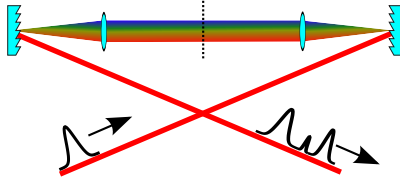


Figure 2.7: A  $4-f$  pulse shaper; the input pulse (lower left), diffraction gratings  $G_1$  and  $G_2$ , and lenses  $L_1$  and  $L_2$  with focal length  $f$ .

acousto-optic programmable dispersive filters [92], and  $4-f$  pulse shapers [93], which we use in this thesis. The operating principle is illustrated in Fig. 2.7. The input pulse is angularly dispersed by diffraction grating  $G_1$ . Lens  $L_1$ , placed one focal length  $f$  away from the grating, produces a spatial Fourier transform of the angularly dispersed beam in the Fourier plane (FP). The transmission amplitude and phase of a spatially varying mask placed in the Fourier plane are mapped directly into the frequency domain. A second lens  $L_2$  and grating  $G_2$  recombine the wavelengths and recollimate the beam, a process which can readily be understood by noting that the device is symmetric about the Fourier plane.

The most direct application of pulse shaping to supercontinuum generation is the temporal compression of the resulting fields through spectral phase compensation [94]. The octave-spanning spectra which are routinely available render this an attractive method of accessing the few-cycle pulse regime, albeit for nanojoule pulse energies. Alternatively, the pump pulse can be shaped, providing a limited degree of control over the dynamics of the supercontinuum generation. A simple adjustment of the pump chirp can optimize the soliton fission and also alter its location in the fibre [95], whilst more complex phase manipulations can influence self-steepening and the soliton self-frequency shift or produce a shorter output [96–98]. In Chapter 4 of this thesis, we adopt a different approach and apply spectrally narrow phase modulations to the pump. These produce local enhancements of the spectral intensity of the supercontinuum.

### 2.6.4 Grating inscription

The production of narrow spectral enhancements in the supercontinuum is desirable for the frequency locking schemes discussed in Section 2.3.1. Such enhancements have been achieved by carrying out the supercontinuum generation in a *fibre grating* — a periodic modulation of refractive index profile of the fibre. Each period of the modulation acts as a weak scatterer, coupling a small fraction of the light between the modes of the fibre. Significant energy transfer between two modes can occur if the grating periodicity matches their longitudinal wavenumber difference. The refractive index modulations can be introduced using ultraviolet inscription [16,99], microbends created by an radio-frequency driven flexural acoustic wave [100,101], or stresses induced by pressure from a grooved plate [102].

One major class of fibre gratings, particularly relevant to this thesis, are fibre Bragg gratings. These resonantly couple forward- and backward-propagating modes at the Bragg wavelength  $\lambda_B$ , determined by the relationship  $\lambda_B = 2n_{\text{eff}}\Lambda$  where  $n_{\text{eff}}$  is the effective refractive index of the fibre and  $\Lambda$  the grating period. Around the Bragg wavelength, fibre Bragg gratings exhibit a *photonic band gap*, in which the propagation is strongly attenuated. Outside of the bandgap, fibre Bragg gratings exhibit strong dispersion which has been used in dispersion-compensation devices [103]. However, in supercontinuum generation the pulses under consideration have considerably greater bandwidth than the bandgap, which is typically a few nanometres. On this scale, the grating acts as a spectrally local phase and amplitude modulation. The first studies of supercontinuum generation in a fibre Bragg grating showed that this modulation resulted in an approximately tenfold enhancement of the local spectral intensity [104]. Subsequently, this enhancement was used to improve the stability of a frequency comb [54]. One of the results of this thesis, presented in Chapter 4 is an improved understanding of the mechanism for this enhancement.

## 2.7 Outline of this thesis

We are now in a position to introduce the major results of this thesis.

### 2.7.1 Blue light generation

As described in Section 2.4, the primary mechanism for the generation of energy at wavelengths shorter than the pump is dispersive wave generation — the perturbation of solitons by cubic- and higher-order dispersion. This blue light greatly contributes to the scientific and technological significance of supercontinuum generation — many of the applications described in Section 2.3 rely on the dispersive waves. Its importance is heightened by the fact that technologies for the generation of tuneable radiation below 700 nm are limited. With few choices of optical gain media, other options are frequency-multiplication of longer wavelength sources or four-wave mixing, which may have limited tuneability and bandwidth and can require amplified laser systems which generally involve significant additional complexity and a reduction of the repetition rate. We were therefore motivated to study of the dispersive wave generation process in more detail with a view to understanding its limitations and possibly identifying parameter choices in which it would be optimized.

Besides this practical goal of improving visible light generation, we were interested in resolving an apparent inconsistency in the accepted picture of femtosecond-pumped supercontinuum generation. Specifically, although this theory attributed the wavelengths shorter than the pump to dispersive wave generation, previous studies of this process had only considered radiation shed by fundamental solitons [14, 15]. However, our simulations showed that in many cases, by the point in the fibre that fundamental solitons had emerged, dispersive wave generation had practically ceased. Instead, the bulk of the dispersive wave energy was created during a well-defined and narrow region during which the pump reached its maximum intensity and began to split into different peaks. Instead of being a fundamental soliton during dispersive wave generation, the pump could be more accurately described as a higher-order soliton undergoing soliton fission, raising the possibility that the agreement between the experimentally observed properties of the dispersive waves and the present theoretical description was partly fortuitous. Chapter 3 presents the results of this investigation.

### 2.7.2 Narrowband enhancement using spectral filtering

Section 2.6.4 discussed how writing a Bragg reflection grating into the generating fibre produced a spectrally narrowband enhancement of the spectrum on the long-wavelength side of the Bragg resonance [104]. This enhancement is useful for frequency-domain applications of supercontinuum generation, such as the interferometric self-referencing used in carrier-envelope phase stabilization [54] described in Section 2.3.1. Despite these experimental demonstrations, and GNLSE simulations which agreed with experiment [105], an intuitive physical explanation of the enhancement had not been presented at the commencement of this thesis. The motivation for the work presented in Chapter 4 is to develop such an explanation. In addition, we sought to ascertain whether such enhancements could be generated through other means. In Chapter 4, we show that the enhancement mechanism can be understood as the action of self-phase modulation on a pulse with a narrowband amplitude or phase feature. We demonstrate this by applying narrowband phase features to a pulse using a pulse shaper, and studying the action of self-phase modulation produced by propagation in a photonic crystal fibre.

## Chapter 3

# Dynamics of dispersive wave generation

Dispersive wave generation is the primary source of blue-shifted radiation in supercontinuum spectra from photonic crystal fibres (PCFs). Additionally, it is analogous to Cherenkov radiation, a ubiquitous and important phenomenon in physics. As the primary means of producing radiation at wavelengths shorter than the pump, dispersive wave generation is very important for supercontinuum applications. Frequency metrology applications [12] exploit the octave-spanning spectra of supercontinuum by measuring the beat tone between the dispersive waves in the blue and the second harmonic of the Raman-shifted solitons in the red. Optical coherence tomography [7], fluorescence microscopy [62], coherent anti-Stokes Raman microscopy [64] and two-photon fluorescence microscopy [63] are all proven or potential applications of dispersive waves in supercontinuum. In general, as a tool for frequency conversion to the blue and near-ultraviolet, dispersive wave generation is seen as a useful alternative to harmonic generation or optical parametric amplification.

This chapter presents a study of dispersive wave generation in femtosecond-pumped supercontinuum. This study led to a publication, “Dispersive wave blue-shift in supercontinuum generation”, which forms the main body of the chapter. One specific aim was to understand the dynamics which shape the short-wavelength edge of the supercontinuum, with a view to possibly extending it or increasing its energy content. Additionally, we sought to reconcile the established description of dispersive wave generation by fundamental solitons with the fact that during supercontinuum generation, significant dispersive wave generation occurs before the soliton fission, when the pump more closely resembles a higher-order soliton.

This chapter is structured as follows: Section 3.1 contains a discussion of the established picture of dispersive wave generation by a fundamental soliton. Section 3.2 presents the paper which contains the main study.

### 3.1 Dispersive wave generation by a fundamental soliton

In nonlinear optics, dispersive wave generation is the process by which higher order dispersion (i.e. cubic and above) perturbs a soliton, causing it to shed energy to low-amplitude linear waves. The first theoretical predictions [14, 15, 76, 106] were in the context of optical communications, where dispersive wave generation was seen as a detrimental energy loss. Another important context was in mode-locked oscillators that were operated near the zero group-delay dispersion. Again, dispersive wave generation was seen as a nuisance, extracting energy from the main pulse [107–109]. The role of dispersive wave generation in supercontinuum was recognized [5] shortly after the spectacular spectral broadening demonstrated by Ranka *et al.* in 2000, leading to several more detailed studies [110–112] which pertain to this thesis and will be considered in more detail below. Dispersive wave generation was also observed in nonlinear pulse propagation experiments in anti-resonant PCF [113]. The spectral recoil of solitons — red- or blue-shifting away from the dispersive wave to conserve the spectral “centre-of-mass” — has been exploited to cancel the Raman self-frequency shift for constant wavelength propagation [114, 115].

The original detailed studies of dispersive wave generation [14, 15, 76] focused on fundamental solitons which were weakly perturbed by higher-order dispersion to produce a low-amplitude temporal pedestal. Although the mechanism is briefly reviewed in the paper which forms the main body of this chapter, we shall now present a more thorough treatment. A fundamental optical soliton is an exact solution  $A_S(T, z)$  of the nonlinear

Schrödinger equation

$$\frac{\partial A(T, z)}{\partial z} = i \frac{\beta_2}{2} \frac{\partial^2 A(T, z)}{\partial T^2} + i \gamma |A(T, z)|^2 A(T, z) \quad (3.1)$$

where  $\beta_2$  is the quadratic dispersion and  $\gamma$  the strength of the third-order instantaneous nonlinearity. As with Section 2.4,  $z$  is the distance along the fibre whilst  $T$  is the time in the comoving frame. For  $\beta_2 < 0$ , the fundamental soliton solution is

$$A_S(T, z) = \sqrt{P_S} \operatorname{sech} \left( \frac{T}{T_S} \right) \exp \left( i \frac{\gamma P_S}{2} z \right) \quad (3.2)$$

where  $P_S$  is the peak power and  $T_S$  the soliton duration, related to the fibre parameters by the fundamental soliton condition

$$T_S^2 \gamma P_S = |\beta_2|. \quad (3.3)$$

The distinguishing characteristic of the fundamental soliton is that in the comoving frame, it is unchanged by propagation except for a phase factor  $\gamma P_S z/2$ . Moving to the laboratory frame, we have

$$E_S(t, z) = A_S(t - \beta_1 z, z) \exp(i \beta_0 z - i \omega_S t) \quad (3.4)$$

$$= \sqrt{P_S} \operatorname{sech} \left( \frac{t - \beta_1 z}{T_S} \right) \exp \left[ i \left( \frac{\gamma P_S}{2} + \beta_0 \right) z - i \omega_S t \right] \quad (3.5)$$

showing that the soliton travels at the group velocity of its central frequency with slightly increased axial wave number  $\frac{\gamma P_S}{2} + \beta_0$  arising from the intensity-dependent refractive index. Here,  $\beta_0$  and  $\beta_1$  are the zeroth- and first-order components of the dispersion relation of the fibre. A dispersion relation for the field comprising a soliton can be obtained by Fourier transforming (3.5) in  $t$  and  $z$ , yielding

$$E_S(\omega, k) = \pi \sqrt{P_S T_S} \operatorname{sech} \left( \frac{\omega - \omega_S}{2} \pi T_S \right) \delta \left\{ k - \left[ \frac{\gamma P_S}{2} + \beta_0 + (\omega - \omega_S) \beta_1 \right] \right\} \quad (3.6)$$

The Dirac delta function is nonzero only for values  $k = \beta_S(\omega)$  where

$$\beta_S(\omega) = \frac{\gamma P_S}{2} + \beta_0 + (\omega - \omega_S) \beta_1 \quad (3.7)$$

is the *soliton wavenumber*. The soliton dispersion curve is parallel to the tangent of the fibre dispersion curve at  $\omega_S$  and offset from it by the nonlinear phase  $\frac{\gamma P_S}{2}$ . Figure 3.1(b) compares the soliton and fibre dispersion relations for a fundamental soliton, shown in Fig. 3.1(a), with intensity full-width at half-maximum (FWHM) duration 50 fs, peak power 46 W and centre wavelength 780 nm. The fibre dispersion relation is a second-order fit to that of NL-20-770, whose parameters were presented in Section 2.4. The stability and robustness of the soliton arises from the fact that fibre and soliton dispersion curves do not intersect, so resonant coupling is impossible if only quadratic dispersion is present [14].

Dispersive wave generation occurs when higher-order dispersion is present, and the fibre and soliton dispersion curves intersect. This is depicted in Fig. 3.2, in which the exact fibre dispersion relation has been used — otherwise the parameters are identical to Fig. 3.1. Principally, it is the positive third-order phase which causes the fibre and soliton dispersion relations to intersect. Mathematically, this intersection requires  $\beta_S(\omega_R) = \beta(\omega_R)$  the widely used condition for dispersive wave generation. Various approximate treatments [14, 15, 116] have shown that energy transfer only occurs if soliton possesses significant spectral intensity at the resonant wavelength. Being low-amplitude radiation in the normal dispersion regime, the dispersive wave broadens into a long pedestal. Furthermore, the soliton and dispersive wave generally have different group velocities and tend to separate, although under certain conditions [117] “light-trapping” can occur so that the dispersive wave remains bound to the soliton.

Dispersive wave emission also affects the soliton. The loss of energy results in temporal broadening so as to maintain the fundamental soliton condition (3.3). Furthermore the soliton is also spectrally shifted away from the resonant wavelength in a process known as “spectral recoil”, a fact which is intuitively explained by observing that in the frequency domain the NLSE (3.1) conserves the first spectral moment, or “centre-of-mass”

$$M(z) = \frac{\int_{-\infty}^{\infty} \omega |A(\omega)|^2 d\omega}{\int_{-\infty}^{\infty} |A(\omega)|^2 d\omega}. \quad (3.8)$$

A proof of this statement is given in Appendix B. Emission in the blue must therefore be accompanied by a shift of the remaining spectrum to the red. Together, these effects reduce the soliton’s spectral intensity at the resonant wavelength until dispersive wave generation and the soliton stabilizes. The spectral recoil is particularly

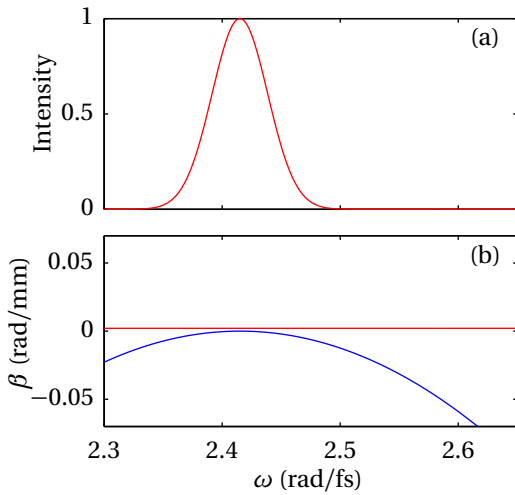


Figure 3.1: Soliton vs fibre dispersion relations for second-order dispersion. (a) Soliton spectrum. (b) Soliton (red) and fibre (blue) dispersion relations.

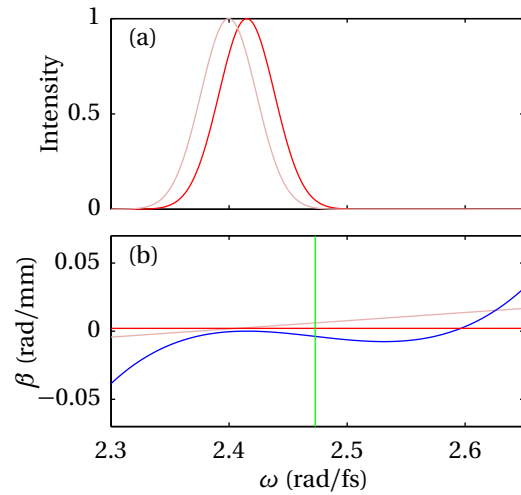


Figure 3.2: Soliton vs fibre dispersion relation with dispersion relation of a PCF. (a) Soliton spectrum. (b) Soliton (solid red) and fibre (blue) dispersion relations. The zero-dispersion frequency (green) is also indicated. In (a) and (b) the soliton spectrum and dispersion relation are redrawn for a lower soliton frequency (faint red).

effective at suppressing dispersive wave generation because the motion of the resonant wavelength roughly “mirrors” the soliton centre wavelength about the zero-dispersion wavelength, as illustrated by the faint lines in Fig. 3.2.

A simulation demonstrating the process is shown in Fig. 3.3. The parameters are those of Fig. 3.2 — a fundamental soliton with centre wavelength 780 nm launched into a length of NL-20-770. Part of the spectrum extends across the zero-dispersion wavelength (shown as a white dashed line), leading to a gradual energy transfer to the resonant wavelength (shown as a green line) during the first 2 m of propagation. The soliton’s centre wavelength (shown as a solid white line) recoils to the red, stabilizing the soliton so that dispersive wave generation effectively ceases. The corresponding movement of the resonant wavelength away from the zero-dispersion wavelength (ZDW) can also be seen.

It should be noted that the shock term and the Raman self-frequency shift both cause the GNLSE to violate conservation of the spectral centre of mass. Appendix B investigates these violations analytically. To give an indication of the magnitude of the shift in the spectral centre of mass, this quantity is plotted in Fig. 3.4 for the simulation of Fig. 3.3. Four cases are shown: the NLSE (equation (3.1)), the NLSE with Raman term, the NLSE with shock term, and the full GNLSE. Over 10 m of propagation, the shock term causes a small ( $\approx 0.1$  nm) blue-shift, whereas Raman scattering causes a significant (8 nm) red shift. However, dispersive wave generation effectively ceases after 1 m (see Fig. 3.3(b)), at which point the Raman-induced change in the spectral centre of mass is only 1.5 nm. This suggests that the Raman self-frequency shift does not play an important role in the spectral recoil mechanism.

Having described dispersive wave generation by a weakly perturbed fundamental soliton, we shall now move on to the main work of this chapter, the dynamics of dispersive wave generation in supercontinuum generation.



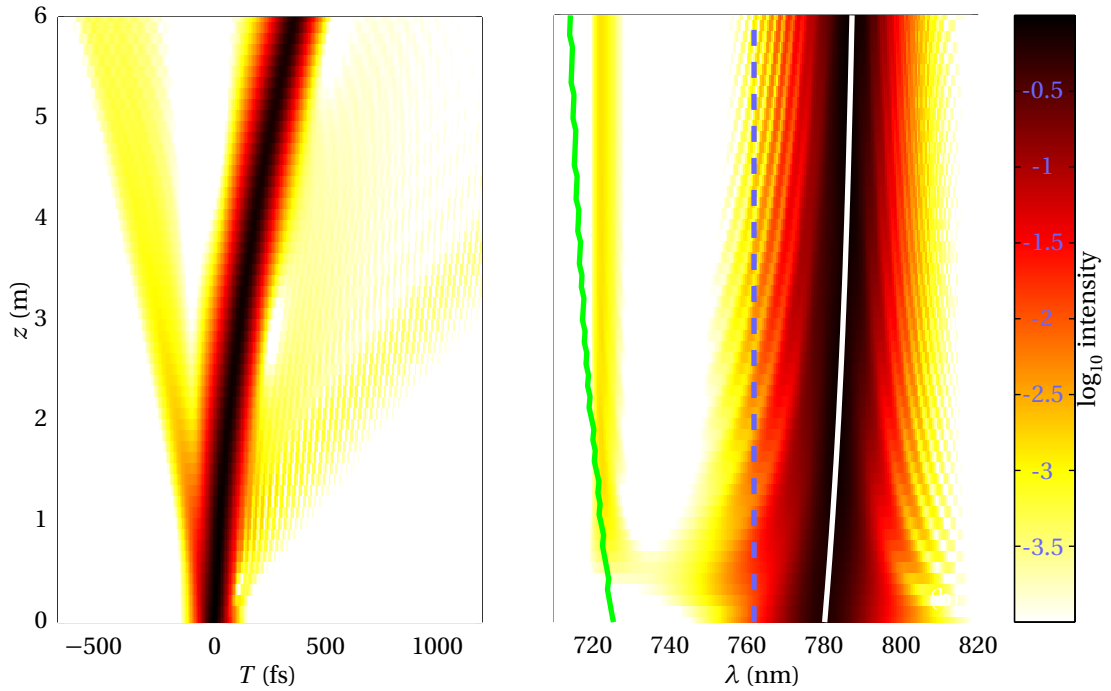


Figure 3.3: Dispersive wave generation by a fundamental soliton; (a) temporal evolution and (b) spectral evolution. The zero-dispersion wavelength (blue dashed), soliton centre wavelength (white solid) and dispersive wave resonant wavelength (green solid) are also shown.

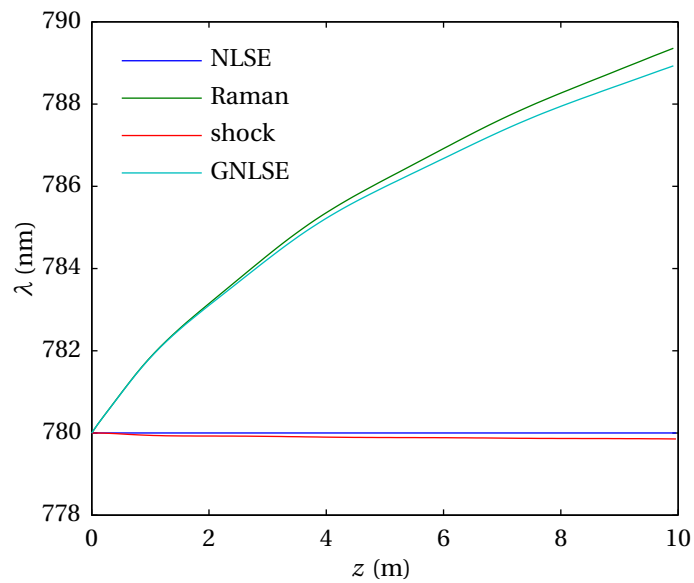


Figure 3.4: Evolution of the spectral centre of mass for the the simulation of Fig. 3.3, for the basic NLSE, the NLSE with shock term, the NLSE with Raman scattering, and the full GNLSE.

### 3.2 Dispersive wave blue-shift in supercontinuum generation

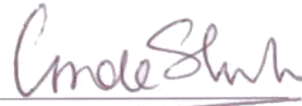
#### 3.2.1 Author's contribution statement

The following signed statement attests that the author of the thesis has made the indicated contributions to a published work contained in this thesis.

Title:	Dispersive wave blue-shift in supercontinuum generation
Journal and issue:	Optics Express, vol. 14, no. 25, pages 11997–12007, December 2006
Authors:	Dane R. Austin, C. Martijn de Sterke, Benjamin J. Eggleton, Thomas G. Brown

We, the authors of the work entitled **Dispersive wave blue-shift in supercontinuum generation**, acknowledge that Dane R. Austin has made the following contributions to the work:

- performed all the computational work;
- provided all the figures
- wrote the text, except for the incorporation of specific comments and corrections.

C. Martijn de Sterke	 Signature	 Date
Benjamin J. Eggleton	 Signature	 Date
Thomas G. Brown	 Signature	 Date

#### 3.2.2 Published work

The following work appeared in *Optics Express* vol. 14 , no. 25, pages 11997–12007 in December 2006.

# Dispersive wave blue-shift in supercontinuum generation

**Dane R. Austin, C. Martijn de Sterke, Benjamin J. Eggleton**

*Centre for Ultrahigh-Bandwidth Devices for Optical Systems, School of Physics, University of Sydney, New South Wales, 2006, Australia*

[daustin@physics.usyd.edu.au](mailto:daustin@physics.usyd.edu.au)

**Thomas G. Brown**

*The Institute of Optics, University of Rochester, Rochester, NY, 14627, USA*

**Abstract:** We numerically study dispersive wave emission during femtosecond-pumped supercontinuum generation in photonic crystal fibres. We show that dispersive waves are primarily generated over a short region of high temporal compression. Despite the apparent complexity of the pump pulse in this region, we show that the dynamics of dispersive wave generation are dominated by a single fundamental soliton. However, any straightforward application of the theory that is thought to describe the blue emission, considerably underestimates the frequency shift. We show that in fact the red-shift of the soliton, caused by spectral recoil from the growing dispersive wave, causes an additional blue-shift of the resonant frequency which is in good agreement with full simulations.

© 2006 Optical Society of America

**OCIS codes:** (060.5530) Pulse propagation and solitons; (060.7140) Ultrafast processes in fibers

---

## References and links

1. R. R. Alfano, *The supercontinuum laser source: fundamentals with updated references*, 2nd ed. (Springer, New York, 2006).
2. A. V. Husakou and J. Herrmann, "Supercontinuum generation of higher-order solitons by fission in photonic crystal fibers," *Phys. Rev. Lett.* **87**, 203901 (2001).
3. J. Ranka, R. Windeler, and A. Stentz, "Visible continuum generation in air-silica microstructure optical fibers with anomalous dispersion at 800 nm," *Opt. Lett.* **25**, 25–27 (2000).
4. J. M. Dudley, G. Genty, and S. Coen, "Supercontinuum generation in photonic crystal fiber," *Rev. Mod. Phys.* **78**, 1135–1184 (2006).
5. N. Akhmediev and M. Karlsson, "Cherenkov radiation emitted by solitons in optical fibers," *Phys. Rev. A* **51**, 2602–2607 (1995).
6. P. K. A. Wai, H. H. Chen, and Y. C. Lee, "Radiations by "solitons" at the zero group-dispersion wavelength of single-mode optical fibers," *Phys. Rev. A* **41**, 426–439 (1990).
7. A. S. Diddams, D. J. Jones, J. Ye, S. T. Cundiff, J. L. Hall, J. K. Ranka, R. S. Windeler, R. Holzwarth, T. Udem, and T. W. Hansch, "Direct Link between Microwave and Optical Frequencies with a 300 THz Femtosecond Laser Comb," *Phys. Rev. Lett.* **84**, 5102–5105 (2000).
8. I. Hartl, X. D. Li, C. Chudoba, R. K. Ghanta, T. H. Ko, J. G. Fujimoto, J. K. Ranka, and R. S. Windeler, "Ultrahigh-resolution optical coherence tomography using continuum generation in an air silica microstructure optical fiber," *Opt. Lett.* **26**, 608–610 (2001).
9. H. N. Paulsen, K. M. Hilligsøe, J. Thogersen, S. R. Keiding, and J. J. Larsen, "Coherent anti-Stokes Raman scattering microscopy with a photonic crystal fiber based light source," *Opt. Lett.* **28**, 1123–1125 (2003).
10. J. Herrmann, U. Griebner, N. Zhavoronkov, A. Husakou, D. Nickel, J. C. Knight, W. J. Wadsworth, P. St. J. Russell, and G. Korn, "Experimental evidence for supercontinuum generation by fission of higher-order solitons in photonic fibers," *Phys. Rev. Lett.* **88**, 173901 (2002).

11. Y. Kodama and A. Hasegawa, "Nonlinear Pulse-Propagation In A Monomode Dielectric Guide," *IEEE J. Quantum Electron.* **23**, 510–524 (1987).
12. J. P. Gordon, "Theory of the soliton self-frequency shift," *Opt. Lett.* **11**, 662–664 (1986).
13. J. N. Elgin, T. Brabec, and S. Kelly, "A perturbative theory of soliton propagation in the presence of 3rd-order dispersion," *Opt. Commun.* **114**, 321–328 (1995).
14. I. Cristiani, R. Tediosi, L. Tartara, and V. Degiorgio, "Dispersive wave generation by solitons in microstructured optical fibers," *Opt. Express* **12**, 124–135 (2004).
15. K. M. Hilligsøe, H. N. Paulsen, J. Thogersen, S. R. Keiding, and J. J. Larsen, "Initial steps of supercontinuum generation in photonic crystal fibers," *J. Opt. Soc. Am. B* **20**, 1887–1893 (2003).
16. G. Genty, M. Lehtonen, and H. Ludvigsen, "Effect of cross-phase modulation on supercontinuum generated in microstructured fibers with sub-30 fs pulses," *Opt. Express* **12**, 4614–4624 (2004).
17. K. Blow and D. Wood, "Theoretical description of transient stimulated Raman scattering in optical fibers," *IEEE J. Quantum Electron.* **25**, 2665–2673 (1989).
18. G. P. Agrawal, *Nonlinear Fibre Optics*, 3rd ed. (Academic Press, San Diego, 2001).
19. Q. H. Ye, C. Xu, X. Liu, W. H. Knox, M. F. Yan, R. S. Windeler, and B. Eggleton, "Dispersion measurement of tapered air-silica microstructure fiber by white-light interferometry," *Appl. Opt.* **41**, 4467–4470 (2002).
20. B. Kibler, J. M. Dudley, and S. Coen, "Supercontinuum generation and nonlinear pulse propagation in photonic crystal fiber: influence of the frequency-dependent effective mode area," *Appl. Phys. B* **81**, 337–342 (2005).
21. C.-M. Chen and P. L. Kelley, "Nonlinear pulse compression in optical fibers: scaling laws and numerical analysis," *J. Opt. Soc. Am. B* **19**, 1961–1967 (2002).
22. D. Skryabin and A. Yulin, "Theory of generation of new frequencies by mixing of solitons and dispersive waves in optical fibers," *Phys. Rev. E* **72**, 016619 (2005).
23. A. Efimov, A. Yulin, D. Skryabin, J. Knight, N. Joly, F. Omenetto, A. Taylor, and P. St. J. Russell, "Interaction of an Optical Soliton with a Dispersive Wave," *Phys. Rev. Lett.* **95**, 213902 (2005).
24. A. Peleg, M. Chertkov, and I. Gabitov, "Inelastic interchannel collisions of pulses in optical fibers in the presence of third-order dispersion," *J. Opt. Soc. Am. B* **21**, 18–23 (2004).
25. D. V. Skryabin, F. Luan, J. C. Knight, and P. St. J. Russell, "Soliton Self-Frequency Shift Cancellation in Photonic Crystal Fibers," *Science* **301**, 1705–1708 (2003).
26. F. Biancalana, D. V. Skryabin, and A. V. Yulin, "Theory of the soliton self-frequency shift compensation by the resonant radiation in photonic crystal fibers," *Phys. Rev. E* **70**, 016615 (2004).

## 1. Introduction

Optical supercontinuum (SC) generation [1] is a versatile source of intense ultra-broadband laser light. The interaction of a narrowband laser pulse with dispersion and nonlinearity [2] produces fields of enormous bandwidth that nonetheless retain the coherent nature of their source. One particularly useful and widespread method of achieving SC generation is injecting femtosecond pulses from a Ti:Sapphire mode-locked laser into small-core ( $\approx 1\mu\text{m}$ ) photonic crystal fibers [3, 4]. The resulting octave-spanning output spectra are due to the combined action of several processes. One of these is dispersive wave emission [5, 6], which is primarily responsible for wavelengths shorter than the pump. Dispersive waves are important for many applications, such as time frequency metrology [7], optical coherence tomography [8], microscopy [9]. Indeed, in many situations SC generation is merely seen as a means of converting light from 800 nm to the visible. To exploit this ability to its fullest, a complete understanding of the dynamics of dispersive wave emission in SC generation is desirable. In this paper we use numerical simulations to explore the limitations of the present understanding involving fundamental solitons [5, 6]. We aim to understand the condition of the pump pulse during dispersive wave generation so as to more accurately predict the emitted wavelengths.

Since dispersive wave emission is but one of a series of interrelated processes leading to SC generation, we now summarize the present understanding [2, 10]. The photonic crystal fibers used for SC generation typically have zero-dispersion wavelength slightly shorter than the Ti:Sapphire pump wavelength. The pump pulses experience anomalous dispersion, which, combined with self-phase modulation, leads to higher-order soliton formation. Both higher order dispersion and the non-instantaneous nonlinear response act as perturbations, causing the higher-order soliton to fission into its constituent fundamental solitons. These solitons are considerably shorter than the pump [11], partly explaining the massive spectral width of the SC. In

addition, stimulated Raman-scattering causes red-shifting, which continues to act on the fundamental solitons via the soliton self-frequency shift [12] well after the break-up is complete. Finally, higher-order dispersion causes solitons to shed energy to dispersive waves (also known as non-solitonic radiation). The spectrum of dispersive waves is usually blue-shifted relative to the pump because of the positive dispersion slope at the pump wavelength.

The original detailed studies of dispersive wave generation [5, 6, 13] were in contexts other than SC generation. They focused on fundamental solitons, which, when weakly perturbed by higher-order dispersion, shed radiation in the form of a low amplitude temporal pedestal. The radiation frequency  $\omega_R$  is governed by phase matching between the soliton and the low amplitude linear waves; that is  $\beta_S(\omega_R) = \beta(\omega_R)$  where  $\beta_S$  is the soliton wavenumber and  $\beta$  is the fiber's linear dispersion curve. The implied assumption that the soliton wavenumber is independent of  $z$  was approximately true in the original studies [5, 6, 13] because the solitons were both fundamental and weakly perturbed. Thus, besides a small nonlinear phase-shift, the solitons propagated undisturbed at the phase and group velocities of the fiber, leading to a simple expression for  $\beta_S$

$$\beta_S(\omega) = \beta(\omega_S) + \beta_1(\omega_S)(\omega - \omega_S) + \frac{\gamma(\omega_S)P_S}{2}, \quad (1)$$

where  $\omega_S$  and  $P_S$  are the soliton's centre frequency, and peak power, subscripts on  $\beta$  denote frequency derivatives, and  $\gamma$  is the fiber's nonlinear coefficient. The power-dependent term represents the nonlinear phase-shift and is often small compared to the other terms in Eq. (1). Equating  $\beta_S$  given in Eq. (1) with the linear wavenumber yields the well-known resonance condition

$$\sum_{n \geq 2} \frac{\beta_n(\omega_S)}{n!} (\omega_R - \omega_S)^n = \frac{\gamma(\omega_S)P_S}{2}, \quad (2)$$

which is commonly used to predict the location of dispersive wave emission [2, 4, 14, 15].

Disagreement between Eq. (2) and experiment is usually attributed to uncertainty in the fiber dispersion curve. However, we shall show that even in simulations, significant disagreement occurs, especially at high powers where dispersive wave generation is most efficient. Explaining this discrepancy is the motivation for this work. In particular, we show that efficient dispersive wave generation occurs over a narrow range of propagation distances before the emergence of distinct fundamental solitons. Examining the state of the pump pulse during this region, we find that the dispersive wave generation is nonetheless well described by a fundamental soliton-like state, provided a red-shift caused by higher-order dispersion is considered.

We note that another mechanism for dispersive wave blue-shift is cross-phase modulation with one of the solitons [16]. It critically depends on the walk-off dynamics between the two components and produces a distinct splitting of the dispersive wave spectrum. Some cross-phase modulation was observed in our work, especially for high input powers. However, additional blue-shift of the dispersive waves was observed even in those cases where significant cross-phase modulation did not occur. We attribute the diminished influence of cross-phase modulation to differences in the walk-off between the solitons and the dispersive wave. The parameters cited by Genty *et al.* [16] are such that the dispersive wave and ejected soliton have similar group velocities, yielding a gradual walk-off that produces a strong cross-phase modulation effect. Here, in contrast, the group velocity of the dispersive waves is considerably slower than that of the ejected soliton, so they quickly fall behind and the cross-phase modulation is weak.

## 2. Preliminary simulation results

In this section we present the results of a numerical simulation of femtosecond-pumped SC generation using typical experimental parameters. We use the scalar Generalized Nonlinear Schrödinger equation [17, 18], the standard formalism for SC generation:

$$\frac{\partial A(T, z)}{\partial z} = \sum_{n \geq 2} \frac{i^{n+1}}{n!} \beta_n \frac{\partial^n A}{\partial T^n} + i\gamma \left( 1 + i\tau_{\text{shock}} \frac{\partial}{\partial T} \right) \left( A(z, T) \int_{-\infty}^{+\infty} R(T') |A(z, T - T')|^2 dT' \right) \quad (3)$$

where  $A(T, z)$  is the time domain envelope,  $T = t - \beta_1 z$  is retarded time,  $z$  is axial propagation distance,  $\beta_n$  and  $\gamma$  are the  $n^{\text{th}}$  order dispersion and nonlinear coefficients evaluated at the reference frequency  $\omega_0$ ,  $\tau_{\text{shock}}$  models the dispersion of the nonlinearity and  $R(T)$  is the usual silica Raman response [18]. Femtosecond-pumped SC generation occurs in millimetres or centimetres of fiber and losses are therefore ignored. The initial conditions were unchirped hyperbolic-secant pulses i.e.  $A(T, 0) = \sqrt{P_0} \text{sech}(T/T_0)$ .

Equation Eq. (3) was solved using the symmetrized Fourier split-step method, using a second order Runge-Kutta algorithm for the nonlinear step. The discretization was sufficient to contain all energy (down to the -40 dB level) in the time and frequency windows, and adaptive step-sizing via step-doubling was used to improve efficiency. The optical photon number was tracked to estimate the global error, which was less than 1%. Although for clarity we here write the reference frequency equal to equal that of the pump, our code used an internal reference frequency approximately equal to the midpoint of the supercontinuum output spectrum so as to most efficiently use the simulated optical bandwidth.

We first consider a single simulation of an  $N = 5$  pump soliton. The other parameters are given in Table 1. The fiber is modeled on Crystal Fibre NL-2.0-740, a typical high air-fill hexagonal photonic crystal fiber designed for nonlinear experiments at 800 nm. Dispersion coefficients were measured using white-light interferometry [19], whilst the nonlinear coefficient was supplied by the manufacturer. We choose  $\tau_{\text{shock}} = 1/\omega_0$ , ignoring the frequency-dependent effective area which has been shown to have negligible effect for this parameter regime [20]. A summary of the results is given in Fig. 1, whilst an animation of the spectral, temporal and spectrographic evolution is linked to Fig. 2. A broad dispersive wave emerges around 629 nm at  $z = 36$  mm, indicated by the vertical lines in Figs. 1(b) and 1(d).

Symbol	Name	Value
$N$	soliton number	5
$P_0$	pump peak power	1365 W
$\lambda_0$	pump centre wavelength	810 nm
$T_0$	pump duration	45 fs
$\beta_2$	quadratic dispersion	-10.64 ps <sup>2</sup> /km
$\beta_3$	cubic dispersion	0.04875 ps <sup>3</sup> /km
$\beta_4$	quartic dispersion	$8.164 \times 10^{-5}$ ps <sup>4</sup> /km
$\gamma$	nonlinear coefficient	96.20 W <sup>-1</sup> km <sup>-1</sup>
$\lambda_{\text{ZDW}}$	zero-dispersion wavelength	749.3 nm
$L$	fiber length	100 mm

Table 1. Simulation parameters

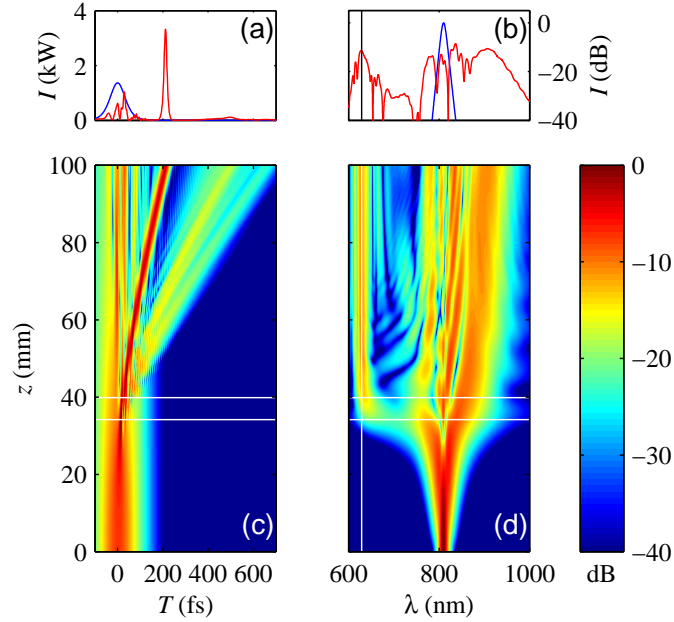


Fig. 1. Supercontinuum generation in 100 mm PCF using a 45 fs fifth-order soliton ( $N = 5$ ) as pump at 800 nm; (a) pump (blue) and output (red) temporal profiles; (b) pump (blue) and output (red) spectra, with dispersive wave marked by black vertical line; (c) temporal intensity; (d) spectral intensity, with dispersive wave generation region marked by white horizontal lines and dispersive wave marked by a white vertical line. Color plots are logarithmic with 40 dB range and normalized to the most intense pixel.

### 3. Soliton wavenumber description

We now consider the validity of using Eq. (2) to solve the phase matching condition to estimate the blue shift. First, in the context of SC generation it is unclear what values to assign  $\omega_S$  and  $P_S$ . For the former, previous authors have implicitly used the pump frequency [14, 15], whilst the latter is either taken to be the pump power, or zero since in any case this term has a only a small effect. Using  $\omega_S = \omega_0$  and  $P_S = 0$ , a resonance at 659 nm is predicted, 30 nm above the simulation result. Alternatively, putting  $P_S = P_0$  predicts 654 nm, still considerably larger. To show that this discrepancy is not an isolated special case, we repeated the simulation with different pump powers, corresponding to launched soliton numbers  $2 \leq N \leq 10$ , and extracted the dispersive wave location. The results are shown in Fig. 3(a), and the well-known blue-shift of the dispersive wave with increasing pump power is evident. Here we note that, in addition, the soliton wavenumber prediction becomes increasingly inaccurate. To ascertain whether any amount of nonlinear phase-shift could explain the discrepancy, we computed the maximum power  $P_{\max}$  over all points  $(T, z)$  in the propagation, and set  $P_S = P_{\max}$  in Eq. (2). Since higher-order soliton evolution involves an initial temporal contraction, we expect this to be significantly higher than the pump peak power and hence cause a larger dispersive wave blue-shift. However, as Fig. 3(a) shows, this is still not sufficient to explain the numerically observed values.

To demonstrate that the nonlinear phase-shift can in no way be wholly responsible for the blue-shift, we inserted the numerically observed blue-shift into Eq. (2) and solved for  $P_S$ , thus finding the peak power required to achieve the observed nonlinear phase-shift. In Fig. 3(b), this

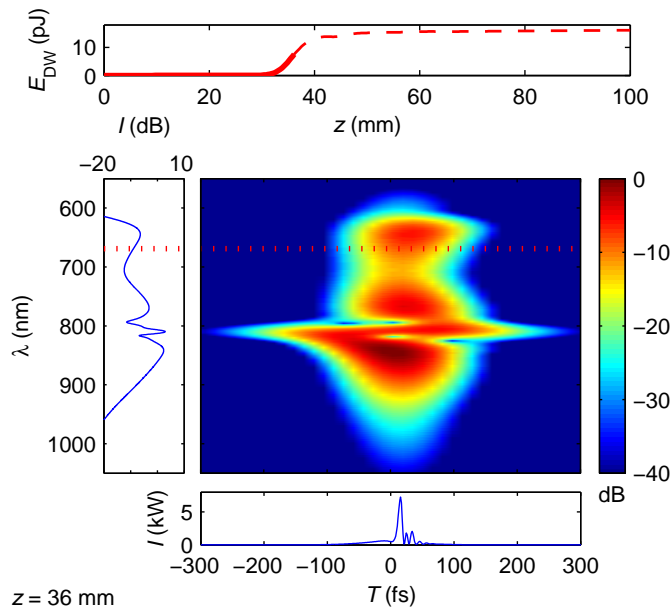


Fig. 2. Animation of spectrum, temporal profile, spectrogram, and energy in the dispersive wave  $E_{DW}$  for the simulation shown in Fig. 1 (2.5 MB). The dispersive wave energy is integrated over all spectral components above the dotted red line. A Gaussian gate function of  $T_{FWHM} = 80$  fs was used for the spectrogram. In the upper axes, the dashed red curve shows the energy in the dispersive wave over the full propagation distance whilst the solid red curve is restricted to  $z$  values up to that of the animation frame. The still image above shows the state at  $z = z_{max} = 36$  mm, the point of maximum temporal intensity of the field.

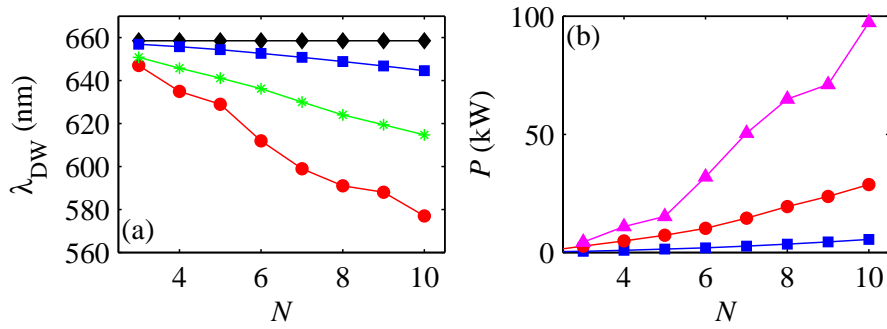


Fig. 3. (a) Wavelength of dispersive wave vs soliton number; as extracted from simulations (red circles); and as predicted from soliton wavenumber using peak power (green stars), pump power (blue squares), and zero power (black diamonds). (b) Temporal intensity vs soliton number, launched pump peak power (blue squares), maximum power achieved over all  $(z, T)$  (red circles), and power that would be required to achieve the numerically observed blue-shift of the dispersive wave through the nonlinear phase-shift (magenta triangles).



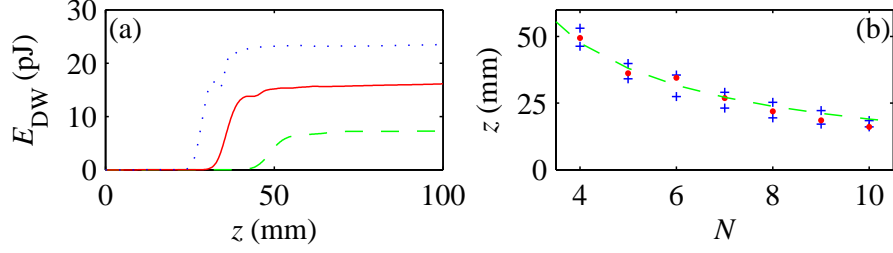


Fig. 4. Dispersive wave generation; (a) energy in dispersive wave vs  $z$  for  $N = 4$  (dashed green),  $N = 5$  (solid red) and  $N = 6$  (dotted blue); (b) Region of efficient dispersive wave generation vs  $N$ , defined by + signs (blue), point of maximum intensity (red dots) and approximate expression for soliton fission point  $L_{D,2}/N$  (green dashed).

is shown to greatly exceed the actual peak power  $P_{\max}$  obtained from the simulations.

Having shown that Eq. (2) becomes increasingly inaccurate with increasing pump power, we now consider the reason for this discrepancy. The soliton wavenumber Eq. (1), used in deriving Eq. (2), describes a fundamental soliton driving a low-amplitude dispersive wave, which can be treated as a small perturbation. Here, however, we have a fifth-order soliton, which even in the absence of perturbations undergoes complex periodic evolution. In addition, higher-order dispersion significantly alters the propagation, as is clear from the large amount of energy in the dispersive wave. Since analytic solution of Eq. (3) is intractable, we numerically examine the state of the pump pulse as dispersive wave generation is occurring.

#### 4. Conditions during dispersive wave generation

As Fig. 1 suggests, efficient dispersive wave generation occurs during a short propagation region. To test this thoroughly, we computed the dispersive wave energy, defined as all energy with wavelength less than 40 nm above the dispersive wave peak, as a function of  $z$ . The results are shown in Fig. 4(a) for several  $N$ , and the discontinuous, sudden nature of dispersive wave generation is apparent. We defined the “dispersive wave generation region” (DWGR) as the  $z$  values over which the dispersive wave energy grows from 20 % to 80 % of its final value. We tested a number of alternative definitions for the dispersive wave energy and DWGR and found that our conclusions were unaffected. For  $N = 5$ , the DWGR is illustrated by the white horizontal lines in Fig. 1, whilst the start and finish are shown for  $3 < N < 10$  in Fig. 4(b). Also shown is the point  $z = z_{\max}$ , defined as the  $z$ -coordinate where the pump pulse reaches its maximum temporal intensity  $P_{\max}$ . For the range of  $N$  considered here,  $z_{\max}$  lies within the DWGR, which is 2–8 mm in length. Furthermore, both the DWGR and  $z_{\max}$  show good agreement with an approximate expression for the soliton fission distance  $z_{\text{fiss}} = L_D/N$ , where  $L_D = T_0^2/|\beta_2|$  is the quadratic dispersion length [4].

We now examine the pump pulse in the DWGR. Although Fig. 2 is linked to an animation showing the complete evolution of the supercontinuum, the still image shows the conditions at  $z = z_{\max} = 36$  mm. Several temporally overlapping structures are evident, including the beginnings of the dispersive wave around 650 nm and a well defined pulse which goes on to become the most intense ejected soliton.

#### 5. Nonlinear wavenumber

To study the phase-matching between linear waves and the evolving pump pulse numerically, we define the nonlinear wavenumber as the spatial frequency including the effects of the non-

linearity. This is easily derived by taking the Fourier transform of Eq. (3) and recasting it in the form

$$\frac{\partial A(\omega', z)}{\partial z} = \left\{ i [\beta_{\text{NL}}(\omega, z) - \beta(\omega_0) - \beta_1(\omega_0)\omega'] - \frac{\alpha_{\text{NL}}(\omega, z)}{2} \right\} A(\omega', z), \quad (4)$$

where  $\omega' = \omega - \omega_0$ , so that  $\beta_{\text{NL}}(\omega, z)$  and  $\alpha_{\text{NL}}(\omega, z)$  are the  $z$ -dependent nonlinear wavenumber and loss respectively. Equating coefficients we find

$$\beta_{\text{NL}}(\omega, z) = \beta(\omega) + \gamma(1 + \tau_{\text{shock}}\omega') \text{Re} \frac{\text{FT} [A(T, z)R(T) * |A(T, z)|^2]}{A(\omega', z)}, \quad (5)$$

where FT denotes the Fourier transform at frequency  $\omega'$ . Using the pre-computed solution  $A(\omega, z)$ , the nonlinear wavenumber can be evaluated as desired. Clearly, at low intensities linear effects dominate and  $\beta_{\text{NL}} \approx \beta$ , whilst for a fundamental soliton at the carrier frequency experiencing quadratic dispersion and self-phase modulation only, Eq. (5) reduces to Eq. (1). The  $N$ -soliton pump pulses are  $N^2$  times more intense, and therefore would “compensate” for a correspondingly larger amount of quadratic dispersion, if it were present. At  $z = 0$ , this leads to

$$\beta_{\text{NL}}(\omega) = \beta(\omega) + \gamma P_0/2 - N^2 \beta_2 \omega'^2, \quad (6)$$

ignoring Raman and self-steepening. The subsequent evolution of the pump is complex and already well understood in terms of soliton-effect compression [21]. Our aim here is to relate the phase-matching between the compressed pump and linear waves during the DWGR to the dispersive wave growth. Figure 5(a) shows the spectrum at the start and end of the DWGR, whilst Fig. 5(b) shows the linear, soliton and nonlinear wavenumbers at the point of maximum intensity  $z_{\text{max}}$ . The linear and nonlinear wavenumbers intersect at  $\nu = 478$  THz, close to the dispersive wave frequency of  $\nu = 476$  THz. By contrast, the soliton wavenumber intersects at  $\nu = 458$  THz, underestimating the blue-shift. For plotting, the transformation  $\beta_{\text{NL}}(\omega)' = \beta_{\text{NL}}(\omega) - \beta(\omega_0) - \beta_1(\omega_0)\omega'$  (defined similarly for  $\beta$  and  $\beta_{\text{S}}$ ) is applied. This removes the linear phase and group velocities (equivalent to the transformation from the lab to the retarded frame) to make the curvature evident. Also, we plot the spectra and wavenumbers against frequency rather than wavelength as that is the natural domain of the latter. Figure 5(c) shows  $\beta_{\text{NL}}$  for various pump powers, and the blue-shift of the intersection point with increasing power is evident. The anomalous behavior of the  $N = 7$  curve around 450 THz is due the rapid change in phase that occurs when self-phase modulation drives the complex spectral amplitude  $A(\omega, z)$  through or close to zero. In general,  $\beta_{\text{NL}}$  is ill-defined for any frequency at which  $A(\omega, z)$  is close to zero. In Fig. 5(d) we present the resonant wavelength obtained from  $\beta_{\text{NL}}$  for the full range of  $N$ , showing good agreement with the simulation data. The average and maximum differences between the two curves are 7 nm and 18 nm respectively.

The evolution of  $\beta_{\text{NL}}$  is shown in the animation attached to Fig. 6(a). The initial condition, as expected from Eq. (6), is roughly parabolic, but after only 5 mm the nonlinear wavenumber has become nearly straight. After soliton fission has occurred, the linear behavior is lost as complex inter-soliton interactions occur. Two simple interpretations are evident from the animation. First for  $z > 50$  mm,  $\beta_{\text{NL}} \approx \beta$  for  $\nu > 470$  THz, showing that nonlinear interactions with the dispersive waves have effectively ceased. Second, the straight section of  $\beta_{\text{NL}}$  at low  $\nu$  for  $z > 50$  mm corresponds to the emergence of a spectrally distinct fundamental soliton, which gradually red-shifts due to Raman scattering.

To verify that the increase of  $\beta_{\text{NL}}$  around  $\nu = 477$  THz is not caused by the influence of the local linear wavenumber, we simulated supercontinuum in a hypothetical fibre with  $\beta_3 = 0$  and  $\beta_4 = 4.459 \times 10^{-4}$  ps<sup>4</sup>/km, chosen to give the same dispersive wave resonance wavelength as before, i.e. 659 nm. The other parameters were identical. The resulting dispersion curve is

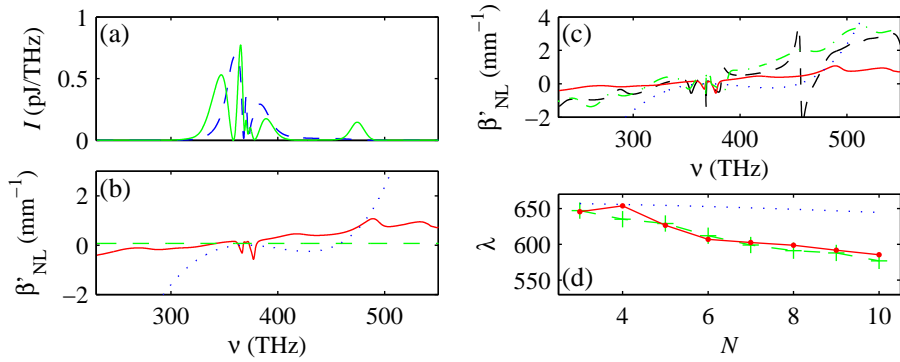


Fig. 5. Nonlinear wavenumber in dispersive wave generation; (a) spectra at the start (blue dashed) and end (green solid) of the dispersive wave generation region for  $N = 5$  pump; (b) nonlinear (red solid), linear (blue dotted) and soliton (green dashed) wavenumber for  $N = 5$  pump; (c) nonlinear wavenumber for  $N = 5$  pump (red solid),  $N = 7$  (black dashed) and  $N = 9$  (green dot-dashed); (d) wavelength of dispersive waves as extracted from simulations (dashed green), predicted by nonlinear wavenumber (solid red) and predicted by soliton wavenumber (dotted blue). All nonlinear wavenumbers are calculated at the point of maximum intensity  $z = z_{\max} = 36$  mm.

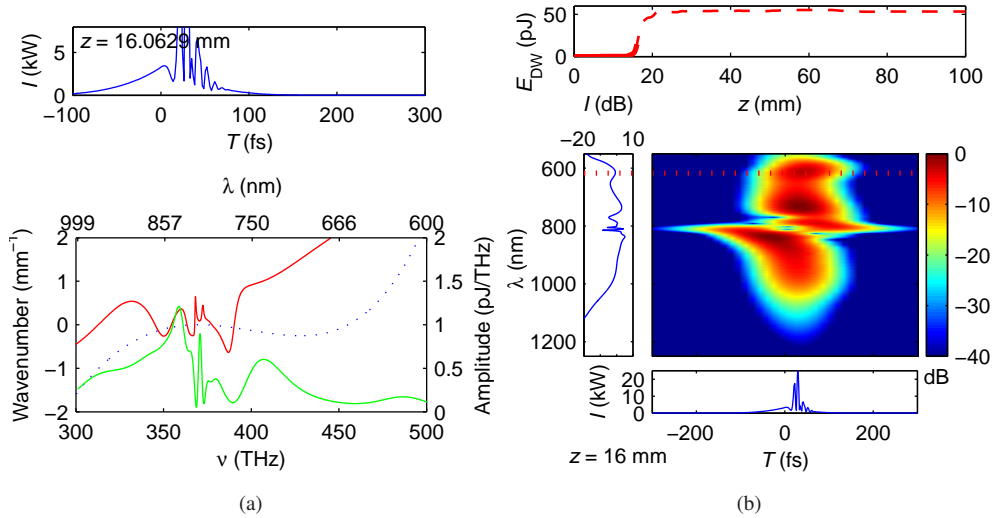


Fig. 6. (a) Animation (2.5 MB) of evolution of nonlinear wavenumber for  $N = 5$  pump; temporal profile (upper axes), spectrum (lower-right y-axis, green), and linear and nonlinear wavenumbers (lower-left y-axis, red and dotted blue respectively). (b) Animation (2.5 MB) of spectrum, temporal profile, spectrogram and dispersive wave generation in supercontinuum using  $N = 10$  pump. Two black dashed lines also appear in the spectrum animation, indicating the original dispersive wave (at the end of the dispersive wave generation region at  $z = 18$  mm) and the subsequent blue-shift caused by additional nonlinear processes.

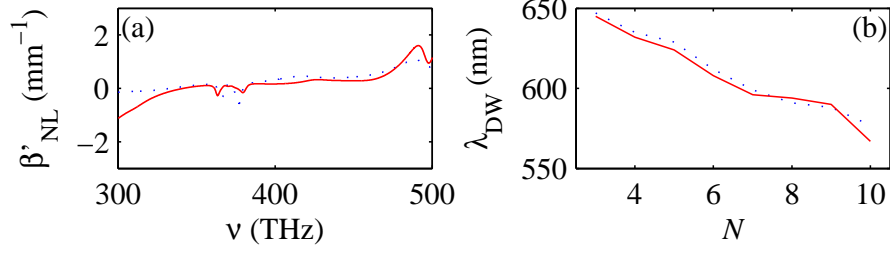


Fig. 7. (a) Nonlinear wavenumber, and (b) wavelength of dispersive waves (left axis) and energy in dispersive waves (right axis), with full Raman response (blue dotted) and pure Kerr nonlinearity (solid red).

symmetric about the pump frequency (in the retarded frame), and the fourth order dispersion creates a second resonance at 1052 nm. Over  $3 < N < 10$ , we found no power-dependent blue-shift of the dispersive wave. Therefore, the blue-shift is not caused merely by the upturn of the linear dispersion curve at high  $\nu$ , or some property of the higher order soliton evolution.

## 6. Spectral recoil of dominant fundamental soliton

Despite the complex multisoliton state of the pump during the DWGR, the nonlinear wavenumber curves are surprisingly linear over a broad frequency range, explaining why the soliton wavenumber has enjoyed reasonable accuracy previously. In Fig. 5(b), the two large deviations of  $\beta_{NL}$  from an approximately straight line occur around the pump frequency ( $\nu = 370$  THz), where the spectral intensity is low since SPM is driving the field through or nearby the origin causing a rapid change in phase. The linear dependence of  $\beta_{NL}$  on frequency is a signature of fundamental soliton propagation, and we attribute it to the dominant effect of the most intense fundamental soliton which forms part of the multisoliton initial state [11]. Since the soliton wavenumber is parallel to the tangent of the linear wavenumber at the soliton's centre frequency, the slight positive slope of  $\beta_{NL}$  in Fig. 5(c) corresponds to a red-shift of the soliton, resulting in a blue-shift of the intersection point with the linear wavenumber curve. This analysis is consistent with previous work, which attributed pump red-shift, in a general sense, to Raman scattering and third-order dispersion [15]. However, here we show that the pump red-shift can be interpreted as the spectral recoil of a fundamental soliton.

We found that the Raman effect has very little influence on the soliton red-shift nor on the dispersive wave phase-matching conditions. In Fig. 7(a), we compare the nonlinear wavenumber at  $z_{max}$  with and without the non-instantaneous Raman response included in the simulation. The difference is minor, and it therefore not surprising that the wavelengths of dispersive wave emission are nearly identical, as shown in Fig. 7(b). Despite this, we found that energy transfer to the dispersive wave was significantly reduced by Raman scattering, consistent with previous numerical results by Dudley *et al.* [4], who attributed the reduction to Raman self-frequency shifting of the first ejected fundamental soliton.

The only remaining effects which break the frequency symmetry are odd orders of dispersion, of which only  $\beta_3$  is considered here. In addition to dispersive wave emission, third-order dispersion causes a spectral recoil of fundamental solitons away from the zero-dispersion wavelength in order to conserve the spectral ‘‘centre of mass’’ [5, 13]. In Eq. (3), both self-steepening and Raman scattering violate the conservation of this quantity; however our simulations show that over the DWGR, the spectral centre of mass remains nearly constant (significant red-shifting occurs afterwards due to the soliton self-frequency shift). We therefore attribute the power-dependent

red-shift of the dominant pump soliton, and corresponding dispersive wave blue-shift, to spectral recoil caused by the dispersive wave emission. This also explains why no power dependent blue-shift was observed in the  $\beta_3 = 0$  case mentioned earlier — the two resonances spaced equidistantly (in frequency space) on either side of the pump cancel out any spectral recoil.

To demonstrate the validity of this argument, we solved Eq. (2) simultaneously with the spectral balance condition

$$\omega_R f_R + \omega_S (1 - f_R) = \omega_0, \quad (7)$$

treating both  $\omega_R$  and  $\omega_S$  as unknowns. The fraction of energy  $f_R$  transferred to the dispersive wave is extracted from the simulations. We therefore calculate a pair of pump soliton and dispersive wave frequencies which are both phase matched and conserve the spectral centre of mass at the pump frequency. As expected, the recoil of the pump soliton increases with  $N$ . Furthermore, the calculated resonant frequency agrees to within 15 nm with the observed dispersive wave emission for  $N \leq 9$ . Whilst a detailed study of the energy transferred to the dispersive wave is beyond the scope of this work, a rough *a priori* estimate of this quantity would enable Eq. (7) to be used in conjunction with Eq. (2) as an improved prediction of the dispersive wave wavelength.

For larger  $N$ , the blue-shift is underestimated, which we attribute to the complicating influence of cross phase modulation and four-wave mixing between the solitonic and dispersive wave components [16, 22, 23] and possibly interactions between the solitons themselves [24]. This is seen by examining the  $N = 10$  case, attached of Fig. 6(b). By the end of the DWGR at  $z = 18$  mm, a spectrally distinct dispersive wave is evident at 585 nm, as indicated by a black dashed line. However, the complex series of interactions that occur with subsequent propagation have the net effect of blue-shifting the peak an additional 10 nm to 575 nm, indicated by the second line. The interactions also introduce fine structure into the dispersive wave spectrum, suggesting that a “clean”, near-transform limited dispersive wave pulse can be produced by truncating the fibre just after the DWGR.

We also note that in fibres with a negative dispersion slope, self-frequency shift compensation of fundamental solitons [25, 26] can occur because the soliton’s recoil to the blue, away from the dispersive wave, opposes the Raman red-shift. Our results suggest that novel dynamics may be observed by performing similar experiments using higher-order solitons, such that the initial spectral recoil “overcompensates” for the Raman red-shift, forcing the pulse to the blue until an equilibrium is reached.

## 7. Summary

We first demonstrated that the dispersive waves emitted in femtosecond pumped supercontinuum generation experience a power-dependent blue-shift which cannot be explained by the standard picture of phase-matched emission by a fundamental soliton at the pump wavelength, even for the highest peak powers attained by the pump during propagation. Closer examination revealed that the majority of dispersive waves are produced in a narrow region where soliton-effect compression produces maximum intensity of the pump pulse. Although soliton fission has not yet progressed to the stage where distinct fundamental solitons are evident, the spatial frequency of the waves is dominated by a single fundamental soliton which is red-shifted by third-order dispersion. The physical interpretation of this red-shift is spectral recoil from the dispersive waves.

TGB acknowledges support through the Denison Distinguished Visitor scheme. This work was supported by an ARC Discovery Grant.

## Chapter 4

# Spectral enhancement using narrowband spectral filtering

In this chapter we describe a general technique for increasing the spectral intensity of an optical pulse in a narrow spectral region. The technique is applicable to supercontinuum insofar as supercontinuum consists of a train of pulses in a  $\chi^{(3)}$  medium. There exist several possible implementations, but in general form, the technique consists of applying a narrowband spectral phase or amplitude filter followed by self-phase modulation (SPM). Amplification occurs in the spectral regions affected by the filter. The technique has been independently discovered in several different contexts and has applications in frequency metrology [54] and nonlinear microscopy [118]. However, a simple intuitive yet quantitative description of the enhancement mechanism was absent from the literature. In this chapter, we identify a link between these contexts and reduce them to a single simple universal principle. Briefly, the enhancement may be understood as interference between the original field, which possesses the spectral feature, and the components generated by SPM, which lack the spectral feature because of the ultrafast gating nature of SPM. Applying this understanding, we demonstrate a novel implementation that overcomes some of the limitations of existing techniques.

Our investigation was prompted by experimental observations of narrowband spectral enhancements caused by the writing of Bragg reflection gratings into supercontinuum-producing fibre. A fibre Bragg grating is a periodic modulation of the fibre's properties — usually the core refractive index — which resonantly couples light into the backwards propagating mode. For the forward propagating mode, a Bragg grating therefore acts as an absorptive filter which acts on the supercontinuum simultaneously with the other effects already present in uniform fibre, such as dispersion, SPM, and Raman scattering. However, the enhancement mechanism relies only on the grating dispersion and SPM, and can be reduced in several steps to the problem of a single pulse with a narrowband phase or amplitude feature experiencing SPM. We therefore discovered a new, universal property of SPM, which was experimentally verified. This led to the publication “Narrowband supercontinuum control using phase shaping” which forms the main part of this chapter.

An overview of the chapter is as follows: Section 4.1 describes the original experimental findings, involving Bragg gratings written onto supercontinuum-generating fibres, which prompted our investigation. Section 4.2 describes how the effect of the grating is incorporated into generalized nonlinear Schrödinger equation (GNLSE) used to model supercontinuum generation. Section 4.3 presents a simulation which illustrates the spectral enhancement in the supercontinuum produced by a Bragg grating. The main results are then given in the form of a paper in Section 4.4.

### 4.1 Background and motivation

In 2004, Westbrook *et al.* [104] demonstrated a 10× enhancement of the supercontinuum spectrum near the resonant wavelength of a Bragg grating inscribed using UV photosensitivity [119, 120] in highly nonlinear fibre. Nonlinear propagation in fibre Bragg gratings had been studied previously [121, 122] and exhibits a variety of novel effects, such as gap soliton formation [123]. However, in these studies the pulse bandwidth was similar to the grating bandwidth, whereas the femtosecond pulses used by Westbrook *et al.* were much more broadband. Westbrook *et al.* also pointed out the potential benefit of local spectral enhancements to frequency metrology applications, and the effect was quickly exploited to improve the signal-to-noise ratio of a frequency comb [54].

This and subsequent investigations [105, 124, 125] established that the enhancement always occurred on the long wavelength side of the bandgap, whilst on the short wavelength side depletion was often observed. The enhancement was often accompanied by the development of a complex spectral structure around the bandgap, and was realised to be related to the grating's dispersion, which is significant even for wavelengths away from the bandgap [103, 126]. Finally, despite the absence of a simple physical explanation, the enhancement was well described by the nonlinear Schrödinger equation.

## 4.2 Theory

A fibre Bragg grating couples forward- and backward-going modes, and this must be incorporated into the GNLSE to model supercontinuum. A general approach is to augment the linear coupled mode theory [127] used for analysis of transmission and reflection spectra of gratings with terms representing the  $\chi^{(3)}$  [122, 128, 129] nonlinearity. When applied to fibre Bragg gratings, coupled mode theory produces coupled differential equations for the longitudinal evolution of the amplitudes of the forward and backward-going modes. However, in this work, along with most other treatments of supercontinuum generation in a fibre Bragg grating [104, 124], coupled mode equations are generally deemed unnecessary because the bandwidths of the pulses encountered in supercontinuum generation greatly exceed the bandgap of the grating, so that the backscattered field is weak and may be neglected. Furthermore, difficulties arise in imposing the appropriate boundary conditions for coupled mode theory: at the start of the grating the amplitude of the forward-going mode must equal the incident field, whilst at the end of the grating the amplitude of the backward-going mode must be zero. This prevents the straightforward integration of the GNLSE used in single-moded problems, and an iterative “shooting method” [130] is required.

For these reasons, in this thesis we treat supercontinuum generation in a fibre Bragg grating as a single-moded problem, with the dispersion and loss profile of the mode appropriately modified to describe the grating interaction. In the grating, the normal modes — those that propagate without coupling — are the *Bloch modes* [126]. They consist of a superposition of forward- and backward-going modes of the uniform fibre. Their wavenumber is given by

$$\beta_G(\omega) = \frac{k_G}{2} \pm \sqrt{\left(\beta(\omega) - \frac{k_G}{2}\right)^2 - \kappa^2} \quad (4.1)$$

where  $k_G$  is the grating wave wavenumber, related to the pitch  $\Lambda$  by  $k_G = 2\pi/\Lambda$ , and  $\beta(\omega)$  is the mode propagation constant in the absence of the grating. At the *Bragg frequency*, defined by  $\beta(\omega_B) = k_G/2$ , the grating induces perfectly tuned coupling between the forward and backward fibre modes. A convenient parameter for describing the properties of the Bloch modes is the normalized detuning

$$\delta = \frac{\beta - \frac{k_G}{2}}{\kappa}. \quad (4.2)$$

For  $|\delta| < 1$ , the Bloch modes possess a complex wavenumber and are therefore evanescent. This spectral region is the *bandgap* of the grating. Except at the *band edges* defined by  $|\delta| = 1$ , where degeneracy occurs, one may identify distinct forward- and backward-going Bloch modes. The forward-going Bloch mode corresponds to the positive (negative) sign in (4.1) for  $\delta > -1$  ( $\delta < -1$ ). Outside the bandgap it has a positive group velocity, indicating energy flow in the positive  $z$  direction. Its field profile is dominated by the forward-going fibre mode, and for large detuning  $|\delta| \gg 1$  its wavenumber approaches that of the forward-going fibre mode i.e.  $\beta_G \approx \beta$ . Inside the bandgap, the imaginary part of the wavenumber is positive indicating attenuation with increasing  $z$ . Corresponding properties apply for the backward-going Bloch mode. The dispersion relation for the Bloch modes is depicted in Fig. 4.1.

To model supercontinuum generation in a fibre Bragg grating, one uses the dispersion relation  $\beta_G(\omega)$  of the forward-going Bloch mode in the GNLSE, which is otherwise unchanged. A few more qualifications are necessary to justify this approximation. We will be considering *apodized* gratings [131], in which the coupling strength  $\kappa(z)$ , and hence the bandgap size, smoothly increases with  $z$  from zero to its peak value and back to zero again. The *local Bloch mode* at  $z$  is defined as the Bloch mode of a longitudinally uniform grating with coupling strength  $\kappa(z)$ . We assume that the apodization is sufficiently smooth so that an adiabatic transition between the local Bloch modes (including the fibre mode  $\kappa = 0$  as a trivial case) occurs for frequencies which are outside the bandgap at the peak coupling strength [132]. The mode amplitude is unchanged by this adiabatic transition. For frequencies which fall within the bandgap, adiabatic transition is impossible [132],

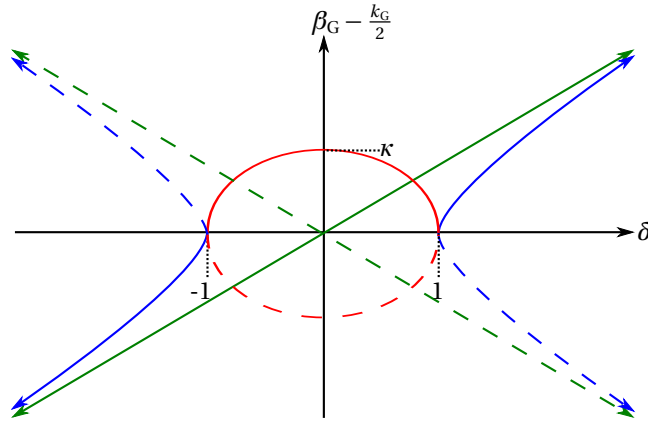


Figure 4.1: Real (blue) and imaginary (red) parts of the dispersion relation of the forward- (solid) and backward-going (dashed) Bloch modes of a fibre Bragg grating. Where the real part is non-zero, the imaginary part is non-zero, and vice versa. The green lines indicate the wavenumber in the absence of the grating.

because when the bandedge moves past any given frequency there is a degeneracy between the forward- and backward-going Bloch modes, and some light is coupled into the latter. Generally we are only interested in the transmitted light outside of the bandgap, which is much smaller than the bandwidths of the pulses involved. The backscattered field is therefore weak and does not participate in nonlinear processes. For these reasons, the backward-going Bloch wave may be ignored.

### 4.3 Example

This section presents simulations of a typical example of the spectral modulation caused by generating supercontinuum with a fibre Bragg grating. The parameters are identical to those in Fig. 2.3, except that a grating with Bragg wavelength 925 nm has been written into the photonic crystal fibre between 200–250 mm. Figure 4.2(a) shows the supercontinuum spectrum just before the grating at  $z = 200$  mm, whilst Figure 4.2(b) compares the spectra with and without the grating at  $z = 250$  mm. The main effect of the grating is to induce a sharp feature at the Bragg wavelength. Enhancement (depletion) occurs on the long (short) wavelength side of the Bragg wavelength. After propagation to the fibre output, shown in Fig. 4.2(c), the enhancement remains. The only other significant difference to the uniform case is the slightly reduced red-shift of the soliton at 960 nm. This can be attributed to energy loss in the grating bandgap reducing the soliton's peak intensity and hence its Raman self-frequency shift.



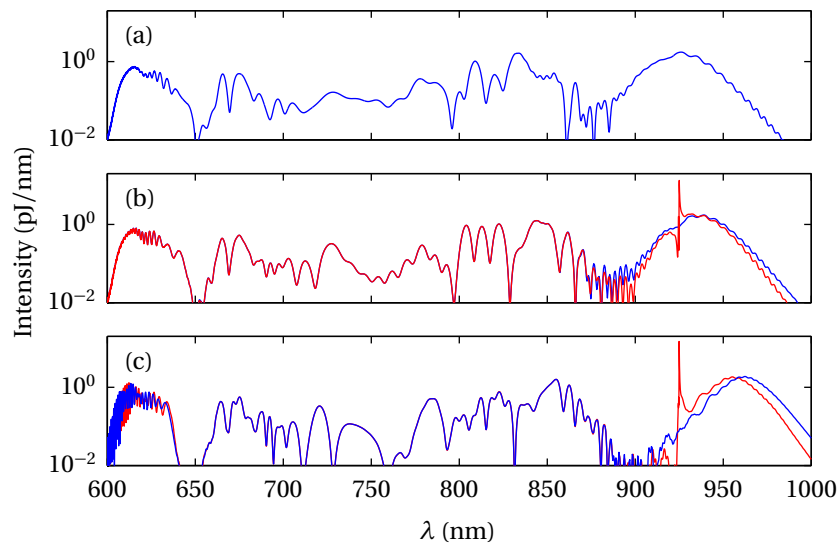


Figure 4.2: Spectra of supercontinuum generation with a Bragg fibre grating; (a) just prior to the grating at  $z = 200$  mm, (b) just after the grating at  $z = 250$  mm (red) and at the same position without the grating (blue), (c) and at the fibre output at  $z = 400$  mm.

## 4.4 Narrowband supercontinuum control using phase shaping

### 4.4.1 Author's contribution statement

The following signed statement attests that the author of the thesis has made the indicated contributions to a published work contained in this thesis.

Title:	Narrowband supercontinuum control using phase shaping
Journal and issue:	Optics Express, vol. 14, no. 26, pages 13142–13150, December 2006
Authors:	Dane R. Austin, Jeremy A. Bolger, C. Martijn de Sterke, Benjamin J. Eggleton, Thomas G. Brown

We, the authors of the work entitled **Narrowband supercontinuum control using phase shaping**, acknowledge that Dane R. Austin has made the following contributions to the work:

- performed the simulations
- performed the experimental work from the starting point of a working Ti:Sapphire oscillator
- provided all the figures
- wrote the text, except for the incorporation of specific comments and corrections.

Jeremy A. Bolger	 Signature	<u>16/FEB/2011</u> Date
C. Martijn de Sterke	 Signature	<u>3/3/2011</u> Date
Benjamin J. Eggleton	 Signature	<u>3-3-2011</u> Date
Thomas G. Brown	 Signature	<u>2 March, 2011</u> Date

### 4.4.2 Published work

The following paper was published in *Optics Express* vol. 14, no. 26, pages 13142–13150 in December 2006.

# Narrowband supercontinuum control using phase shaping

Dane R. Austin, Jeremy A. Bolger, C. Martijn de Sterke, and Benjamin J. Eggleton

*Centre for Ultrahigh-bandwidth Devices for Optical Systems (CUDOS), School of Physics,  
University of Sydney, New South Wales 2006, Australia*

Thomas G. Brown

*The Institute of Optics, University of Rochester, Rochester, NY, 14627, USA*  
[daustin@physics.usyd.edu.au](mailto:daustin@physics.usyd.edu.au)

**Abstract:** We study theoretically, numerically and experimentally the effect of self-phase modulation of ultrashort pulses with spectrally narrow phase features. We show that spectral enhancement and depletion is caused by changing the relative phase between the initial field and the nonlinearly generated components. Our theoretical results explain observations of supercontinuum enhancement by fiber Bragg gratings, and predict similar enhancements for spectrally shaped pulses in uniform fiber. As proof of principle, we demonstrate this effect in the laboratory using a femtosecond pulse shaper.

© 2006 Optical Society of America

**OCIS codes:** (230.1480) Bragg reflectors; (320.7140) Ultrafast processes in fibers; (190.4370) Nonlinear optics, fibers; (190.4380) Nonlinear optics, four-wave mixing

---

## References and links

1. R. R. Alfano, *The supercontinuum laser source: fundamentals with updated references*, 2nd ed. (Springer, New York, 2006).
2. I. Hartl, X. D. Li, C. Chudoba, R. K. Ghanta, T. H. Ko, J. G. Fujimoto, J. K. Ranka, and R. S. Windeler, "Ultrahigh-resolution optical coherence tomography using continuum generation in an air silica microstructure optical fiber," *Opt. Lett.* **26**, 608–610 (2001).
3. A. S. Diddams, D. J. Jones, J. Ye, S. T. Cundiff, J. L. Hall, J. K. Ranka, R. S. Windeler, R. Holzwarth, T. Udem, and T. W. Hansch, "Direct Link between Microwave and Optical Frequencies with a 300 THz Femtosecond Laser Comb," *Phys. Rev. Lett.* **84**, 5102–5105 (2000).
4. K. Mori, T. Morioka, and M. Saruwatari, "Group-velocity dispersion measurement using supercontinuum picosecond pulses generated in an optical-fiber," *Electron. Lett.* **29**, 987–989 (1993).
5. A. V. Husakou and J. Herrmann, "Supercontinuum generation of higher-order solitons by fission in photonic crystal fibers," *Phys. Rev. Lett.* **87**, 203901 (2001).
6. D. TÜRKE, W. Wohlleben, J. Teipel, M. Motzkus, B. Kibler, J. Dudley, and H. Giessen, "Chirp-controlled soliton fission in tapered optical fibers," *Appl. Phys. B* **83**, 37–42 (2006).
7. S. Xu, D. Reitze, and R. Windeler, "Controlling nonlinear processes in microstructured fibers using shaped pulses," *Opt. Express* **12**, 4731–4741 (2004).
8. M. Tianprateep, J. Tada, T. Yamazaki, and F. Kannari, "Spectral-Shape-Controllable Supercontinuum Generation in Microstructured Fibers Using Adaptive Pulse Shaping Technique," *Japanese J. of Appl. Phys.* **43**, 8059–8063 (2004).
9. P. S. Westbrook, J. W. Nicholson, K. S. Feder, and A. D. Yablon, "Improved supercontinuum generation through UV processing of highly nonlinear fibers," *J. Lightwave Technol.* **23**, 13–18 (2005).
10. J. C. Travers, R. E. Kennedy, S. V. Popov, J. R. Taylor, H. Sabert, and B. Mangan, "Extended continuous-wave supercontinuum generation in a low-water-loss holey fiber," *Opt. Lett.* **30**, 1938–1940 (2005).
11. F. Lu, Y. Deng, and W. Knox, "Generation of broadband femtosecond visible pulses in dispersion-micromanaged holey fibers," *Opt. Lett.* **30**, 1566–1568 (2005).

12. P. S. Westbrook, J. W. Nicholson, K. S. Feder, Y. Li, and T. Brown, "Supercontinuum generation in a fibre grating," *Appl. Phys. Lett.* **85**, 4600–4602 (2004).
  13. K. Kim, S. A. Diddams, P. S. Westbrook, J. W. Nicholson, and K. S. Feder, "Improved stabilization of a 1.3  $\mu\text{m}$  femtosecond optical frequency comb by use of a spectrally tailored continuum from a nonlinear fiber grating," *Opt. Lett.* **31**, 277–279 (2006).
  14. Y. Li, F. C. Salisbury, Z. Zhu, T. G. Brown, P. S. Westbrook, K. S. Feder, and R. S. Windeler, "Interaction of supercontinuum and Raman solitons with microstructure fiber gratings," *Opt. Express* **13**, 998–1007 (2005).
  15. P. S. Russell, "Bloch Wave Analysis of Dispersion and Pulse-Propagation in Pure Distributed Feedback Structures," *J. Mod. Opt.* **38**, 1599–1619 (1991).
  16. P. Westbrook and J. Nicholson, "Perturbative approach to continuum generation in a fiber Bragg grating," *Opt. Express* **14**, 7610–7616 (2006).
  17. C.-M. Chen and P. L. Kelley, "Nonlinear pulse compression in optical fibers: scaling laws and numerical analysis," *J. Opt. Soc. Am. B* **19**, 1961–1967 (2002).
  18. B. J. Eggleton, R. E. Slusher, C. M. de Sterke, P. A. Krug, and J. E. Sipe, "Bragg Grating Solitons," *Phys. Rev. Lett.* **76**, 1627–1630 (1996).
  19. A. Präkelt, M. Wollenhaupt, C. Sarpe-Tudoran, A. Assion, and T. Baumerta, "Filling a spectral hole via self-phase modulation," *Appl. Phys. Lett.* **87**, 121113 (2005).
  20. A. M. Weiner, "Femtosecond pulse shaping using spatial light modulators," *Rev. Sci. Instrum.* **71**, 1929 (2000).
- 

## 1. Introduction

Supercontinuum (SC) generation [1] in optical fibres is a striking effect with applications in imaging [2], frequency metrology [3], and interferometry [4]. The large spectral broadening, often spanning more than an octave, results from the interaction of an intense laser pulse with the fiber's dispersion and cubic nonlinearity [5]. Attention has recently turned to tailoring and improving SC for specific applications. The pump wavelength, duration, energy, and fiber nonlinearity and dispersion can be chosen to gain a limited degree of control, whilst more complex methods include pump chirp control [6], pump spectral shaping [7, 8], UV postprocessing [9], cascading different fibres [10] and tapering [11]. Another such scheme involves writing a Bragg grating in the fiber, resulting in a spectrally narrow enhancement of up to 15 dB around the long-wavelength side of the Bragg resonance [12]. This wavelength selective amplification is useful in applications that use only a small part of the spectrum, such as frequency-comb stabilization, where Bragg gratings were shown to improve the signal-to-noise ratio by 24 dB [13].

This paper generalizes and strengthens grating-enhanced SC generation in two ways. First, although semi-analytic results and modeling agree qualitatively with experiments [14], an intuitive physical explanation has not been presented. Whilst the enhancement has been linked to the magnitude of dispersion around the grating bandgap [15], experimental and calculated spectra exhibit complex and unexplained features such as depletion on the short wavelength side of the bandgap and fine spectral fringes with varying period. To realize the scheme's full potential these effects must be understood. Providing a simple explanation involving interference between initial and nonlinearly generated components is our main goal here. Additionally, we generalize this notion to arbitrarily shaped narrowband spectral phase features. We show that the phase features can be imparted on the field either continuously throughout the fiber, as is the case with Bragg gratings, or as an initial condition before nonlinear pulse propagation commences, as schematically shown in Fig. 1. We implement the latter configuration using a femtosecond pulse shaper, and as proof of principle demonstrate a tunable spectral enhancement after nonlinear propagation in a uniform photonic crystal fibre. This scheme could potentially address one practical disadvantage of Bragg gratings, namely, their limited tunability.

## 2. Nonlinear pulse propagation in Bragg grating

Supercontinuum generation in a fibre Bragg grating has recently been well described by Westbrook and Nicholson using a perturbative form of the nonlinear Schrödinger equation (NLSE) [16]. Here, we focus on the dynamics of the enhancement mechanism for a single pulse rather

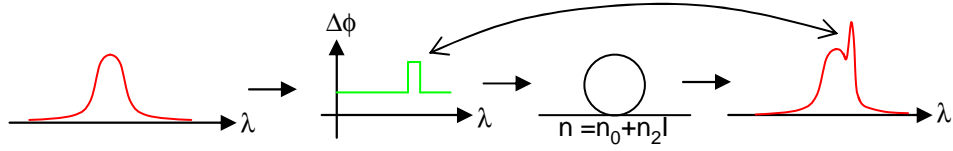


Fig. 1. Spectral enhancement via narrow spectral phase features and nonlinear propagation; an ultrashort pulse (red) passes through a spectral filter whose phase response (green) is flat except for a narrowband feature. The pulse then propagates through a nonlinear medium, such as a small-core silica microstructured optical fibre. Upon propagation, the output acquires a spectral enhancement corresponding to the narrowband phase feature.

than full supercontinuum description [16]. Our primary aim is an intuitive, quantitative description of the enhancement mechanism rather than full broadband agreement with the NLSE. The key technical difference between this work and Ref. [16] is that we consider the nonlinearity as a perturbation to the linear evolution in the presence of the grating, whereas Ref. [16] treats the grating as a perturbation to the full nonlinear solution for a uniform fibre.

We initially consider a fibre Bragg grating, and a single transform-limited incident pulse, rather than the complicated fields associated with SC generation. This is justified since the use of scaling laws [17], in combination with experimental parameters [12, 13] indicate that the gratings were written after the soliton fission point, so the SC field consists of a train of discrete pulses. Since the grating is apodized, incident pulses are coupled into the forward-propagating Bloch mode [15], permitting the use of the NLSE rather than coupled mode equations. The narrowband grating dispersion cannot be represented over the full pulse bandwidth by the usual Taylor expansion of dispersion coefficients, unlike previous studies of nonlinear propagation in Bragg gratings [18] where the pulse bandwidth was small or comparable to the bandgap. We therefore work in the frequency domain, and have

$$\frac{\partial A(\omega', z)}{\partial z} = i\beta_T(\omega)A(\omega', z) + i\gamma B(\omega', z), \quad (1)$$

where  $A(\omega', z)$  is the Fourier transform of the field envelope,  $\beta_T(\omega)$  the transformed wavenumber,  $\gamma = 80 \text{ W}^{-1} \text{ km}^{-1}$  is the fiber's nonlinear coefficient and  $B(\omega', z) = \text{FT}[|A(T, z)|^2 A(T, z)]$  is the Fourier transform of the usual self-phase modulation term, where  $T$  is retarded time. Bandgap reflection is ignored for reasons discussed below. In this frame,  $\omega' = \omega - \omega_0$  is the frequency relative to the carrier  $\omega_0$ . The transformed wavenumber is

$$\beta_T(\omega) = \beta(\omega) - \beta_F(\omega_0) - (\omega - \omega_0) \left. \frac{d\beta_F}{d\omega} \right|_{\omega=\omega_0}, \quad (2)$$

where  $\beta(\omega)$  and  $\beta_F(\omega)$  are the wavenumbers with and without the grating. Equation (2) transforms  $\beta(\omega)$  from the laboratory frame to a comoving frame with the phase and group velocity of the uniform fibre at  $\omega_0$  - we do not wish to “transform away” the grating dispersion. The grating is modeled as a 1-D photonic bandgap [15], with Bragg wavelength  $\lambda_B$ . In the chosen frame,  $\beta_T = 0$  away from the bandgap,  $\beta_T < 0$  for  $\lambda < \lambda_B$ , since  $\beta < \beta_F$ , and  $\beta_T > 0$  for  $\lambda > \lambda_B$  since  $\beta > \beta_F$ . We ignore background fiber dispersion because of the short propagation lengths under consideration.

Though our analysis is perfectly general, for our modelling we choose the experimental parameters of Li *et al.* [14]: grating Bragg wavelength  $\lambda_B = 950 \text{ nm}$  and coupling strength  $\kappa = 600 \text{ m}^{-1}$ , and pulse duration  $T_{\text{FWHM}} = 150 \text{ fs}$  and centre wavelength  $\lambda_0 = 945 \text{ nm}$ . The pulse bandwidth (6.3 nm) considerably exceeds that of the grating (0.7 nm), so only a small

fraction of the pulse energy is affected, justifying the absence of the bandgap reflection in Eq. (1). At the bandgap edges the transformed wavenumber is  $\pm\kappa$ , so the typical grating length scale  $L_G = 1/\kappa = 1.67$  mm is much smaller than the nonlinear length  $L_{NL} = 1/(\gamma P_0) = 25$  mm where  $P_0 = 0.5$  kW is the pulse peak power.

Neglecting the nonlinearity, Eq. (1) the field evolves linearly as

$$A_L(\omega', z) = A(\omega', 0) \exp[i\beta_T(\omega)z], \quad (3)$$

and the effect of the grating is thus to rotate the field's spectral phase in opposite directions on either side of the gap. To treat the nonlinearity, we make two simplifications. First, all our calculations are truncated to first order in  $z/L_{NL}$ ; equivalently we assume  $z \ll L_{NL}$ . Whilst this may seem overly restrictive, we show that much of the essential physics can be explained by this simple model. We then write

$$A(\omega', z) \approx A_L(\omega', z) + A_{NL}(\omega', z), \quad (4)$$

with  $A_{NL}(\omega', z)$  the nonlinear contribution correct to first order in  $z/L_{NL}$ . Without the grating, the nonlinearity causes self-phase modulation (SPM). The equivalent frequency domain description of SPM is intrapulse four-wave mixing (FWM) between all energy conserving frequency combinations in the pulse spectrum  $A_L(\omega', z)$ . Hence the second simplification: since the FWM contribution at frequency  $\omega'$  results from the many mixing processes just described, the spectrally narrow effect of the grating on  $A_{NL}(\omega', z)$  is small. Alternatively the spectrally narrow feature is broad and weak in time, lacking nonlinear effect. By ignoring the grating's effect on the FWM, the nonlinear term  $B(\omega, z)$ , which drives  $A_{NL}(\omega', z)$ , can be evaluated at  $z = 0$ .

Formally, we proceed by substituting Eq. (4) into Eq. (1). By the first assumption, only  $A_L(\omega', z)$  terms remain in the nonlinear driving term, which by the second assumption can be evaluated at  $z = 0$ . We obtain

$$\frac{\partial A_{NL}(\omega', z)}{\partial z} = i\beta_T(\omega)A_{NL}(\omega', z) + i\gamma B(\omega', 0) \quad (5)$$

which can be solved using integrating factors to yield

$$A_{NL}(\omega', z) = \frac{\gamma B(\omega', 0) \left[ e^{i\beta_T(\omega)z} - 1 \right]}{\beta_T(\omega)}. \quad (6)$$

This forms the starting point to explain a key feature of the reported spectra: depletion for wavelengths below the bandgap, accompanying the enhancement on the long wavelength side. For now, we consider  $A_{NL}(\omega', z)$  in the initial stages of propagation i.e.  $z \ll L_G$ ; equivalently we ignore grating dispersion of the nonlinear terms. This additional assumption is not intrinsic to our formalism and is only required for the simple argument which follows. In this limit, Eq. (6) reduces to

$$A_{NL}(\omega', z) \approx i\gamma B(\omega', 0)z. \quad (7)$$

The argument proceeds by considering the relative phases of the two terms in Eq. (4) for various cases. Initially, the pulse is transform limited at  $T = 0$ , so  $\angle A(\omega', 0) = \angle B(\omega', 0) = 0$ . Thus  $\angle A_L(\omega', z) = \beta_T(\omega)z$  and from Eq. (7),  $\angle A_{NL}(\omega', z) = \pi/2$ , leading to the simple vector construction in Fig. 2. For  $\lambda < \lambda_B$ ,  $\beta_T(\omega) < 0$  and the resultant vector is shortened, corresponding to a depletion of the spectrum, whereas for  $\lambda > \lambda_B$ ,  $\beta_T(\omega) > 0$  leading to an enhancement. By rotating the spectral phase for a narrow wavelength range without changing the nonlinear

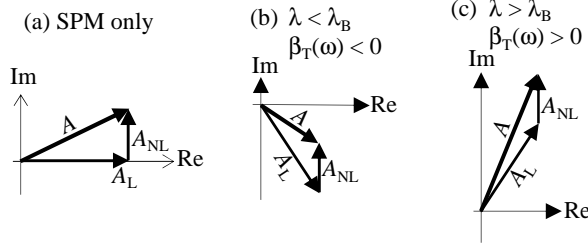


Fig. 2. Phasor diagrams showing interference between strong linear and weak nonlinear components after a short propagation length; (a) self-phase modulation only, (b) short wavelength side of Bragg resonance and (c) long wavelength side.

processes, therefore, the grating alters the phase angle between the original field at a frequency, and the nonlinearly generated field at that same frequency, thereby changing the vector sum.

As noted, Westbrook and Nicholson [16] presented approximate formulae for supercontinuum generation in a Bragg grating. We now compare their results with the argument just presented here. Since we assume  $z \ll L_G$ , the analogous result in Ref. [16] is Eq. (4), which shows an interference whose sign is affected by the sign of the wavenumber, but is otherwise very difficult to interpret. Note that, like Westbrook and Nicholson [16], we use the basic assumption that the grating's influence on nonlinear processes is negligible. Our argument requires the additional assumptions of a weak nonlinearity, so that  $z \ll L_{NL}$ , and transform limited pulses. In return, however, we provide the simple physical interpretation described above, and show that the sign of the interference depends only on the sign of the transformed wavenumber.

Additional spectral features arise when we consider grating dispersion of the nonlinear contributions once they are generated, i.e. for  $z > L_G$ . Combining Eqs (3), (4) and (6) we obtain

$$\left| \frac{A(\omega', z)}{A(\omega', 0)} \right| \approx 1 + \left| \frac{B(\omega', 0)}{A(\omega', 0)} \right| \frac{2\gamma \sin^2 \left[ \frac{\beta_T(\omega)z}{2} \right]}{\beta_T(\omega)} \quad (8)$$

for transform-limited pulses. The factor of 1/2 in the sine argument in Eq. (8) arises because the nonlinear contribution is generated along the entire length, so that the contribution generated near the end of the fibre is not affected by the grating. We now point out the salient features of Eq. (8) plotted as the solid red curve in Fig. 3(b). For reference, the transformed wavenumber  $\beta_T$  outside the bandgap is shown in Fig. 3(a). The sign of the  $\beta_T(\omega)$  term in the numerator determines whether Eq. (8) corresponds to enhancement or depletion. We shall “approach” the bandgap from the long wavelength side, where  $\beta_T(\omega) > 0$  and enhancement occurs. As expected, well away from the bandgap there is no spectral modulation owing to the rapid falloff of the transformed wavenumber. Moving closer,  $\beta_T(\omega)$  begins to increase monotonically and hence the  $\sin^2$  argument in Eq. (8) increases. For small  $\beta_T(\omega)z$  (e.g. at 950.5 nm), an enhancement proportional to  $z^2$  is observed. Closer to the bandgap, however,  $\beta_T(\omega)z > 1$  and the oscillatory behaviour of the sine term in Eq. (8) becomes important. The enhancement goes through a maximum where  $\beta_T(\omega)z \approx \pi$ . (The relation is not exact because of the  $\beta_T(\omega)$  term in the denominator of Eq. (8)). The enhancement peak therefore moves to longer wavelengths with increasing  $z$ . Even closer to the bandedge, fine spectral fringes appear since  $\beta_T(\omega)z > 2\pi$ . However, because of the large  $\beta_T(\omega)$  term in the numerator of Eq. (8), the amplitude of these fringes is very small. Published experimental spectra have suggested the presence of fine fringes [12, 14], but limited resolution prevents quantitative comparison with Eq. (8). As shown in Fig. 4, Eq. (8) agrees well with the exact numerical solution over a typical experimen-

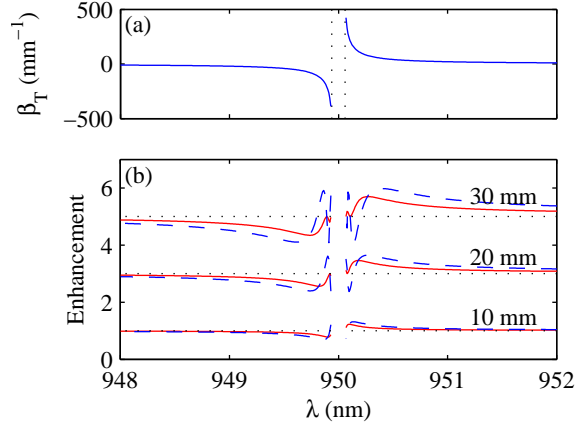


Fig. 3. Nonlinear spectral enhancement due to a narrowband 1-D photonic bandgap; (a) transformed wavenumber (blue solid) outside bandgap (black dotted); (b) relative spectral modulation resulting from a grating over the full 30 mm propagation length (red solid, Eq. (8) in text) and from a spectral filter of equivalent overall phase (blue dashed, Eq. (11) in text). Dashed black is a baseline, indicating the result in the absence of enhancement or suppression.

tal propagation length of  $L = 30$  mm. The approximation begins to break down for  $z > L_{NL}$  as second-order nonlinear effects begin to dominate.

Our Eq. (8) is essentially a special case of Eq. (3) in Ref. [16], employing our additional assumptions of a weak nonlinearity and a transform-limited pulse. In return for this loss of generality we can predict numerous qualitative features of the spectrum, as discussed in the paragraph above. Indeed, the NLSE results given in Fig. 1b of Ref. [16] show spectral fringes whose period and visibility decrease approaching the bandgap, consistent with Eq. (8). Our work, in offering physical insight and simple analytic results, is therefore complementary to Ref. [16], which is useful for rapid numerical approximation of grating-enhanced supercontinuum spectra.

The grating phase profile thus changes femtosecond pulse propagation, particularly the relative phase between the incident pulse and nonlinearly generated components, causing asymmetric spectral modulation around the Bragg wavelength. Our interpretation applies to any Bragg grating enhanced supercontinuum experiment where the grating is written after the soliton fission point, where the field incident on the grating consists of discrete solitons. We now discuss in Sec. 3 a generalization of the concept to a wider class of experimental geometries. Section 4 is concerned with establishing proof of principle of this generalization.

### 3. Nonlinear pulse propagation with arbitrary narrow phase feature

The simplifications in the theoretical analysis in Sect. 2 remain valid if the phase is applied as a single narrowband phase discontinuity of  $\Delta\phi(\omega) = \beta_T(\omega)L$  at  $z = 0$  mm. This means that the two roles played by the grating in the process, namely the inscription of a phase feature, and providing the medium for nonlinear propagation, can be separated. In other words, the process is equivalent to inscribing a spectral feature, by whatever means, followed by self-phase modulation in a fiber. Since this insight allows the two elements to be selected and optimized independently, it broadens the possible application of this process.

We now treat the more general situation in which the application of the spectral feature and



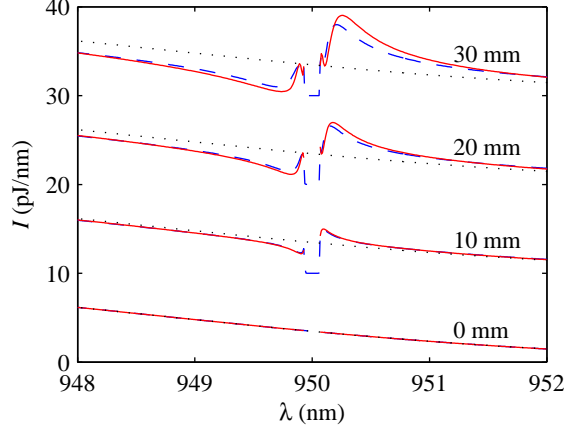


Fig. 4. Exact (blue dashed) and approximate (red solid, Eq. (8) in text) pulse spectra under propagation through a 30 mm Bragg grating, shown on a linear scale with vertical offsets added for clarity. The initial pulse (black dotted) is repeated for comparison.

the nonlinear propagation are separated. Instead of solving Eq. (1) for a transform limited pulse with a narrowband dispersive term, as in the previous section, we use the initial condition

$$A(\omega', 0) = A(\omega', 0^-)e^{i\Delta\phi(\omega)}, \quad (9)$$

where  $A(\omega', 0^-)$  is the transform limited pulse before the phase discontinuity. Since we are ignoring fibre dispersion and the phase feature has been incorporated into the initial condition, we solve Eq. (1) with  $\beta_T(\omega) = 0$ . As with the previous section, we work to first order in  $z/L_{NL}$ . However, whereas before we ignored the grating's influence on the nonlinear contribution, here we ignore the effect of the phase filter instead. This enables us to evaluate the nonlinear driving term at  $z = 0^-$  i.e. with a transform limited pulse, and we obtain

$$A(\omega', z) = A(\omega', 0^-)e^{i\Delta\phi(\omega)} + i\gamma z B(\omega', 0^-). \quad (10)$$

The relative enhancement is then given by

$$\left| \frac{A(\omega', z)}{A(\omega', 0^-)} \right| \approx 1 + \left| \frac{B(\omega', 0^-)}{A(\omega', 0^-)} \right| \gamma z \sin \Delta\phi(\omega). \quad (11)$$

Equation Eq. (11) is shown as the dashed blue curve in Fig. 3 for  $L = 30$  mm. Compared with Eq. (8), the fringes are larger close to the bandgap because Eq. (11) does not have the large phase term in the denominator. Also, the sign of the effect (enhancement or depletion) is now determined by the sign of  $\sin \Delta\phi(\omega)$  rather than simply  $\beta_T(\omega)$  as in Eq. (8). Physically, both of these differences correspond to the entire grating phase  $\beta_T(\omega)L$  being pre-applied at  $z = 0$  mm, before any nonlinear components are generated, rather than continuously throughout the propagation. Besides this, the two curves are qualitatively similar.

This generalization may now be applied to other, narrow phase perturbations of the pulse. We therefore posit a scenario in which a narrowband phase feature is imprinted on a pulse *prior to* propagation through a nonlinear medium. The experiment described in the following section tests such a scenario. We note that the application of spectrally narrow amplitude features, followed by self-phase modulation was earlier considered by Präkelt *et al.* [19], though not in the context of super continuum generation. Moreover their treatment is qualitative and does give rise to quantitative predictions.

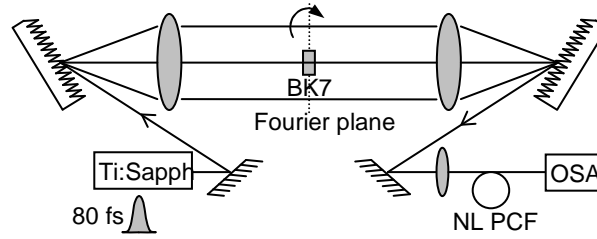


Fig. 5. Experimental setup: BK7 glass in the Fourier plane of a 4- $f$  femtosecond pulse shaper imparts spectrally narrow phase delays on Ti:Sapphire mode-locked laser pulses, which are then injected into nonlinear photonic crystal fibre (PCF). Rotating the glass about the horizontal transverse axis (dotted) affects the phase delay without changing its spectral extent.

#### 4. Experiment

In our experiment we show that our theory correctly describes spectral enhancement of femtosecond pulses which have narrowband phase features applied before nonlinear propagation in photonic crystal fibre. Because this technique limits the spectral enhancement to be within the pump spectrum, its purpose here is to demonstrate proof of principle of the ideas developed in the previous section. A more complicated geometry which permits a wider choice of enhancement wavelengths is described in section 5.

We applied spectrally narrow phase features to 80 fs pulses with centre wavelength  $\lambda_0 = 778$  nm from a modelocked Ti:Sapph laser using a 4- $f$  femtosecond pulse shaper [20] as in Fig. 5. A ruled reflection grating (1800 rules/mm) disperses the spectrum which is then imaged by a lens ( $D = 50$  mm,  $f = 200$  mm) onto the Fourier plane. A transparent phase mask in the Fourier plane imparts a phase profile  $\Delta\phi(\omega)$ , then a second lens and grating pair recollimate the beam which is coupled into 4.5 m of small core PCF (Crystal Fibre NL-1.8-750) with measured zero dispersion wavelength  $\lambda_{ZD} = 760$  nm and manufacturer specified nonlinearity  $\gamma = 99$  W $^{-1}$ km $^{-1}$ . The output is spectrally resolved on an optical spectrum analyser. Our phase mask was a  $d = 92$   $\mu$ m thick piece of polished BK7 glass, which was rotated to adjust the effective thickness and hence phase delay within a range equivalent to 74-80 wavelengths at a wavelength  $\lambda_D = 778$  nm.

Figure 6(a) shows the enhancement and depletion achievable with a pulse peak power of approximately 14 W, giving a nonlinear length  $L_{NL} = 0.7$  m. Without the phase mask, SPM has only a small effect. With a phase delay such that  $\sin\Delta\phi = 1$ , a 5 dB enhancement is observed as predicted by Eq. (11), whilst a corresponding depletion is seen for  $\sin\Delta\phi = -1$ . Across the width of the feature  $\Delta\lambda = 1.7$  nm, the enhancement is not uniform; because of the wavelength dependent phase delay ( $\phi \propto 2\pi/\lambda$ ) the relatively large thickness produces a perceptible change in phase over the spectral feature. Material dispersion also plays a small role in the asymmetry. Figure 6(b) shows the spectral intensity at  $\lambda_D$  from a series of spectra taken with varying delay. As predicted in Eq. (11), sinusoidal dependence on  $\Delta\phi$  with period  $2\pi$  is observed.

#### 5. Discussion

It is clear from simulation, theory, and our proof of principle experiment, that the sort of enhancements first reported by Li *et al.* [14] may be generalized to other situations in which a narrowband phase feature is imposed on a pulse, with the pulse then subject to propagation in a Kerr-like nonlinear medium. The nonlinear propagation has the effect of imprinting a pre-

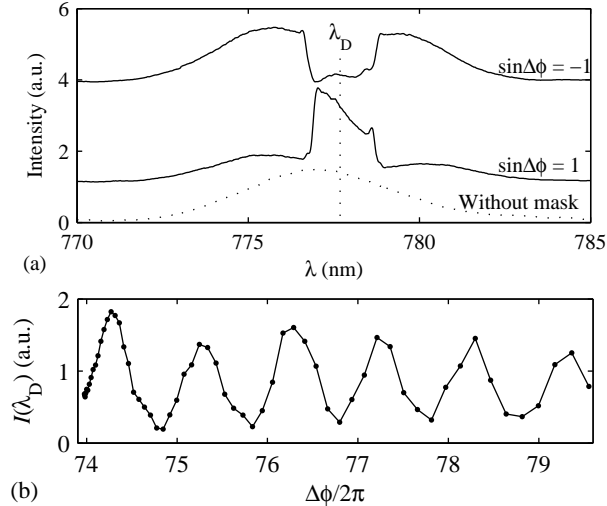


Fig. 6. (a) Output spectra: no phase mask (bottom), phase delay causing enhancement (middle) and depletion (top). Vertical offsets have been added for clarity. (b) Spectral intensity at phase delayed wavelength vs phase delay.

conditioned phase feature on the spectral density of the pulse. While it is not easy to separate the phase filtering and propagation when using a Bragg grating, our experiment clearly shows the distinct roles of phase filtering and propagation. This insight follows immediately from our quantitative, yet intuitive theoretical description of the process, which differs from that of Westbrook and Nicholson [16] which provides less physical insight, and that of Präkelt *et al.* [19], which is qualitative.

In our geometry, the enhancement is limited to within the pump spectrum. Its main purpose is to verify the theoretical development in this paper. To obtain spectral peaks at other frequencies, a high power could be propagated through enough fibre to generate a supercontinuum encompassing all required enhancement wavelengths. The resulting field, consisting of various pulses distributed over the spectrum, would have phase features applied using the pulse shaper and would then be re-injected into a second fibre for subsequent spectral enhancement and further broadening. This scheme is similar to that of Li *et al.* [14] with the Bragg grating substituted by a pulse shaper. In addition, replacing the BK7 glass phase mask with a liquid-crystal spatial light modulator [20] would allow far greater control of the applied phase and attenuation. We note that the experiments presented here are reminiscent of those of Präkelt *et al.* However, their work, in which the self-phase modulation occurs in a water jet, was not conducted in the context of fiber supercontinuum generation.

In conclusion, we have shown that Bragg gratings cause nonlinear spectral enhancement by inducing relative phase rotation between linear and nonlinear components. Our experiment confirms that any narrow phase feature followed by nonlinear propagation exhibits similar effects. Though the enhancement was restricted to within the pump spectrum, it nonetheless demonstrates that our theoretical argument is sound. The analytic result and simple explanation will, we believe, enable spectral tailoring of supercontinuum light sources in novel ways.

TGB acknowledges support through the Denison Distinguished Visitor scheme. This work was supported by an Australian Research Council Discovery Grant.

# Chapter 5

## Summary and outlook

In this thesis, we studied one theoretical aspect of supercontinuum generation in photonic crystal fibres, and also demonstrated a technique for achieving a narrowband spectral enhancement in the supercontinuum. In this chapter, we discuss and reflect upon the significance of these findings and highlight areas for future work.

### 5.1 Dispersive wave generation

The dispersive wave generation study of Chapter 3 had several motivations. We began with the qualitative objection to the accepted theory of SC generation that during the region of efficient dispersive wave production, isolated fundamental solitons are not actually present, so that phase matching arguments based on the properties of fundamental solitons cannot represent the complete picture. The key figure demonstrating this is Fig. 2 of the paper. Quantitatively, we noted that the phase matched wavelengths predicted by the accepted theory do not agree with simulation results, as shown in Fig. 3(a) of the paper. We also desired an improved understanding of the limitations of DWG from an applications standpoint, particularly the achievable blue-shift and conversion efficiency. The study improved the qualitative aspects of the theory by showing that, despite the apparent complexity of the pump pulse in the region of efficient dispersive wave generation, for the purposes of phase matching it could be well approximated by a fundamental soliton as long as spectral recoil was taken into account, as shown in Fig. 5(b) of the paper. The quantitative accuracy of the theory was also improved by taking into account the spectral recoil using a simple spectral balance argument, given by Eq. (7) of the paper. However, this amendment is not completely satisfying because of the need for an *a priori* estimate of the fraction of energy converted into the dispersive wave. Given that in practice, uncertainty over the fibre dispersion curve and input power generally results in greater uncertainty in the phase-matched wavelength than the theoretical inaccuracies mentioned above, it is unlikely that eq. (7) will be used in practical fibre design situations.

With regard to improving the utility of dispersive wave generation for applications, the study makes clear that for a clean spectrum, the fibre length should be carefully chosen so that the end face coincides with the end of the dispersive wave generation region (DWGR), as illustrated by Fig. 4(b) of the paper (Section 3.2). The DWGR is shown to coincide quite closely with the soliton fission point, providing a simple prescription for choosing fibre lengths. This recommendation dovetails well with studies of the shot-to-shot coherence [4] which show that during propagation the coherence rapidly degrades after the soliton fission occurs.

The finding that spectral recoil of the pump away from the zero-dispersion wavelength causes a rapid cessation of dispersive wave generation suggests that placing a second dispersion zero at longer wavelengths could improve conversion efficiency by providing its own compensatory spectral recoil, so that the pump pulse is “bound” at both shorter and longer wavelengths. We provided indirect evidence for this in Section 6 of the paper by simulating a hypothetical fibre with only even orders of dispersion, so that the dispersion curve was symmetric about the pump wavelength and a second dispersion zero at 1052 nm appears. No spectral recoil was observed — however we did not perform a systematic study of the conversion efficiency. There have been several other studies of supercontinuum generation in a fibre with a second zero-dispersion wavelength [114,133–136]. Besides the expected second dispersive wave, other novel effects include a self-frequency shift cancellation [114], paired propagation of the soliton and dispersive wave [133], and greater spectral density [136]. However, none have explicitly mentioned the second dispersive wave balancing spectral recoil and

preventing shutoff of dispersive wave generation, although Hilligsøe *et al.* [136], using a fibre with dispersion zeros at 780 nm and 945 nm and pumping at 790 nm, show almost complete conversion of energy into the dispersive waves at 650 nm and 1100 nm. The efficiency is not compared with the single zero-dispersion wavelength (ZDW) case but could easily be greater. This evidence suggests that fibres with two closely spaced dispersion zeros may be a possible route towards increasing the spectral intensity of blue light generation in supercontinuum. Such fibres may be fabricated through tapering [137]. Finally, we mention that fibres with highly customized dispersion profiles may now be fabricated [138]. The nonlinear wavenumber introduced in Chapter 3 may assist understanding of dispersive wave generation in these fibres, and help guide their design.

## 5.2 Narrowband spectral enhancements

In Chapter 4 we presented a general theory of spectral modulation caused by the Kerr nonlinearity acting on pulses with spectrally narrow phase features. In our model, the key effect is the interference between the narrowband field corresponding to the phase feature, and the remainder of the pulse as it undergoes self-phase modulation. The theory explains recent observations of local spectral enhancement of supercontinuum in fibre Bragg gratings (FBGs), with the phase feature produced by dispersion around the grating bandgap and the pulses being Raman-shifted fundamental solitons emitted by the soliton fission. We demonstrated another implementation of the effect by propagating spectrally shaped pulses in uniform fibre.

Since fibre Bragg gratings couple forward- and backward-propagating fundamental modes, their period is approximately one half of the wavelength, and they must generally be written using ultraviolet inscription. Furthermore, they are not particularly sensitive to external conditions, limiting their tuneability. An alternative which overcomes these restrictions is a long-period grating (LPG), which couples the fundamental mode with a higher-order mode [139]. Because the Bloch modes of a LPG generally have a significant component in the cladding, they are more sensitive to external conditions than FBGs and may be tuned using mechanisms such as temperature adjustment or immersion in different fluids. It is also possible to write dynamically tunable LPGs using, for example, radio-frequency driven acoustic waves [100, 101] or stresses introduced by a grooved plate [102]. Our realization that a Bragg grating was not necessary for the supercontinuum enhancement, and that the phase feature could be applied by another method, suggested the use of LPGs. Since the completion of this thesis, we demonstrated a temperature-tuneable spectral enhancement in a photonic crystal fibre with a long-period grating spliced in the middle [16]. Subsequent work demonstrated a similar effect in a dynamically tunable LPG written using a radio-frequency driven acoustic wave. An enhancement of 6 dB was achieved, tuneable over a 20 nm range [100].

Subsequent to the completion of this work, we learned that a related theory had been developed to describe the refilling of a spectral hole — a narrow amplitude feature — in the presence of self-phase modulation *and* two-photon absorption by Fischer *et al.* [118]. They have developed this into a new form of nonlinear microscopy and used it to measure neuronal activity [140]. The theory of spectral hole refilling is conceptually similar to our work in that the key process is interference between a narrowband field corresponding to the amplitude feature, and the remainder of the pulse as it undergoes self-phase modulation and two-photon absorption [141]. To date, this work has focused mainly amplitude-only features. It is therefore worthwhile investigating whether using a phase feature or some combination of the two holds any advantage.

In our model, self-phase modulation is only treated to first order. An important situation which falls outside of this approximation is the effect of a spectrally narrow feature upon a propagating soliton. This would require including quadratic dispersion and propagating beyond the first order in the nonlinear length. This problem has been partially treated in the various theoretical studies which complement our model. The role played by the Raman self-frequency shift in determining whether or not the trajectory in  $(\omega, z)$  space of a soliton will interact with a grating was studied by Li *et al.* [105]. Treating the grating rather than the nonlinearity as a perturbation allows efficient estimation of the effect of a grating on highly complex supercontinuum fields [124]. It was noted by Li *et al.* that solitons may regenerate after spectrally narrow attenuation by a photonic band gap. Furthermore, it is possible that the self-stabilizing nature of solitons may enable a much greater spectral enhancement upon extended propagation. This is a promising topic for further investigation.

# Appendix A

## Numerical methods

To solve the generalized nonlinear Schrödinger equation (GNLSE), we used a second-order procedure related to the split-step Fourier method [66]. We shall derive a procedure for propagating the field from  $z$  to  $z + h$ . We start by writing the formally exact solution to (2.9)

$$A(\omega, z + h) = \int_z^{z+h} \exp[(z + h - z')L(\omega)] N(\omega, z') dz' + \exp[hL(\omega)] A(\omega, z). \quad (\text{A.1})$$

The first summand is an integral over all source contributions at  $z'$  between  $z$  and  $z + h$ , each with an appropriate linear propagator from  $z'$  to  $z + h$ . The second summand linearly propagates the initial condition from  $z$  to  $z + h$ .

The first summand cannot be evaluated analytically. To derive a second-order method, we use the trapezoidal rule, writing

$$\int_z^{z+h} \exp[(z + h - z')L(\omega)] N(\omega, z') dz' \approx \frac{h}{2} \{ \exp[hL(\omega)] N(\omega, z) + N(\omega, z + h) \} + O(h^3). \quad (\text{A.2})$$

Since the second summand on the right-hand side,  $N(\omega, z + h)$ , depends on  $A(\omega, z + h)$ , a first-order estimation of the latter quantity is required. We use

$$\begin{aligned} A_1(\omega) &= [hN(\omega, z) + A(\omega, z)] \exp[hL(\omega)] \\ &\approx A(\omega, z + h) \end{aligned} \quad (\text{A.3})$$

from which the  $N(\omega, z + h)$  is calculated. Equation (A.2) can then be directly evaluated.

This method differs slightly from the standard split-step treatment in that we write the nonlinearity as a source term, rather than as an operator applied to  $A(T, z)$ . We do this because the frequency dependence of the nonlinearity caused by the self-steepening term prevents this operator from being written as a scalar-valued function in either of the time or frequency domains, unlike the linear operator which is a scalar-valued function in the frequency domain. We therefore find the derivation more straightforward if the nonlinearity is treated as a source term.

To discretize the time- and frequency axes, we first chose ranges for these axes which ensured all pulse energy remained in the time-frequency domain down to the  $10^{-4}$  intensity level. The discretization of the axes then followed from the mathematics of the discrete Fourier transform. The  $z$ -axis was discretized automatically using an adaptive step-size routine.

## Appendix B

# Conservation laws of the nonlinear Schrödinger equation

In this Appendix we derive two conservation laws for the nonlinear Schrödinger equation

$$\frac{\partial A(T, z)}{\partial z} = i \frac{\beta_2}{2} \frac{\partial^2 A(T, z)}{\partial T^2} + i\gamma |A(T, z)|^2 A(T, z). \quad (\text{B.1})$$

The first is of the energy

$$U = \int_{-\infty}^{\infty} |A(\omega)|^2 d\omega. \quad (\text{B.2})$$

The second is of the spectral first moment

$$M = \frac{\int_{-\infty}^{\infty} \omega |A(\omega)|^2 d\omega}{U}. \quad (\text{B.3})$$

### B.1 Energy conservation

Using the identity  $d|A|^2 = 2\Re A^* dA$ , where  $\Re$  denotes the real part, one has

$$\frac{dU}{dz} = \int_{-\infty}^{\infty} 2\Re A^*(\omega, z) \frac{dA(\omega, z)}{dz} d\omega. \quad (\text{B.4})$$

Inserting (B.1), one obtains

$$\frac{dU}{dz} = -2\Im \int_{-\infty}^{\infty} \frac{\beta_2}{2} \omega^2 |A(\omega, z)|^2 + \gamma \text{FT} [|A(T, z)|^2 A(T, z)] d\omega \quad (\text{B.5})$$

where FT denotes the Fourier transform and  $\Im$  denotes the imaginary part. The dispersive term in (B.5) is real and hence does not contribute. The nonlinear term is written out in full, yielding

$$\int_{-\infty}^{\infty} \text{FT} [|A(T, z)|^2 A(T, z)] d\omega = \int d\omega_1 \int d\omega_2 \int d\omega A(\omega_1, z) A(\omega_2, z) A^*(\omega_1 + \omega_2 - \omega) A^*(\omega). \quad (\text{B.6})$$

One makes the change of variables  $\omega'_1 = \omega$ ,  $\omega'_2 = \omega_1 + \omega_2 - \omega$ ,  $\omega' = \omega_1$ . (The absolute value of the determinant of the Jacobian of this transformation is unity and therefore no scaling factor is introduced.) Upon performing the substitution and taking the complex conjugate, the right-hand side of (B.6) emerges unchanged. It is therefore real, and thus via (B.5)  $U$  is constant.

## B.2 Conservation of spectral centre of mass

The proof begins similarly to that of conservation of energy, and one obtains

$$U \frac{dM}{dz} = -2\Im \int_{-\infty}^{\infty} \frac{\beta_2}{2} \omega^3 |A(\omega, z)|^2 + \gamma \omega \text{FT} [|A(T, z)|^2 A(T, z)] d\omega. \quad (\text{B.7})$$

The dispersive term is once again real, leaving the nonlinear term

$$G(z) = \int d\omega_1 \int d\omega_2 \int d\omega A(\omega_1) A(\omega_2) A^*(\omega_1 + \omega_2 - \omega) A^*(\omega) \omega. \quad (\text{B.8})$$

We will show that  $G(z)$  is real by examining

$$2\Im G(z) = G(z) - G^*(z). \quad (\text{B.9})$$

Applying the same transformation to the conjugated term as in Section B.1, we obtain

$$2\Im G(z) = \int d\omega_1 \int d\omega_2 \int d\omega A(\omega_1) A(\omega_2) A^*(\omega_1 + \omega_2 - \omega) A^*(\omega) (\omega - \omega_1). \quad (\text{B.10})$$

One now makes the substitution  $\omega' = \omega_1 + \omega_2 - \omega$ ,  $\omega'_1 = \omega_2$ ,  $\omega'_2 = \omega_1$ . Dropping the primes the result is the negative of (B.10), and hence is equal to zero.

## B.3 Violation of conservation laws due to self-steepening and Raman scattering

### B.3.1 Self-steepening

The inclusion of the standard shock term  $\tau_{\text{shock}} = 1/\omega_0$  leads to the following form for the nonlinear term in the GNLSE

$$i\gamma(1 + i\tau_{\text{shock}})A(z, T)|A(z, T)|^2 \leftrightarrow i\frac{\gamma}{\omega_0} \omega \int d\omega_1 \int d\omega_2 \int d\omega A(\omega_1, z) A(\omega_2, z) A^*(\omega_1 + \omega_2 - \omega) A^*(\omega) \quad (\text{B.11})$$

where the double-headed arrow denotes the Fourier transform. In the frequency domain, the shock term is therefore a factor of  $\omega$  in front of the nonlinear term. Therefore, with the shock term present, the proof of conservation of *energy* is identical to that conservation of *spectral centre of mass* without the shock term i.e. that of Section B.2. However, for the spectral centre of mass, the nonlinear term has a factor of  $\omega^2$ . Conservation of the spectral centre of mass requires

$$\Im \int d\omega_1 \int d\omega_2 \int d\omega A(\omega_1, z) A(\omega_2, z) A^*(\omega_1 + \omega_2 - \omega, z) A^*(\omega, z) \omega^2 = 0. \quad (\text{B.12})$$

In general, this condition does not hold — it is violated, for example, by a chirped Gaussian pulse. There are at least two special cases for which it does hold: i) a transform-limited pulse, for which the spectral phase is a straight line ii) a pulse whose spectrum possesses a frequency of conjugate-symmetry i.e.  $A(-\omega) = A^*(\omega)$ . This is equivalent to pulse with constant instantaneous frequency.

Some treatments extend the shock term to incorporate the frequency dependence of the effective area and the effective index [84, 142, 143]. This introduces a degree of arbitrariness which leads to violation of both energy and spectral centre-of-mass conservation.

### B.3.2 Raman response

Inclusion of the Raman response in the NLSE and repeating the steps for conservation leads to the condition

$$\Im \int d\omega_1 \int d\omega_2 \int d\omega A(\omega_1, z) A(\omega_2, z) A^*(\omega_1 + \omega_2 - \omega, z) A^*(\omega, z) R(\omega - \omega_1) = 0. \quad (\text{B.13})$$



### B.3 Violation of conservation laws due to self-steepening and Raman scattering

---

Performing the substitution of Section B.1, conjugating, and exploiting the fact that the Raman response is real and hence satisfies  $R(-\omega) = R^*(\omega)$ , one finds that the left hand side of (B.13) is indeed zero, and hence the Raman term preserves energy conservation.

For the spectral centre-of-mass, repeating the steps of Section B.2 leads to

$$\Im \int d\omega_1 \int d\omega_2 \int d\omega A(\omega_1)A(\omega_2)A^*(\omega_1 + \omega_2 - \omega)A^*(\omega)\omega R(\omega - \omega_1) = 0. \quad (\text{B.14})$$

In general, for a real causal Raman response, this condition is not satisfied.

# Bibliography

- [1] Alfano, R. & Shapiro, S. Emission in the Region 4000 to 7000 Å Via Four-Photon Coupling in Glass. *Phys. Rev. Lett.* **24**, 584 (1970). 6
- [2] Alfano, R. R. & Shapiro, S. L. Observation of self-phase modulation and small-scale filaments in crystals and glasses. *Phys. Rev. Lett.* **24**, 592 (1970). 6, 9, 11
- [3] Ranka, J., Windeler, R., & Stentz, A. Visible continuum generation in air-silica microstructure optical fibers with anomalous dispersion at 800 nm. *Opt. Lett.* **25**, 25 (2000). 6, 8, 9, 10
- [4] Dudley, J. M., Genty, G., & Coen, S. Supercontinuum generation in photonic crystal fiber. *Rev. Mod. Phys.* **78**, 1135 (2006). 6, 11, 16, 18, 52
- [5] Husakou, A. V. & Herrmann, J. Supercontinuum generation of higher-order solitons by fission in photonic crystal fibers. *Phys. Rev. Lett.* **87**, 203901 (2001). 6, 10, 16, 22
- [6] Alfano, R. R. The supercontinuum gains momentum. *Laser Focus World* **41** (2005). 7
- [7] Hartl, I., Li, X. D., Chudoba, C., Ghanta, R. K., Ko, T. H., Fujimoto, J. G., Ranka, J. K., & Windeler, R. S. Ultrahigh-resolution optical coherence tomography using continuum generation in an air silica microstructure optical fiber. *Opt. Lett.* **26**, 608 (2001). 6, 13, 22
- [8] Ell, R., Morgner, U., Kärtner, F. X., Fujimoto, J. G., Ippen, E. P., Scheuer, V., Angelow, G., Tschudi, T., Lederer, M. J., Boiko, A., & Luther-Davies, B. Generation of 5-fs pulses and octave-spanning spectra directly from a ti:sapphire laser. *Opt. Lett.* **26**, 373 (2001). 6
- [9] Nisoli, M., Silvestri, S. D., & Svelto, O. Generation of high energy 10 fs pulses by a new pulse compression technique. *Appl. Phys. Lett.* **68**, 2793 (1996). 6
- [10] Dudley, J. M., Genty, G., & Eggleton, B. J. Harnessing and control of optical rogue waves in supercontinuum generation. *Opt. Express* **16**, 3644 (2008). 8
- [11] Luan, F., Skryabin, D. V., Yulin, A. V., & Knight, J. C. Energy exchange between colliding solitons in photonic crystal fibers. *Opt. Express* **14**, 9844 (2006). 8
- [12] Diddams, A. S., Jones, D. J., Ye, J., Cundiff, S. T., Hall, J. L., Ranka, J. K., Windeler, R. S., Holzwarth, R., Udem, T., & Hansch, T. W. Direct Link between Microwave and Optical Frequencies with a 300 THz Femtosecond Laser Comb. *Phys. Rev. Lett.* **84**, 5102 (2000). 8, 12, 22
- [13] Nagarajan, V., Johnson, E., Schellenberg, P., Parson, W., & Windeler, R. A compact versatile femtosecond spectrometer. *Rev. Sci. Instrum.* **73**, 4145 (2002). 8, 12
- [14] Akhmediev, N. & Karlsson, M. Cherenkov radiation emitted by solitons in optical fibers. *Phys. Rev. A* **51**, 2602 (1995). 8, 15, 21, 22, 23
- [15] Wai, P. K. A., Chen, H. H., & Lee, C. Y. Radiations by “solitons” at the zero group-dispersion wavelength of single-mode optical fibers. *Phys. Rev. A* **41**, 426 (1990). 8, 21, 22, 23
- [16] Yeom, D.-I., Bolger, J. A., Marshall, G. D., Austin, D. R., Kuhlmeier, B. T., Withford, M. J., de Sterke, C. M., & Eggleton, B. J. Tunable spectral enhancement of fiber supercontinuum. *Opt. Lett.* **32**, 1644 (2007). 8, 20, 53

- [17] Stoicheff, B. P. Characteristics of stimulated Raman radiation generated by coherent light. *Phys. Lett.* **7**, 186 (1963). 9
- [18] Brewer, R. G. Frequency shifts in self-focused light. *Phys. Rev. Lett.* **19**, 8 (1967). 9
- [19] Bloembergen, N. Nonlinear optics: past, present, and future. *IEEE J. Sel. Topics in Quantum Electron.* **6**, 876 (2000). 9
- [20] Shimizu, F. Frequency broadening in liquids by a short light pulse. *Phys. Rev. Lett.* **19**, 1097 (1967). 9
- [21] Alfano, R. R. & Shapiro, S. Direct distortion of electronic clouds of rare-gas atoms in intense electric fields. *Phys. Rev. Lett.* **24**, 1217 (1970). 9
- [22] Alfano, R. R., Hope, L. L., & Shapiro, S. L. Electronic mechanism for production of self-phase modulation. *Phys. Rev. A* **6**, 433 (1972). 9
- [23] Corkum, P. B., Ho, P. P., Alfano, R. R., & Manassah, J. T. Generation of infrared supercontinuum covering 3-14  $\mu\text{m}$  in dielectrics and semiconductors. *Opt. Lett.* **10**, 624 (1985). 9, 10
- [24] Manassah, J., Ho, P., Katz, A., & Alfano, R. Ultrafast supercontinuum laser source. *Photonics Spectra* **18**, 53 (1984). 9
- [25] Lin, C. & Stolen, R. H. New nanosecond continuum for excited-state spectroscopy. *Appl. Phys. Lett.* **28**, 216 (1976). 9, 10, 11, 12
- [26] Hasegawa, A. & Tappert, F. Transmission of stationary nonlinear optical pulses in dispersive dielectric fibers. *Appl. Phys. Lett.* **23**, 171 (1973). 10
- [27] Mollenauer, L. F., Stolen, R. H., & Gordon, J. P. Experimental observation of picosecond pulse narrowing and solitons in optical fibers. *Phys. Rev. Lett.* **45**, 1095 (1980). 10
- [28] Satsuma, J. & Yajima, N. Initial value-problems of one-dimensional self-modulation of nonlinear-waves in dispersive media. *Prog. Theor. Phys., Suppl.* pages 284–306 (1974). 10, 15
- [29] Stolen, R., Mollenauer, L., & Tomlinson, W. Observation of pulse restoration at the soliton period in optical fibers. *Opt. Lett.* **8**, 186 (1983). 10
- [30] Kodama, Y. & Hasegawa, A. Nonlinear pulse-propagation in a monomode dielectric guide. *IEEE J. Quantum Electron.* **23**, 510 (1987). 10, 15, 16
- [31] Beaud, P., Hodel, W., Zysset, B., & Weber, H. Ultrashort pulse propagation, pulse breakup, and fundamental soliton formation in a single-mode optical fiber. *IEEE J. Quantum. Elect.* **23**, 1938 (1987). 10
- [32] Schütz, J., Hodel, W., & Weber, H. Nonlinear pulse distortion at the zero dispersion wavelength of an optical fibre. *Opt. Commun.* **95**, 357 (1993). 10
- [33] Gouveia-Neto, A., Faldon, M., & Taylor, J. Solitons in the region of the minimum group-velocity dispersion of single-mode optical fibers. *Opt. Lett.* **13**, 770 (1988). 10
- [34] Islam, M., Sucha, G., Bar-Joseph, I., Wegener, M., Gordon, J., & Chemla, D. Femtosecond distributed soliton spectrum in fibers. *J. Opt. Soc. Am. B* **6**, 1149 (1989). 10
- [35] Morioka, T., Mori, K., & Saruwatari, M. More than 100-wavelength-channel picosecond optical pulse generation from single laser source using supercontinuum in optical fibres. *Electron. Lett.* **29**, 862 (1993). 10
- [36] Morioka, T., Kawanishi, S., Mori, K., & Saruwatari, M. Nearly penalty-free, less-than-4ps supercontinuum gbit-s pulse generation over 1535-1560nm. *Electron. Lett.* **30**, 790 (1994). 10
- [37] Mogilevtsev, D., Birks, T. A., & Russell, P. St. J.. Group-velocity dispersion in photonic crystal fibers. *Opt. Lett.* **23**, 1662 (1998). 10
- [38] Broderick, N., Monro, T., Bennett, P., & Richardson, D. Nonlinearity in holey optical fibers: measurement and future opportunities. *Opt. Lett.* **24**, 1395 (1999). 10

## BIBLIOGRAPHY

---

- [39] Herrmann, J., Griebner, U., Zhavoronkov, N., Husakou, A., Nickel, D., Knight, J. C., Wadsworth, W. J., Russell, P. St. J., & Korn, G. Experimental evidence for supercontinuum generation by fission of higher-order solitons in photonic fibers. *Phys. Rev. Lett.* **88**, 173901 (2002). 10
- [40] Birks, T. A., Wadsworth, W. J., & Russell, P. St. J. Supercontinuum generation in tapered fibers. *Opt. Lett.* **25**, 1415 (2000). 10
- [41] Kelley, P. L. Self-focusing of optical beams. *Phys. Rev. Lett.* **15**, 1005 (1965). 11
- [42] Genty, G., Dudley, J., & Eggleton, B. Modulation control and spectral shaping of optical fiber supercontinuum generation in the picosecond regime. *Appl. Phys. B: Lasers Opt.* **94**, 187 (2009). 11
- [43] Solli, D. R., Ropers, C., & Jalali, B. Active control of rogue waves for stimulated supercontinuum generation. *Phys. Rev. Lett.* **101**, 233902 (2008). 11
- [44] Agrawal, G. P. *Fibre-Optics Communications Systems*. John Wiley & Sons, Inc. (1997). 11
- [45] Snyder, A. W. & Love, J. D. *Optical Waveguide Theory*. Chapman & Hall, London (1996). 11
- [46] Birks, T. A., Knight, J. C., & St. J. Russell, P. Endlessly single-mode photonic crystal fiber. *Opt. Lett.* **22**, 961 (1997). 11
- [47] Schnatz, H., Lipphardt, B., Helmcke, J., Riehle, F., & Zinner, G. First phase-coherent frequency measurement of visible radiation. *Phys. Rev. Lett.* **76**, 18 (1996). 12
- [48] Udem, T., Reichert, J., Holzwarth, R., & Hänsch, T. W. Accurate measurement of large optical frequency differences with a mode-locked laser. *Opt. Lett.* **24**, 881 (1999). 12
- [49] Udem, T., Reichert, J., Holzwarth, R., & Hänsch, T. W. Absolute Optical Frequency Measurement of the Cesium  $D_1$  Line with a Mode-Locked Laser. *Phys. Rev. Lett.* **82**, 3568 (1999). 12
- [50] Diddams, S., Jones, D., Ma, L., Cundiff, S., & Hall, J. Optical frequency measurement across a 104-THz gap with a femtosecond laser frequency comb. *Opt. Lett.* **25**, 186 (2000). 12
- [51] Reichert, J., Holzwarth, R., Udem, T., & Hänsch, T. Measuring the frequency of light with mode-locked lasers. *Opt. Commun.* **172**, 59 (1999). 12
- [52] Jones, D. J., Diddams, S. A., Ranka, J. K., Stentz, A., Windeler, R. S., Hall, J. L., & Cundiff, S. T. Carrier-envelope phase control of femtosecond mode-locked lasers and direct optical frequency synthesis. *Science* **288**, 635 (2000). 12
- [53] Udem, T., Holzwarth, R., & Hänsch, T. Optical frequency metrology. *Nature* **416**, 233 (2002). 12
- [54] Kim, K., Diddams, S. A., Westbrook, P. S., Nicholson, J. W., & Feder, K. S. Improved stabilization of a 1.3  $\mu\text{m}$  femtosecond optical frequency comb by use of a spectrally tailored continuum from a nonlinear fiber gratings. *Opt. Lett.* **31**, 277 (2006). 12, 20, 21, 38
- [55] Alfano, R. R. *The supercontinuum laser source: fundamentals with updated references*. Springer, New York, 2nd ed. (2006). 12
- [56] Alfano, R. R. *Biological events probed by ultrafast laser spectroscopy*. Academic Press (1982). 12
- [57] Ye, Q. H., Xu, C., Liu, X., Knox, W. H., Yan, M. F., Windeler, R. S., & Eggleton, B. Dispersion measurement of tapered air-silica microstructure fiber by white-light interferometry. *Appl. Opt.* **41**, 4467 (2002). 12
- [58] Shang, H. Chromatic dispersion measurement by white-light interferometry on metre-length single-mode optical fibres. *Electron. Lett.* **17**, 603 (1981). 12
- [59] Léonard, J., Lecong, N., Likforman, J., Crégut, O., Haacke, S., Viale, P., Leproux, P., & Couderc, V. Broadband ultrafast spectroscopy using a photonic crystal fiber: application to the photophysics of malachite green. *Opt. Express* **15**, 16124 (2007). 13
- [60] Huang, D., Swanson, E. A., Lin, C. P., Schuman, J. S., Stinson, W. G., Chang, W., Flotte, T., Gregory, K., Puliafito, C. A., & Fujimoto, J. G. Optical coherence tomography. *Science* **254**, 1178 (1991). 13

- [61] Povazay, B., Bizheva, K., Unterhuber, A., Hermann, B., Sattmann, H., Fercher, A. H., Drexler, W., Apolonski, A., Wadsworth, W. J., Knight, J. C., Russell, P. St. J., Vetterlein, M., & Scherzer, E. Submicrometer axial resolution optical coherence tomography. *Opt. Lett.* **27**, 1800 (2002). 13
- [62] McConnell, G. Confocal laser scanning fluorescence microscopy with a visible continuum source. *Opt. Express* **12**, 2844 (2004). 13, 22
- [63] Palero, J., Boer, V., Vijverberg, J., Gerritsen, H., & Sterenborg, H. Short-wavelength two-photon excitation fluorescence microscopy of tryptophan with a photonic crystal fiber based light source. *Opt. Express* **13**, 5363 (2005). 13, 22
- [64] Paulsen, H. N., Hilligsøe, K. M., Thogersen, J., Keiding, S. R., & Larsen, J. J. Coherent anti-Stokes Raman scattering microscopy with a photonic crystal fiber based light source. *Opt. Lett.* **28**, 1123 (2003). 13, 22
- [65] Boyd, R. *Nonlinear Optics*. Academic Press (2003). 15
- [66] Agrawal, G. *Nonlinear Fiber Optics*. Elsevier (2001). 15, 16, 17, 54
- [67] Foster, M., Gaeta, A., Cao, Q., & Trebino, R. Soliton-effect compression of supercontinuum to few-cycle durations in photonic nanowires. *Opt. Express* **13**, 6848 (2005). 15
- [68] Chen, C. M. & Kelley, P. L. Nonlinear pulse compression in optical fibers: scaling laws and numerical analysis. *J. Opt. Soc. Am. B* **19**, 1961 (2002). 15
- [69] Drazin, P. G. *Solitons: An Introduction*. Cambridge University Press, Cambridge (1993). 15
- [70] Taylor, J. R. *Optical Solitons: Theory and Experiment*. Cambridge University Press (1992). 15
- [71] Russell, J. St. J.. Report of 14th Meeting of the British Association for the Advancement of Science. 15
- [72] Denschlag, J., Simsarian, J. E., Feder, D. L., Clark, C. W., Collins, L. A., Cubizolles, J., Deng, L., Hagley, E. W., Helmerson, K., Reinhardt, W. P., Rolston, S. L., Schneider, B. I., & Phillips, W. D. Generating Solitons by Phase Engineering of a Bose-Einstein Condensate. *Science* **287**, 97 (2000). 15
- [73] Dudley, J., Peacock, A., & Millot, G. The cancellation of nonlinear and dispersive phase components on the fundamental optical fiber soliton: a pedagogical note. *Opt. Commun.* **193**, 253 (2001). 15
- [74] Tai, K., Hasegawa, A., & Bekki, N. Fission of optical solitons induced by stimulated Raman effect. *Opt. Lett.* **13**, 392 (1988). 15
- [75] Wai, P. K. A., Menyuk, C. R., Lee, Y. C., & Chen, H. H. Nonlinear Pulse-Propagation in the Neighborhood of the Zero-Dispersion Wavelength of Monomode Optical Fibers. *Opt. Lett.* **11**, 464 (1986). 15
- [76] Elgin, J. N., Brabec, T., & Kelly, S. A perturbative theory of soliton propagation in the presence of 3rd-order dispersion. *Opt. Commun.* **114**, 321 (1995). 15, 22
- [77] Genty, G., Lehtonen, M., & Ludvigsen, H. Effect of cross-phase modulation on supercontinuum generated in microstructured fibers with sub-30 fs pulses. *Opt. Express* **12**, 4614 (2004). 16
- [78] Skryabin, D. & Yulin, A. Theory of generation of new frequencies by mixing of solitons and dispersive waves in optical fibers. *Phys. Rev. E* **72**, 016619 (2005). 16
- [79] Efimov, A., Yulin, A., Skryabin, D., Knight, J., Joly, N., Omenetto, F., Taylor, A., & Russell, P. Interaction of an Optical Soliton with a Dispersive Wave. *Phys. Rev. Lett.* **95**, 213902 (2005). 16
- [80] Gordon, J. Theory of the soliton self-frequency shift. *Opt. Lett.* **11**, 662 (1986). 16
- [81] Woodbury, E. J. & Ng, W. K. Ruby laser operation in near IR. *Proc. Inst. Radio Eng.* **50**, 2367 (1962). 16
- [82] Eckhardt, G., Hellwarth, R. W., McClung, F. J., Schwarz, S. E., Weiner, D., & E.J., W. Stimulated Raman Scattering From Organic Liquids. *Phys. Rev. Lett.* **9**, 455 (1962). 16
- [83] Stolen, R. H. & Ippen, E. P. Raman gain in glass optical waveguides. *Appl. Phys. Lett.* **22**, 276 (1973). 16

## BIBLIOGRAPHY

---

- [84] Blow, K. & Wood, D. Theoretical description of transient stimulated Raman scattering in optical fibers. *IEEE J. Quantum Electron.* **25**, 2665 (1989). 16, 17, 56
- [85] Mamyshev, P. V. & Chernikov, S. V. Ultrashort-pulse propagation in optical fibers. *Opt. Lett.* **15**, 1076 (1990).
- [86] Brabec, T. & Krausz, F. Nonlinear optical pulse propagation in the single-cycle regime. *Phys. Rev. Lett.* **78**, 3282 (1997). 16
- [87] Afshar V., S. & Monro, T. M. A full vectorial model for pulse propagation in emerging waveguides with subwavelength structures part i: Kerr nonlinearity. *Opt. Express* **17**, 2298 (2009). 16
- [88] Tran, T. X. & Biancalana, F. An accurate envelope equation for light propagation in photonic nanowires: new nonlinear effects. *Opt. Express* **17**, 17934 (2009). 16
- [89] Dudley, J. M., Barry, L. P., Bolland, P. G., Harvey, J. D., Leonhardt, R., & Drummond, P. D. Direct measurement of pulse distortion near the zero-dispersion wavelength in an optical fiber by frequency-resolved optical gating. *Opt. Lett.* **22**, 457 (1997). 18
- [90] Weiner, A. M. Femtosecond pulse shaping using spatial light modulators. *Rev. Sci. Instrum.* **71**, 1929 (2000). 18
- [91] Leaird, D. & Weiner, A. Femtosecond direct space-to-time pulse shaping. *IEEE J. Quantum. Elect.* **37**, 494 (2001). 18
- [92] Kaplan, D. & Tournois, P. Acousto-optic spectral filtering of femtosecond laser pulses. In *Ultrafast optics IV: selected contributions to the 4th International Conference on Ultrafast Optics, Vienna, Austria*, page 105. Springer Verlag (2004). 20
- [93] Weiner, A. M., Heritage, J. P., & Kirschner, E. M. High-resolution femtosecond pulse shaping. *J. Opt. Soc. Am. B* **5**, 1563 (1988). 20
- [94] Schenkel, B., Paschotta, R., & Keller, U. Pulse compression with supercontinuum generation in microstructure fibers. *J. Opt. Soc. Am. B* **22**, 687 (2005). 20
- [95] Türke, D., Wohlleben, W., Teipel, J., Motzkus, M., Kibler, B., Dudley, J., & Giessen, H. Chirp-controlled soliton fission in tapered optical fibers. *Appl. Phys. B* **83**, 37 (2006). 20
- [96] Xu, S., Reitze, D., & Windeler, R. Controlling nonlinear processes in microstructured fibers using shaped pulses. *Opt. Express* **12**, 4731 (2004). 20
- [97] Omenetto, E., Taylor, A., Moores, M., & Reitze, D. Adaptive control of femtosecond pulse propagation in optical fibers. *Opt. Lett.* **26**, 938 (2001). 20
- [98] Tianprateep, M., Tada, J., Yamazaki, T., & Kannari, F. Spectral-Shape-Controllable Supercontinuum Generation in Microstructured Fibers Using Adaptive Pulse Shaping Technique. *Japanese J. Appl. Phys.* **43**, 8059 (2004). 20
- [99] Westbrook, P. S., Nicholson, J. W., Feder, K. S., & Yablon, A. D. Improved supercontinuum generation through uv processing of highly nonlinear fibers. *J. Lightwave Technol.* **23**, 13 (2005). 20
- [100] Bolger, J. A., Luan, F., Yeom, D.-I., Tsoy, E. N., de Sterke, C. M., & Eggleton, B. J. Tunable enhancement of a soliton spectrum using an acoustic long-period grating. *Opt. Express* **15**, 13457 (2007). 20, 53
- [101] Kim, H. S., Yun, S. H., Kwang, I. K., & Kim, B. Y. All-fiber acousto-optic tunable notch filter with electronically controllable spectral profile. *Opt. Lett.* **22**, 1476 (1997). 20, 53
- [102] Savin, S., Dignonnet, M. J. F., Kino, G. S., & Shaw, H. J. Tunable mechanically induced long-period fiber gratings. *Opt. Lett.* **25**, 710 (2000). 20, 53
- [103] Eggleton, B. J., Stephens, T., Krug, P. A., Dhosi, G., Brodzeli, Z., & Ouellette, F. Dispersion compensation using a fibre grating in transmission. *Electron. Lett.* **32**, 1610 (1996). 20, 39

- [104] Westbrook, P. S., Nicholson, J. W., Feder, K. S., Li, Y., & Brown, T. Supercontinuum generation in a fibre grating. *Appl. Phys. Lett.* **85**, 4600 (2004). 20, 21, 38, 39
- [105] Li, Y., Salisbury, F. C., Zhu, Z., Brown, T. G., Westbrook, P. S., Feder, K. S., & Windeler, R. S. Interaction of supercontinuum and raman solitons with microstructure fiber gratings. *Opt. Express* **13**, 998 (2005). 21, 39, 53
- [106] Höök, A. & Karlsson, M. Ultrashort solitons at the minimum-dispersion wavelength: effects of fourth-order dispersion. *Opt. Lett.* **18**, 1388 (1993). 22
- [107] Curley, P., Spielmann, C., Brabec, T., Krausz, F., Wintner, E., & Schmidt, A. Operation of a femtosecond Ti:sapphire solitary laser in the vicinity of zero group-delay dispersion. *Opt. Lett.* **18**, 54 (1993). 22
- [108] Salin, F., Grangier, P., Georges, P., & Brun, A. Pulse propagation near zero group-velocity dispersion in a femtosecond dye laser. *Opt. Lett.* **15**, 1374 (1990). 22
- [109] Brabec, T. & Kelly, S. Third-order dispersion as a limiting factor to mode locking in femtosecond solitary lasers. *Opt. Lett.* **18**, 2002 (1993). 22
- [110] Husakou, A. V. & Herrmann, J. Supercontinuum generation, four-wave mixing, and fission of higher-order solitons in photonic-crystal fibers. *J. Opt. Soc. Am. B* **19**, 2171 (2002). 22
- [111] Hilligsøe, K. M., Paulsen, H. N., Thogersen, J., Keiding, S. R., & Larsen, J. J. Initial steps of supercontinuum generation in photonic crystal fibers. *J. Opt. Soc. Am. B* **20**, 1887 (2003). 22
- [112] Cristiani, I., Tediosi, R., Tartara, L., & Degiorgio, V. Dispersive wave generation by solitons in microstructured optical fibers. *Opt. Express* **12**, 124 (2004). 22
- [113] Fuerbach, A., Steinvurzel, P., Bolger, J., & Eggleton, B. Nonlinear pulse propagation at zero dispersion wavelength in anti-resonant photonic crystal fibers. *Opt. Express* **13**, 2977 (2005). 22
- [114] Skryabin, D. V., Luan, E., Knight, J. C., & Russell, P. St. J.. Soliton self-frequency shift cancellation in photonic crystal fibers. *Science* **301**, 1705 (2003). 22, 52
- [115] Biancalana, F., Skryabin, D. V., & Yulin, A. V. Theory of the soliton self-frequency shift compensation by the resonant radiation in photonic crystal fibers. *Phys. Rev. E* **70** (2004). 22
- [116] Karpman, V. I. Radiation of solitons described by a high-order cubic nonlinear Schrödinger equation. *Phys. Rev. E* **62** (2000). 23
- [117] Gorbach, A. & Skryabin, D. Light trapping in gravity-like potentials and expansion of supercontinuum spectra in photonic-crystal fibres. *Nat. Photon.* **1**, 653 (2007). 23
- [118] Fischer, M. C., Ye, T., Yurtsever, G., Miller, A., Ciocca, M., Wagner, W., & Warren, W. S. Two-photon absorption and self-phase modulation measurements with shaped femtosecond laser pulses. *Opt. Lett.* **30**, 1551 (2005). 38, 53
- [119] Hill, K., Fujii, Y., Johnson, D., & Kawasaki, B. Photosensitivity in optical fiber waveguides: Application to reflection filter fabrication. *Appl. Phys. Lett.* **32**, 647 (1978). 38
- [120] Meltz, G., Morey, W., Glenn, W., *et al.* Formation of Bragg gratings in optical fibers by a transverse holographic method. *Opt. Lett.* **14**, 823 (1989). 38
- [121] Aceves, A. & Wabnitz, S. Self-induced transparency solitons in nonlinear refractive periodic media. *Phys. Lett. A* **141**, 37 (1989). 38
- [122] Christodoulides, D. N. & Joseph, R. I. Slow bragg solitons in nonlinear periodic structures. *Phys. Rev. Lett.* **62**, 1746 (1989). 38, 39
- [123] Eggleton, B. J., Slusher, R. E., de Sterke, C. M., Krug, P. A., & Sipe, J. E. Bragg grating solitons. *Phys. Rev. Lett.* **76**, 1627 (1996). 38
- [124] Westbrook, P. & Nicholson, J. Perturbative approach to continuum generation in a fiber Bragg grating. *Opt. Express* **14**, 7610 (2006). 39, 53

## BIBLIOGRAPHY

---

- [125] Nicholson, J. W., Westbrook, P. S., & Feder, K. S. Localized enhancement of supercontinuum generation using fiber bragg gratings. In *Lasers and Electro-Optics, 2005.(CLEO). Conference on*, vol. 3, pages 1891–1893 Vol. 3 (2005). 39
- [126] Russell, P. St. J.. Bloch wave analysis of dispersion and pulse-propagation in pure distributed feedback structures. *J. Mod. Opt.* **38**, 1599 (1991). 39
- [127] Erdogan, T. Fiber grating spectra. *J. Lightwave Technol.* **15**, 1277 (1997). 39
- [128] Sipe, J. E., de Sterke, C. M., & Eggleton, B. J. Rigorous derivation of coupled mode equations for short, high-intensity grating-coupled, co-propagating pulses. *J. Mod. Opt.* **49**, 1437 (2002). 39
- [129] Winful, H. G. & Cooperman, G. D. Self-pulsing and chaos in distributed feedback bistable optical devices. *Appl. Phys. Lett.* **40**, 298 (1982). 39
- [130] Press, W. H., Teukolsky, S. A., Vetterling, W. T., & Flannery, B. P. *Numerical Recipes in C, The Art of Scientific Computing*. Cambridge University Press (1992). 39
- [131] Hill, K. & Meltz, G. Fiber Bragg grating technology fundamentals and overview. *J. Lightwave Technol.* **15**, 1263 (2002). 39
- [132] Johnson, S. G., Bienstman, P., Skorobogatiy, M. A., Ibanescu, M., Lidorikis, E., & Joannopoulos, J. D. Adiabatic theorem and continuous coupled-mode theory for efficient taper transitions in photonic crystals. *Phys. Rev. E* **66**, 066608 (2002). 39
- [133] Frosz, M., Falk, P., & Bang, O. The role of the second zero-dispersion wavelength in generation of supercontinua and bright-bright soliton-pairs across the zero-dispersion wavelength. *Opt. Express* **13**, 6181 (2005). 52
- [134] Genty, G., Lehtonen, M., Ludvigsen, H., & Kaivola, M. Enhanced bandwidth of supercontinuum generated in microstructured fibers. *Opt. Express* **12**, 3471 (2004). 52
- [135] Efimov, A., Taylor, A., Omenetto, F., Yulin, A., Joly, N., Biancalana, F., Skryabin, D., Knight, J., & Russell, P. Time-spectrally-resolved ultrafast nonlinear dynamics in small-core photonic crystal fibers: Experiment and modelling. *Opt. Express* **12**, 6498 (2004). 52
- [136] Hilligsøe, K. M., Andersen, T. V., Paulsen, H. N., Nielsen, C. K., Molmer, K., Keiding, S., Kristiansen, R., Hansen, K. P., & Larsen, J. J. Supercontinuum generation in a photonic crystal fiber with two zero dispersion wavelengths. *Opt. Express* **12**, 1045 (2004). 52, 53
- [137] Nguyen, H., Kuhlmeiy, B., Mägi, E., Steel, M., Domachuk, P., Smith, C., & Eggleton, B. Tapered photonic crystal fibres: properties, characterisation and applications. *Appl. Phys. B: Lasers Opt.* **81**, 377 (2005). 53
- [138] Zhang, W. Q., Ebendorff-Heidepriem, H., Monroe, T. M., & V., S. A. Fabrication and supercontinuum generation in dispersion flattened bismuth microstructured optical fiber. *Opt. Express* **19**, 21135 (2011). 53
- [139] Vengsarkar, A., Lemaire, P., Judkins, J., Bhatia, V., Erdogan, T., & Sipe, J. Long-period fiber gratings as band-rejection filters. *J. Lightwave Technol.* **14**, 58 (1996). 53
- [140] Fischer, M., Liu, H., Piletic, I., Escobedo-Lozoya, Y., Yasuda, R., & Warren, W. Self-phase modulation signatures of neuronal activity. *Opt. Lett.* **33**, 219 (2008). 53
- [141] Samineni, P., Perret, Z., Warren, W. S., & Fischer, M. C. Measurements of nonlinear refractive index in scattering media. *Opt. Express* **18**, 12727 (2010). 53
- [142] Kibler, B., Dudley, J. M., & Coen, S. Supercontinuum generation and nonlinear pulse propagation in photonic crystal fiber: influence of the frequency-dependent effective mode area. *Applied Physics B: Lasers and Optics* **81**, 337 (2005). 56
- [143] Karasawa, N., Nakamura, S., Nakagawa, N., Shibata, M., Morita, R., Shigekawa, H., & Yamashita, M. Comparison between theory and experiment of nonlinear propagation for a-few-cycle and ultrabroadband optical pulses in a fused-silica fiber. *IEEE J. Quantum. Electron.* **37**, 398 (2001). 56